Quark Nugget Dark Matter : Cosmic Evidence and Detection Potential

by

Kyle Lawson

B.Sc., The University of Western Ontario, 2005
M.Sc., The University of British Columbia, 2008

A THESIS SUBMITTED IN PARTIAL FULFILLMENT OF
THE REQUIREMENTS FOR THE DEGREE OF

DOCTOR OF PHILOSOPHY

in

The Faculty of Graduate and Postdoctoral Studies

(Physics)

THE UNIVERSITY OF BRITISH COLUMBIA

(Vancouver)

February, 2015

Abstract

I present a dark matter model in which the dark matter is composed of very heavy "nuggets" of Standard Model quarks and antiquarks. This model was originally motivated by the fact that the matter and dark matter mass densities are observed to have similar scales. If these two forms of matter originate through completely distinct physical processes then their densities could easily have existed at vastly different scales. However, if the dark and the visible matter are co-produced, this similarity in scales is a natural outcome. In the model considered here dark matter and the baryonic matter share an origin in Standard Model strong force physics.

The main goal of this work is to establish the testable predictions of this model. The physical properties of the nuggets are set by well understood nuclear physics and quantum electrodynamics, allowing many definite observable consequences to be predicted. To this end, I devote special attention to the structure of the surface layer of the nuggets from which the majority of observable consequences arise.

With this basic picture of nugget structure in place, I will discuss the consequences of their interactions with a number of different environments. Particular attention is given to the galactic centre and to the early universe, as both are sufficiently dense to allow for significant levels of matter-dark matter interaction. The emitted radiation, in both cases, is shown to be consistent with observations.

Finally, I discuss the consequences of a nugget striking the earth. In this context, I will demonstrate that the nuggets produce effects observable in cosmic ray detectors. Based on these considerations, I discuss the nugget detection potential for experiments primarily devoted to the study of high energy cosmic rays.

Preface

Much of the original research contained in this dissertation has previously been published in several versions.

Many of the details of Chapter 2 are adapted from work previously published in, The Electrosphere of Macroscopic 'Quark Nuclei': A Source for Diffuse MeV Emissions from Dark Matter, (Forbes, Lawson and Zhitnitsky, 2010 [40]) as is the material of Chapter 4. Many of the detailed nuclear physics calculations of that work were due to Michael Forbes, my primary efforts came in translating those results in observational consequences. The results of Chapter 5 are taken from, Isotropic Radio Background from Quark Nugget Dark Matter, (Lawson and Zhitnitsky, 2013 [81]). The underlying research was originally proposed by Ariel Zhitnitsky and conducted collaboratively. Many of the details of Chapter 6 are taken from independent research presented in the solo author papers, Quark Matter Induced Extensive Air Showers [73] and, Atmospheric Radio Signals From Galactic Dark Matter [77]. This research arose out of, and was strongly influenced by, extensive discussions with Ariel Zhitnitsky, but was pursued largely independently.

I have previously presented aspects of this work at; the Winter Nuclear and Particle Physics Conference, Banff, AB (2009); the Lake Louise Winter Institute, Lake Louise, AB (2009) [75]; UWO Physics and Astronomy Department Colloquium, London, ON (2009); the Winter Nuclear and Particle Physics Conference, Banff, AB (2010); the Lake Louise Winter Institute, Lake Louise, AB (2010) [76]; APS Northwestern Meeting, Vancouver, BC (2012); the International Symposium on Very High Energy Cosmic Ray Interactions, Berlin, Germany (2012) [78] and CERN, Geneva, Switzerland (2014) [79]; as well as the Snowmass meeting, Stanford, California (2013) [82].

Table of Contents

Appendices

List of Figures

Chapter 1

Dark Matter and Baryogenesis

1.1 Introduction

The matter content of the universe is predominantly in the form of dark matter, which carries an average energy density five times larger than that of the visible matter[1]. The large scale behavior of the dark matter is well understood in terms of its gravitational interaction with the surrounding visible matter. However, at present we have no microscopic understanding of its properties or origin. While many theories have been put forward none has received any observational verification[2] and most require the introduction of new physics beyond the standard model for which we have no evidence. As such, the physical nature of the dark matter remains one of the most important open questions in cosmology.

The physical properties of visible matter, as represented by the Standard Model, are better understood than those of the dark matter. However, there remains an important outstanding question related to the origin of the visible matter content of the universe. While the basic physical laws apparently treat matter and antimatter identically, we observe a large global asymmetry between the two - namely the visible universe is almost entirely composed of matter with only trace amounts of antimatter. The source of this asymmetry has not been established, nor does it have any mechanism by which to arise within the context of Standard Model physics. The process by which the present day matter dominated universe emerges from a (presumably)

[1]Current best measurements suggest a universe dominated by the cosmological constant (Λ) and cold dark matter, the so called ΛCDM cosmology, with the relative energy densities divided as $\Omega_\Lambda = 0.7181, \Omega_{DM} = 0.236, \Omega_B = 0.0461$ and negligible contributions from photons and neutrinos [56]. Here Ω is the fraction of the critical density represented by each of the components of the universe as defined in appendix A.

[2]There have been some tantalizing recent results in ground based detectors, but the data remains confusing and, at times, seemingly contradictory. The current state of these investigations will be briefly reviewed at the beginning of chapter 6.

matter/antimatter symmetric initial state is known as baryogenesis, and is the second outstanding question in cosmology to be addressed here.

It is intriguing that, while the dark matter dominates over visible, it does so by what is seemingly only a geometric factor: $\Omega_{DM} \approx 5\Omega_{vis}$. Had these two forms of matter originated at different epochs and through radically different physical processes their densities could easily be separated by many orders of magnitude. This seemingly coincidental common scale in energy density may, in fact, hint at a deeper relation between baryogenesis and the origin of the dark matter. Motivated by this possible connection this work will consider a model in which the dark matter emerges as a necessary byproduct of baryogenesis. This connection is made possible if the baryon asymmetry develops at the QCD[3] phase transition in the early universe. The details of this model will be outlined in the following section. In this context, it is important to note where the dominant component of the visible mass of the universe resides. The majority of visible matter is baryonic and, as such, its mass is determined primarily by the QCD binding energy associated with protons and neutrons, rather than the masses of the individual quarks[4]. As such, the similar mass densities of the visible and dark matter may imply a link between the dark matter and the QCD scale.

Before turning to the specific model to be considered here, it will be useful to review some general considerations relating to baryogenesis. An important measure of the matter/antimatter asymmetry is the baryon-to-photon ratio [56]

$$\eta \equiv \frac{n_B - n_{\bar{B}}}{n_\gamma} = 6 \times 10^{-10}. \tag{1.1}$$

Here n_B and $n_{\bar{B}}$ are the observed baryon and antibaryon number densities and n_γ is the photon density. This ratio will remain constant with the universe's expansion once whatever process creates the baryon asymmetry ceases to act and the CMB photons[5] decouple from the matter content. Had no form of baryogenesis occurred, the universe would contain equal numbers of protons and antiprotons, with a total density much lower than presently observed. In fact, were the asymmetry not present baryon annihilation

[3]Quantum chromodynamics (QCD) is the theory governing the strong force interactions of the Standard Model. Some of its basic details are outlined in appendix B.

[4]In the Standard Model the light quarks within the proton and neutron acquire masses at the MeV scale through the Higgs mechanism. The observed mass of the nucleons is however, much larger than that of three quarks due to the contribution from the strong force binding energy.

[5]The cosmic microwave background (CMB), along with some other relevant cosmology, is reviewed in appendix A.

would continue until expansion dilutes the universe to the point where the mean free path of a proton is longer than the Hubble scale. In this freeze out scenario the matter-to-photon ratio would be some ten orders of magnitude smaller than presently observed with, $n_B = n_{\bar{B}} \approx 10^{-20} n_\gamma$. It would seem that there must be some process which is capable of generating the matter dominance observed today. It should be noted that the asymmetry as a fraction of the total baryonic matter content, $\Delta n/N = (n_B - n_{\bar{B}})/(n_B + n_{\bar{B}})$, remains small until the QCD phase transition even if it originates at an earlier epoch. Before the phase transition the early universe plasma contained deconfined light quarks which are thermally abundant in numbers essentially equal to the photon abundance. After the phase transition, at temperatures below $T \sim 100$MeV, the quarks are confined in nucleons which are too heavy to be created in thermal collisions. At this point, the only possible interactions are inelastic scattering or the annihilation of matter with antimatter and the ratio $\Delta n/N$ rapidly drops to its present day value of $\Delta n/N \sim 1$. Thus, even if the baryon asymmetry is present before the QCD phase transition, it does not become an order one effect until this time.

Any dynamical process which generates a baryon asymmetry must meet the three Sakharov Conditions [105]. These are:

- The violation of baryon number ,
- Charge parity (CP) symmetry violation,
- Non-equilibrium processes.

The first condition allows for the creation or removal of baryons or antibaryons independently. CP violation is necessary as the relevant process must preferentially remove antibaryons over baryons[6]. Finally these processes must be out of equilibrium in order to assure that antibaryon destruction occurs at a different rate than its reverse process of antibaryon creation.

In the model of interest here the baryon asymmetry is only an apparent one. Consequently, it does not require the introduction of a baryon number violating process and leaves the global baryonic charge of the universe unchanged. The required CP violation and non-equilibrium conditions are provided by the physics of the QCD phase transition. To demonstrate how this is possible, I will now turn from general considerations to the specifics of the model.

[6] Charge Parity (CP) symmetry is the combination of the charge reversal and mirror reflection symmetries.

1.2 Dark matter as compact composite objects

Since the existence of dark matter was firmly established a wide variety of models for its physical nature have been proposed. The majority of these models assume that the dark matter is comprised of a new fundamental particle whose properties should be chosen to match the observational constraints coming from dark matter searches. There is presently no evidence for the existence of suitable beyond Standard Model particles (except possibly the existence of the dark matter itself) and their physical properties are not well constrained. Rather than treating the dark matter as a new, yet to be discovered, particle this work will consider the possibility that the dark matter may be composite in nature and involve large numbers of known particles.

The first proposal that dark matter may be not a new fundamental particle but conventional Standard Model particles in a novel phase was that described by Witten [122]. This model suggested that, at sufficiently large densities, the presence of strange quarks could make a quark matter state energetically favorable to nuclear matter. This is possible because Pauli exclusion requires that each additional particle be placed in a higher energy state. Thus, at some large density, it becomes favorable to begin adding heavier strange quarks rather than ultrarelativistic u and d quarks. Droplets of matter in this phase are referred to as strangelets and have been suggested as a dark matter candidate. There is, at present, no evidence for the existence of strangelets but their possible stability is not ruled out (see for example [85, 86].)

The original suggestion for the formation of strangelets [122], in sufficient numbers to explain the dark matter, required that the QCD phase transition be first-order (though it is now believed to be a second-order crossover.) In this picture, bubbles of the nucleating low temperature phase grow and it is the pressure of the bubble walls that is responsible for compressing regions of the high temperature phase to sufficient density that they form strange quark matter. In addition to the now disfavored requirement of a first-order phase transition, this model also requires more efficient cooling of the shrinking bubbles than is theoretically predicted[7].

The model under consideration here is a modification of this original proposal in that it invokes axion domain walls, which may form at the phase

[7]The strangelet model also requires that baryogenesis occur at an early epoch of the universe's history and provides no mechanism for generating the observed asymmetry. While not an explicit failure of the model, which was intended only to explain the dark matter, it does leave unanswered one of the fundamental problems to be addressed here.

transition, as a means by which to compress the high temperature quark gluon plasma to sufficient densities to form quark matter (the properties and dynamics of these walls are reviewed in appendix B.4.) The resulting objects, known as quark nuggets or antiquark nuggets depending on their composition, will end up in a high density quark matter state which is now thought more likely to be a colour superconductor than a form of strange quark matter. If the QCD phase transition results in the production of nuggets of quarks and antiquarks, the question becomes whether these objects could possible serve as the dark matter.

Large inherent uncertainties remain in the formation process and in the high density structure of the QCD phase diagram (particularly in the case of nonzero θ which, as discussed below, will be of relevance here[8].) However, it is not necessary for our purposes to present an in depth discussion of quark matter. Instead, I will use generic considerations and energy scales to extract the basic properties any such objects must display. A brief review of the properties of quark matter and colour superconductivity, with a particular emphasis on the properties relevant to the present analysis, is given in section 2.1.

This idea may at first seem counterintuitive as these objects are macroscopically large and interact strongly with visible matter. However, there is a range of allowed parameter space in which models of this type of feasible. The basic idea is that gravitational probes of the dark matter are sensitive to the mass density of the dark matter, while all possible non-gravitational observations depend on the product of the number density and the interaction cross section. As such, it is not the interaction strength which is observationally constrained but rather the cross section to mass ratio (σ/M). Thus, even strongly interacting, macroscopically large objects may serve as the dark matter, provided they are sufficiently dense.

The local dark matter mass density is estimated at roughly 1 GeV/c^2 cm^{-3} (i.e. $\sim 2\times10^{-27}$ kg/cm^3). In order to remain bound to the galaxy, the dark matter should carry an average velocity near 200km/s as determined from virial equilibrium. This translates to a dark matter flux of

$$\Phi_{DM} = n_{DM} v_{gal} \approx \left(\frac{1\mathrm{GeV/c^2}}{M_{DM}}\right) 10^{11}\mathrm{m^{-2}s^{-1}}. \tag{1.2}$$

For WIMP dark matter with a mass near the 100GeV/c^2 scale this implies a relatively large flux and, in order to avoid direct detection constraints,

[8]The vacuum angle θ is a free parameter appearing in the fundamental theory of QCD which parameterizes the degree of CP violation present in the theory. For further details see appendix B.

requires that the dark matter is coupled to visible matter at a level below the electroweak scale. For comparative value, a state of the art dark matter experiment such as CDMSII publishes exclusion limits up to, at most, a dark matter mass at the TeV scale [14].

Alternatively, if the dark matter is sufficiently massive, the flux may become small enough to evade detection even without the requirement of a strongly suppressed interaction strength. In the case of quark nuggets with a baryonic charge B_N the flux expression 1.2 is more usefully formulated as

$$\Phi_{Nuggets} \approx \left(\frac{10^{24}}{B_N}\right) \text{km}^{-2}\text{yr}^{-1}. \tag{1.3}$$

Given that the nuggets must carry a baryonic charge larger (and possibly several orders of magnitude larger) than 10^{24}, these events are infrequent enough to avoid detection by conventional dark matter searches.

Similar considerations apply in the case of constraints on the dark matter coming from astrophysical observations. The frequency of direct scattering events is determined by the ratio of the nugget's physical cross section to mass ratio, and the strength of their electromagnetic coupling to various astrophysical plasmas scales with the charge to mass ratio. Both of these are increasingly suppressed for increasing nugget mass. As such, the nuggets behave almost identically to any other type of collisionless cold dark matter. Their coupling to the lighter baryonic matter is primarily gravitational so that they form extended dark matter halos rather than clumping as the visible matter does.

To place meaningful constraints on this class of dark matter models requires either the indirect analysis of galactic and cosmological data able to sample over large volumes, or the use of much larger direct detection experiments. These two complementary search techniques will be discussed in the following chapters.

1.3 Baryogenesis through charge separation

As suggested above, the similar energy densities of the baryonic and dark matter components of the universe may argue for some deeper connection in their origins. This work draws on the possibility that both the baryon asymmetry and the dark matter may be generated at the time of the QCD phase transition [95, 126, 127]. Some background on the QCD physics relevant to the following discussion may be found in appendix B.

At temperatures well above the phase transition the universe contains a quark-gluon plasma rather than the discrete baryons observed today. As the temperature drops, the effective QCD coupling strength increases, and the quarks are forced into colour singlet protons and neutrons which are the low energy particles of the low temperature phase.

The phase transition provides the requisite non-equilibrium physics and, as discussed further in appendix B, may also allow for sufficient CP violation to satisfy the second Sakharov condition. In the high temperature phase, the CP violating θ term is expected to have been non-zero, so that CP violating interactions were generally as common as those respecting CP symmetry. During the phase transition QCD physics contains no small parameters and, as such, all processes must occur at essentially the same rate[9]. After the phase transition the dynamics of the axion allow the value of θ to relax from $\theta \sim 1$ to its present near zero value. At this point QCD becomes a CP preserving theory as it is observed to be today. Once this relaxation has occurred the Standard Model (and many of its proposed extensions) allows for too little CP violation to explain the observed degree of baryogenesis. In this way, the QCD phase transition may satisfy the requirements of non-equilibrium physics and CP violation without contradicting present limits on the scale of strong CP violation. However, there is no mechanism at this scale for explicitly violating baryon number conservation.

Rather than relying on the introduction of a new baryon number violating process, the baryogenesis model considered here preserves global baryonic charge, instead using CP violating processes to separate the matter from the antimatter. In this sense it is not a "baryogenesis" process but rather one of charge separation. A more detailed description of this process is given in [126]. Possible evidence of a related process in heavy ion collisions is discussed in [68]. In this picture axion domain walls, related to the 2π periodicity of the θ parameter, form at the QCD phase transition and carry sufficient energy to compress the quarks and antiquarks of the quark-gluon plasma down to densities at or above the nuclear scale. As CP symmetry is strongly violated along these walls, the reflection coefficients of quarks and antiquarks may be quite different. The differential escape probabilities will result in an excess of either quarks or antiquarks inside the contracting wall. The excess quarks remaining within the nugget, do not have antimatter particles with which to annihilate, and are compressed by the collapsing wall until the internal Fermi pressure becomes sufficient

[9] For comparison the theory of QED includes the fine structure constant, the small value of which favours processes involving the fewest possible photon-fermion interactions.

to halt collapse. On formation these objects essentially become dark in the manner discussed above.

As a natural consequence of the order one CP violation present when $\theta \neq 0$ the rate of nugget formation is likely to differ from that of antinugget formation by a geometric factor. If the efficiency of forming nuggets of antiquarks is higher than for quarks the result, at the end of the nugget formation process, will be a universe with an excess of antimatter bound in the nuggets and a corresponding excess of matter in the plasma of hadronic matter. Annihilation of the free matter and antimatter not confined to the nuggets continues within the early universe plasma until the antimatter has completely annihilated away and only the excess of matter remains. It is this component which makes up the visible universe as observed today. It should be noted that the small value of the baryon to photon ratio in expression 1.1 implies that the process of nugget formation need not be highly efficient, the vast majority of the original baryonic content of the universe does annihilate to photons. Observationally, the antiquark nuggets must be favoured over quark nuggets by a factor of $\sim 3/2$. This would result in a baryon distribution between visible matter, nuggets and antinuggets of,

$$B_{vis} : B_n : B_{\bar{n}} \approx 1 : 2 : 3 \tag{1.4}$$

consistent with the observed matter to dark matter ratio ($\Omega_{DM} \approx 5\Omega_{vis}$) and a universe with zero net baryon number. While this ratio cannot be estimated with any level of precision, it can be argued that this order one proportionality is to be expected. This is because the nuggets continue to interact with the surrounding baryons as long as the temperatures are at the QCD scale. At these energies all processes, including those violating CP symmetry, are expected to occur at the same scale. As the value of this temperature is critical in establishing the degree of baryogenesis it will be further discussed below, a more extensive estimation may be found in [95].

This general picture may be made more specific if we assume that the relaxation of the θ term occurs through the axion mechanism (a brief review of axion physics is given in appendix B or, for more details, see, for example, the recent review article [109] and references therein.) In this case the domain walls are associated with transitions in the axion field, and we may estimate the basic properties of the nuggets from the assumed properties of the (as yet unobserved) axion. The following discussion will give a qualitative outline of the formation of the nuggets in this scenario, going only as far as needed to motivate some of the basic assumptions required to establish the phenomenological consequences of quark nugget dark matter. It is these consequences that are to be the primary focus of this work.

As discussed in appendix B the axion domain wall has a sandwich structure, with a hard core capable of reflecting some fraction of the quarks incident on it. As these walls form, some will collapse into closed surfaces which then further collapse down to smaller sizes, condensing the nuggets out of the quark gluon plasma. From basic considerations of this process we are able to estimate the size of the nuggets that will be produced.

Across the axion domain wall the energy density will be at the typical quark condensate scale:

$$\rho \sim m_q < \bar{\psi}\psi > \sim m_q \Lambda_{QCD}^3. \tag{1.5}$$

Here m_q is the quark mass, and $< \bar{\psi}\psi >$ is the vacuum expectation value (VEV) of the quark field. The quark VEV is generally expected to occur at the characteristic energy scale of QCD interactions, $\Lambda_{QCD} \sim 100$MeV. The thickness of the wall is set by the axion length scale, $l_a \sim m_a^{-1}$, where m_a is the axion mass. It is the introduction of this new length scale into the dynamics of the phase transition which allows the development of macroscopically large objects carrying a very large baryonic charge. Without such a scale all structures would evolve at the much smaller femtometer scale associated with QCD energies.

Suppose that, as argued above, there is a high density phase of hadronic matter which is energetically favourable at low energies to free baryons by an amount Δ. In this case, the change in potential energy associated with a quark nugget of radius R and baryon number B is,

$$U = 4\pi\sigma_a R^2 - \Delta B. \tag{1.6}$$

Where σ_a is the surface tension of the axion domain wall. From this expression we can see that there will be some minimum baryonic charge for which the energy cost of the domain wall is overcome by the lower binding energy of the quarks[10]. The radial size at which this occurs is,

$$R = \frac{2\sigma_a}{n_B \Delta} = 2\frac{m_q}{m_a \Delta}\frac{< \bar{\psi}\psi >}{n_B}, \tag{1.7}$$

where n_B is the baryon density in the nugget such that $B = \frac{4}{3}\pi R^3 n_B$. The quark condensate, the nugget baryon density and the binding gap must be at the QCD scale up to geometric factors so that $R \sim \frac{m_q}{m_a \Lambda_{QCD}}$.

[10]This analysis is conducted in a more rigorous way in [95] which also incorporates pressure terms and reflection coefficients at the domain wall. That analysis gives results similar to those obtained in this simplified static case as all processes, with the exception of the axion wall, must occur at or near the scale set by Λ_{QCD}.

If we assume that the axion mass falls in the allowed range of $10^{-6}eV < m_a < 10^{-3}$eV, then the nugget radius may vary by,

$$10^{-6}\text{cm} < R_N < 10^{-2}\text{cm}. \tag{1.8}$$

Assuming that the resulting quark nugget is of roughly nuclear density this may be converted into a total baryon number for the nuggets of

$$10^{23} < B_N < 10^{33}. \tag{1.9}$$

These values will be taken as an estimate of the basic scale at which the nuggets are likely to exist.

Finally, a brief discussion of the baryon to photon ratio, as given in equation 1.1, is in order. At the phase transition all the quarks not confined to nuggets form into baryons. Baryon-antibaryon pairs are too heavy to be formed in thermal collisions, and annihilations begin to rapidly decrease their density. At this time the baryons remain energetic enough that they are able to penetrate into the still forming nuggets. As the baryons cool, and the nuggets settle into an ordered high density phase, the probability that a baryon will be reflected from a nugget grows. Once the baryon temperature falls below the superconducting gap of the quark matter the probability that a baryon or antibaryon can penetrate the nugget becomes very small, and the nuggets effectively freeze out. At this time the baryon number is falling rapidly, $n_B \approx n_{\bar{B}} \sim exp(-m_N/T)$, where m_n is the nucleon mass and T is the temperature of the plasma. If the matter decouples from the nuggets at a temperature T_f, then the scale of baryogenesis will be the same as the baryon density at this temperature. In this case the baryon to photon ratio is given by

$$\eta \sim \left(\frac{m_N}{T_f}\right)^{3/2} e^{-m_N/T_f}. \tag{1.10}$$

As it is exponentially dependent on temperature, this fraction can vary by several orders of magnitude across the possible physical values of T_f. While this means that the value of η cannot be predicted with any precision in this model, one can work backwards from the observed value and make a consistency check on the model. The value of η, as given in equation 1.1, implies a nugget freeze out temperature of $T_f \approx 40$MeV [95]. This value is fully consistent with the structure of quark matter as presently understood. The quark matter, and the domain wall which binds it, exist at the QCD scale set by the temperature at which chiral symmetry breaking and quark confinement occur. This transition happens at $T \sim 100$MeV, and nugget formation must occur entirely below this energy scale. Once the nuggets have started to form the next relevant energy scale is the binding gap of the colour superconducting phase. The exact value of the gap is not well established, and depends on the form of quark matter realized in the nuggets. Across a wide range of possible quark matter phases the binding gap is found to be in the few tens of MeV range [16, 17, 102]. Below this scale the transmission coefficient at the quark matter surface falls rapidly, so this should represent a lower limit on the possible freeze out temperature for the nuggets. It should also be noted that the absolute lower limit on the freeze out temperature is set by the point where baryon-antibaryon annihilation would cease due to the universe's expansion, even if no form of baryogenesis had occured. This will happen when the baryon collision rate falls below the Hubble time, which coincides with a temperature of $T \sim 22$MeV and would result in a baryon to photon ratio ten orders of magnitude lower than observed. The limits set by the phase transition and the freeze out of nuclear annihilations between, 100MeV$< T <$20MeV naturally cover the energy scale of nuclear physics, and the formation temperature of the quark nuggets should be expected to fall in this range. It should also be noticed that, as the nuggets effectively decouple from the remaining nucleons at an energy in the tens of MeV range, they have no impact on big bang nucleosynthesis which occurs at energies an order of magnitude lower.

While this discussion of nugget formation remains qualitative because of the inherent complexity of any quantitative details and the accompanying uncertainties, I will take the basic properties of the nuggets and the order of magnitude estimates made here as indicative of the range of possible physical properties for the nuggets and as an argument that they may represent a viable dark matter candidate. These preliminary arguments will allow for the formulation of some basic properties of the nuggets, and allow estimations of their phenomenological consequences for present and future observations.

Chapter 2

Nugget Structure

The structure of a quark nugget may be divided into two basic components; the central quark matter, composed of light standard model quarks; and the surrounding electromagnetically bound leptons. This surface layer, known as the electrosphere, consists of electrons in the case of a quark nugget and positrons in the case of an antiquark nugget. These two structures, and their relevant properties, will be discussed below. Much of this discussion is influenced by previous work, my own participation was primarily to the detailed calculations related to the structure of the electrosphere as discussed in section 2.2.

For reference a schematic picture of the nuggets' structure, and the way that it maps onto various sources of electromagnetic emission discussed below, is given in figure 2.1.

2.1 Quark matter

The nuggets of this model are composed of quark matter of densities within a few orders of magnitude of nuclear density, $\rho_{QM} \sim 1-100$ MeV fm^{-3}. This density range is not sufficiently large that asymptotic freedom[11] may be exploited to study the ground state structure, which must instead be studied using more complicated non-perturbative means. A full determination of the structure of the QCD phase diagram remains an outstanding problem, and the exact form of quark matter realized in the nuggets must, therefore, remain uncertain for the present. Fortunately, the surrounding electrosphere (to be discussed in the following section) prevents direct observation of the quark matter surface in all relevant contexts. For this reason, the internal structure of the nugget is mostly important for establishing the lower boundary conditions of the electrosphere (such as surface density, electric field strength and the total radius of the nugget) and for estimating the scale

[11] The asymptotic freedom of QCD implies that, while strongly coupled at low energies, the high energy limit of the theory is weakly interacting and may be treated using perturbation theory [53, 99]. For a limited review of this phenomenon see appendix B.

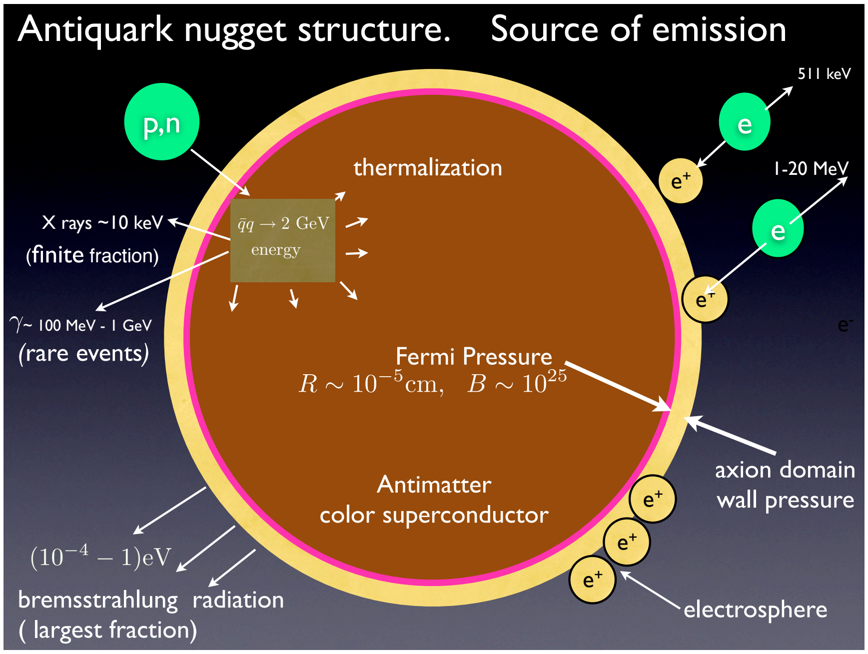

Figure 2.1: Schematic picture of the structure of a quark nugget showing the sources of various emission processes to be discussed in chapters 3 and 5. Figure adapted from [82].

at which nuclear annihilations, occurring within the quark matter, transfer energy to the electrosphere from which it is emitted in a modified form.

Many of the details considered here were originally discussed in the context of strangelets and strange stars or quark stars [15, 67, 84]. These are hypothetical objects similar to neutron stars composed, either wholly or partially, of quark matter rather than nuclear matter. Stars of this form are possible if, at sufficiently large densities, quark matter is energetically favourable to nuclear matter. The quark matter of which these objects would be composed is essentially identical to that which is found in the quark nuggets considered here and, as such, many of the results may be carried over.

The form of quark matter most likely to be realized in the nuggets, is a colour superconductor. As in the case of a conventional superconductor, this state occurs when a weak attraction between charge carriers near the Fermi surface causes the elementary charges to form pairs. In such a state the fundamental modes are no longer individual charges but these bound Cooper pairs[12]. In a sense, the pairing mechanism involved in a colour superconductor is easier to understand than that in a conventional superconductor. Within the context of QCD there are several attractive quark-quark interactions (the most obvious being the mechanism by which quarks are bound in colourless mesons and baryons) and these naturally become weak at large momenta. The paired quarks are now bosonic, and form a condensate which is the quantum ground state of the superconductor. As individual quark pairs cannot form colour singlets, this ground state breaks local colour SU(3) symmetry. At asymptotically large densities, the Fermi surface quarks are sufficiently energetic that they interact in the weak coupling limit of asymptotic freedom, and the problem may be treated perturbatively. In the case where Fermi surface quarks are in the asymptotically free limit, and the difference in mass between the u,d and s quarks is negligible, it is found that the ground state is a colour-flavour locked (CFL) superconductor [16]. In this state, the pairing mechanism connects the colour and flavour indices of the quarks forming Cooper pairs. All fermionic excitations and all eight gluons are gapped at the 10-100MeV scale and, because the quarks carry electric charge, the photon also picks up a gap at this scale.

Moving to lower densities the momentum carried by quarks at the Fermi surface drops, and the effects of the larger s quark mass begin to become relevant. At these densities the CFL phase is stressed by the increased energetic cost of adding an s quark, rather than a u or d, in a particular momentum state. This stress favours a depletion of strange quarks and gives a net electric charge to the quark matter. Lowering the density also causes the coupling between quarks to run towards its vacuum value in the strong coupling regime. As the interaction strength grows, ever higher order interactions must be considered until any suitable description becomes fully non-perturbative. This makes it impossible to predict exactly how the phase structure of quark matter extrapolates between the asymptotically dense CFL phase and the low density nuclear phase.

For the purposes of the present work, which is to take a mainly phenomenological standpoint, the exact nature of the quark matter realized in the core of the nugget is not a primary concern. It will simply be noted here that, in order for this proposal to explain the presence of dark matter it is

[12]At large densities fermions can only be scattered to states which are not already occupied. As such, the low energy interactions of a given system involve those states near the Fermi surface which can be scattered to an unoccupied higher momentum space state with only a small additional energy.

necessary that the nuggets must be stable on timescales longer than the age of the universe. At present there are several proposed quark matter phases which may meet this condition.

One final component of the quark nugget which is unique to this model is the axion domain wall, mentioned in section 1.3, and appendix B and analyzed in detail in [41]. This structure is important in the initial formation of the quark nuggets, introducing the macroscopic length scale necessary in this process, and may be important in maintaining their absolute stability on cosmic timescales. A more detailed description of the axion domain wall and its properties and evolution is given in appendix B.

Having established some basic properties of the core of the quark nuggets, I now turn to the surface layer of leptons, which will be more important in extracting observable properties of the nuggets.

2.2 The electrosphere

Independent of the form of quark matter realized in the core of the quark nugget, the decreasing pressure near the quark surface will necessarily result in the accumulation of a net electric charge at the quark surface, positive in the case of quark matter and negative in the case of antiquark matter. This is evident in the case where the nugget is composed of nuclear matter but, even if the core of the nugget is in a charge neutral phase (for example the CFL phase) the falling chemical potential near the quark surface results in a depletion of s quarks relative to the much lighter u and d quarks. This will, as in the purely nuclear case, result in a net electric charge.

The structure of this outer layer of leptons has been considered previously in the context of strangelets and quark stars [15, 67]. As the electric fields established by the quark matter in these situations will be similar to those at the surface of a quark nugget many of these earlier results also apply in the model considered here. However, these earlier studies were generally limited to treating the leptons as massless and considering plane parallel geometries. As will be seen below, the low energy emission from the nuggets originates primarily from the lower density outer regions of the electrosphere where the lepton density scales as $n_e \sim (m_e T)^{3/2}$. A detailed treatment of these emission mechanisms will therefore require a full description of the electrosphere's structure accounting for the mass of the electron and for thermal effects. To this end the remainder of this section will establish the density profile of the electrosphere from the quark matter surface out to the low density limit far from the nugget. In this outer limit the full spherical geometry of the nuggets will also need to be taken into account.

The strong electric potential near a quark matter surface will support a surrounding distribution of leptons, much as typical nuclei are surrounded by a distribution of electrons. To model the electrosphere structure we begin with the Poisson equation, which relates the electrostatic potential to the charge distribution:

$$\nabla^2\phi(\vec{r}) = -4\pi e n(\vec{r}). \tag{2.1}$$

Here ϕ is the electric potential and n is the number density of charges in the electrosphere. This may be re-expressed in terms of the lepton chemical potential $\mu(\vec{r}) = -e\phi(\vec{r})$. In the two examples to be considered below, I will discuss regions of the electrosphere close enough to the quark nugget that the spherical geometry of the nugget may be neglected and the density will vary only with the height (z) above the quark surface. Under this simplification I may reformulate the Poisson equation, in terms of chemical potential and density, as

$$\frac{d^2}{dz^2}\mu(z) = 4\pi e^2 n_e(z). \tag{2.2}$$

Outside the quark matter the only relevant charges are electrons and positrons and their number density is determined by the local chemical potential:

$$n(\mu) = 2\int \frac{d^3\vec{p}}{(2\pi)^3}\left[\frac{1}{1+e^{(E-\mu)/T}} - \frac{1}{1+e^{(E+\mu)/T}}\right]. \tag{2.3}$$

Here $E = \sqrt{p^2 + m_e^2}$ is the particle energy. The first term in the integrand of equation 2.3 represents the contribution from electrons while the second is due to positrons. In [40] the equations 2.1 and 2.3 were self consistently solved in the spherically symmetric case to obtain a solution to the lepton density valid across all radial distances and dependent only on the chemical potential at the surface of the nugget. The results of this computation are shown in figure 2.2. The details of the extrapolation between the lower density outer layers and the ultrarelativistic regime near the nugget surface will allow for the relative strength of the 511keV line and the MeV continuum to be exactly computed in the following chapter.

Rather than an in depth discussion of the details of figure 2.2 and the calculations behind it, I will simply demonstrate the basics of the calculation in two limiting cases for which analytic results may be obtained. In what follows these results are sufficient to discuss the 511keV and MeV band emission profiles separately, while the full numerical treatment is necessary for an analysis of their relative scales.

2.2.1 The Boltzmann limit

First consider the low density regime far from the quark matter surface. In this regime, which will be denoted as the "Boltzmann" regime, the electric field strength is screened by the high density inner regions of the electrosphere and thermal effects come to dominate the lepton distribution. In this limit we can take the number density in equation 2.3 to be,

$$n(\mu) \approx 2 \int \frac{d^3\vec{p}}{(2\pi)^3} e^{(\mu - m_e - p^2/2m)/T} \approx \sqrt{2} \left(\frac{m_e T}{\pi} \right)^{3/2} e^{(\mu - m_e)/T} \tag{2.4}$$

Here m_e is the mass of the electron. The Boltzmann regime may extend over a substantial fraction of the electrosphere as seen in figure 2.2. To further simplify matters I will assume that we may neglect the curvature of the quark matter surface so that the density is dependent only on the height above the quark surface and we may use the plane parallel form of the Poisson equation. In terms of the number density this gives the expression,

$$\frac{1}{n}\frac{d^2 n}{dz^2} - \frac{1}{n^2}\left(\frac{dn}{dz}\right)^2 = \frac{4\pi\alpha}{T} n \tag{2.5}$$

which is solved by

$$n_B(z) = \frac{T}{2\pi\alpha} \frac{1}{(z + z_0)^2}. \tag{2.6}$$

Here z_0 is the height within the electrosphere at which these approximations become valid and above which the fall off in density is fixed by this expression. This regime will persist so long as the height $(z + z_0)$ remains small with respect to the radial size of the quark nugget. Once the height becomes comparable to the nugget size the spherical terms in the Poisson equation become relevant and the fall off in the number density becomes exponential with distance from the nugget.

2.2.2 The ultrarelativistic limit

Near the quark matter surface the chemical potential is in the 10-100MeV range, the average positron energy is also be near this scale and the rest energy in expression 2.3 may safely be neglected. Under astrophysical conditions the electrosphere temperature will also be well below the chemical potential so that the full density expression given in equation 2.3 reduces to,

$$n_e[\mu] \approx 2 \int_0^{\mu} \frac{d^3\vec{p}}{(2\pi)^3} \approx \frac{\mu^3}{3\pi^2}. \tag{2.7}$$

The extent of the ultrarelativistic regime is considerably smaller than the physical size of the quark nugget itself so that we may also simplify the Poisson equation to the plane parallel limit as in the case of the Boltzmann regime. In this limit the number density falls as,

$$n_{UR} \approx \frac{\mu_0^3}{3\pi(1+z/z_0)^3}, \quad z_0 \equiv \sqrt{\frac{3\pi}{2\alpha}}\frac{1}{\mu_0}. \tag{2.8}$$

This density expression may also be formulated in terms of the chemical potential,

$$\mu_{UR} = \sqrt{\frac{3\pi}{2\alpha}}\frac{1}{z+z_0} \tag{2.9}$$

which may in turn be converted to an electric field strength near the quark surface,

$$E(z) = -\frac{1}{e}\frac{d\mu}{dz} = \sqrt{\frac{2}{3\pi}}\frac{\mu_0^2}{(1+z/z_0)}. \tag{2.10}$$

Note that for typical values of μ_0 this implies that the surface electric fields carry nuclear scale energy densities, a fact that will become important in a discussion of positrons ejected from the quark surface that will come in section 3.3.

The number densities given in equations 2.6 and 2.8 may be used to establish the production rates of various types of emission from the nugget as discussed in the main body of this work as well as the thermal properties of the nuggets discussed in the following appendix C.

2.3 Charge equilibrium

As discussed in section 2.2.1 the distribution of leptons, far from the quark matter surface, is influenced by the temperature of the nugget. As the outermost leptons are only weakly bound this temperature also influences the total ionization levels of the nuggets. As the temperature increases positrons further evaporate from the electrosphere. In the case of matter nuggets the nugget will fall into a static equilibrium with the surrounding galactic matter. The temperature will be determined by the rate of energy absorption through collisions with surrounding matter and photons which is balanced by the rate of thermal emission. The temperature will be low as will the net ionization of the nuggets.

In the case of nuggets of antimatter the situation is more complicated. The annihilation of galactic matter within the quark nuggets will increase the temperature of the nuggets (thus affecting the ionization levels) while any difference in the flux of galactic ions and electrons onto the nugget may also change the overall charge dynamics. This net charge, in turn, is important in determining the rate at which charged particles annihilate with the nugget.

As the positron density increases gradually across the electrosphere, a galactic electron incident on an antiquark nugget annihilates with a probability very near one. Conversely, the quark matter surface is very sharp, resulting in a relatively large probability of galactic ions being reflected. The preferential annihilation of positrons will begin to generate a negative charge on the nuggets. This charge will increase until the electric field of the nugget is sufficient to prevent the escape of charged ion with a velocity typical of the interstellar medium. Once this field strength is reached the ion will become bound to the nugget and may reflect off the surface as many times as is necessary for annihilation to occur.

This situation is complicated by the possibility of charge exchange interactions between the nugget and the incident ion. If such a charge exchange process occurs it may neutralize the ion, for example converting a proton to a neutron. In this case the incident particle may escape without annihilating. The ratio of charge exchange interactions to annihilation interactions will set the relative rate at which electrons and baryons annihilate with the nugget. As the interstellar medium is primarily composed of hydrogen, this ratio would be very near one in the absence of charge exchange processes. However, the possibility of charge deposition without annihilation means that this ratio may be less than one. This process will be discussed further when we estimate the relative strengths of various forms of emission from the nugget is section 4.2.

With the physical properties of the electrosphere established from conventional physical properties we are now in a position to discuss the observational consequences of this dark matter model. These observational consequences will primarily arise through the annihilation of galactic matter within an antiquark nugget.

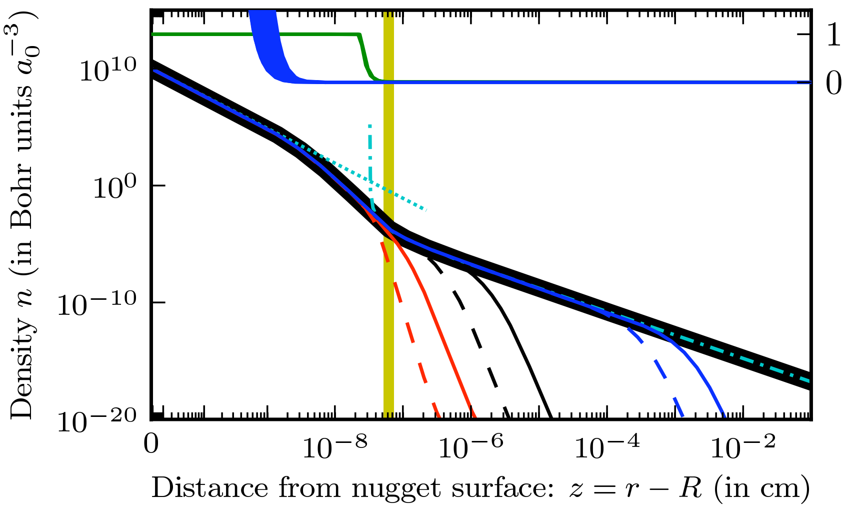

Figure 2.2: Radial density profile of the electrosphere of a quark nugget. The positron density in Bohr units are shown for nuggets with baryon number 10^{20} (red), 10^{24} (black) and 10^{33} (blue). The solid curves assume a nuclear density core while the dashed curves assume a density 100 times larger than nuclear. The thick black band is the density profile neglecting nugget curvature. The cyan curves show the relativistic (dotted) and Boltzmann (dot-dash) approximations discussed in the text. The yellow band indicates the region from which the microwave emission discussed in section 3.2 originates. The upper two curves give the annihilation rate of incident electrons relative to the maximum positronium formation rate. These rates are used to establish the relative emission strengths as discussed in chapter 4. Figure taken from [40].

Chapter 3

Motivation from Galactic Observations

3.1 Introduction

In the search for dark matter, indirect detection techniques rely on astrophysical observations to reveal the presence of dark matter through its potential non-gravitational interactions. Thus far, no such detection has yielded an unambiguous dark matter signal. There have, however, been several suggestive observations warranting further consideration. This chapter will highlight several galactic observations, spanning many orders of magnitude in energy, which have been suggested as possibly containing signatures of the dark matter. Based on these observations it will be argued that the contribution to the galactic spectrum of quark nugget dark matter, in the mass range considered here, is fully consistent with present observations and may offer a source for several observed emission features. The underlying uncertainty in the diffuse galactic backgrounds means that none of these observations may be attributed to the dark matter with any certainty. However, the observations discussed below are generally taken as being indicative of the presence of emission sources which have not, at present, been directly identified. These sources may, with further investigation, prove to be conventional astrophysical populations but, at present, they have attracted interest as possible indications of non-gravitational dark matter interactions. If the dark matter does consist of nuggets of quark matter then they could provide emission much like that observed. If, however, the apparent excess emission is found to be attributed to conventional astrophysical sources then these observations will serve to impose strong constraints on the existence of quark nuggets.

The material of this chapter serves primarily as background and motivation for the material to follow, and is primarily based on work done by myself and others predating my thesis research. It is presented here strictly for completeness, readers interested in further details should consult the cited original works.

The scale of the possible observational consequences of quark nuggets is strongly suppressed by their small cross section to mass ratio. However, there is nothing fundamentally weak about the interactions of these objects with the surrounding visible matter. As they are entirely governed by well known QED and nuclear physics, it is possible to calculate the emission spectrum expected when a quark nugget or antinugget interacts with visible matter in a particular environment. Once this emission spectrum is established, we are in a position to observationally constrain the allowed range of nugget mass scales. This is done by comparing the predicted spectrum to observations of regions where both the visible and dark matter densities are high. Following the standard terminology I will refer to this process for constraining dark matter properties as indirect detection, that is, techniques in which the astrophysical consequences of a dark matter candidate are searched for, generally in the form of an additional component in diffuse emission.

In this analysis, I will emphasize diffuse emission sources which may arise from either self interaction of the dark matter or from the interaction of the dark matter with the visible matter of the interstellar medium. In the case of self interacting dark matter (for example the annihilation of a dark matter particle with its antimatter partner) the interaction rate is scaled by the line of sight integral

$$\int dr\ n_{DM}^2\ v\ \sigma_{DM-DM} \tag{3.1}$$

in which the integral runs over the thickness of the dark matter distribution, v is the relative velocity, n_{DM} is the dark matter density and σ_{DM-DM} is the dark matter self interaction cross section. Alternatively, for interactions between dark and visible matter we have to include both the dark matter and visible matter distributions,

$$\int dr\ n_{DM}\ v\ \sigma_{DM-vis} n_{vis} \tag{3.2}$$

with the integral again running across the thickness of the interaction region. In this case the relevant cross section is that for interactions between visible and dark matter. For most dark matter models, the contribution from dark matter self interaction and interaction with visible matter can be of similar magnitude unless the interaction strengths are tuned to suppress one or the other. However, in the case of quark nugget dark matter the self interaction rate is suppressed, with respect to interactions with visible matter, by the extra factor of the nugget baryonic charge appearing in the dark matter number density. As such, the following section will focus on determining the spectrum generated by matter striking a quark nugget, rather than the interaction between nuggets[13].

The dark matter number density, as it appears in equation 3.2, is not known directly. The mass density of the dark matter is inferred from the kinematics of the visible matter and from simulations of large scale structure formation. It is generally assumed that the dark matter has a spherically symmetric distribution rather than tracing the disk and bulge structures observed in the the visible matter. The mass distribution is frequently taken to have a Navarro-Frenk-White type profile [94] with the density scaling as,

$$\rho_{DM}(r) \sim \frac{1}{r(1+r/r_s)^2} \tag{3.3}$$

where r_s is a characteristic scale length of a given dark matter profile. This profile give a good description of the dark matter distribution on large scales, but seems to predict a stronger than expected cusp in the galactic centre. Within numerical simulations the central divergence is regulated by the resolution of the simulation, however the discrepancy with observation seems to extend to scales beyond this resolution limit. Weak lensing measurements strongly favour a central, constant density, core to the dark matter distribution. This distribution is expected independent of the actual form taken by the dark matter. While they do carry a baryonic charge the nuggets will not behave like conventional baryonic matter. Their small cross section to mass ratio prevents any significant level of clumping as discussed in section 1.2. This uncertainty in the structure of the dark matter should be kept in mind for the following discussion, as it directly affects the scale and morphology of any dark matter contribution to the direct spectrum.

As the observational consequences highlighted below are strongly associated with the galactic centre, within the presumed core of the dark matter distribution, and as the emission traces both visible and dark matter (as in equation 3.2) they will be strongly correlated with the visible matter distribution with a slightly stronger spherical morphology favoured by the contribution from the dark matter distribution.

In addition to the underlying uncertainty in the dark matter distribution the total scale of any quark nugget contribution to the spectrum will depend

[13]This is further justified by the fact that the nuggets exist as complex many body objects, represented by macroscopically large multiparticle wave functions. In any given collision there is unlikely to be a large wave function overlap and thus the most likely outcome is simply elastic scattering.

on the average baryon number of the nuggets. Once the dark matter mass distribution, $\rho(r)$, has been estimated in a particular region the quark nugget number density (which is the factor actually appearing in the line of sight integral of expression 3.2) is given by,

$$n_N(r) = \frac{\rho(r)}{M_N}, \quad M_N = m_B B, \tag{3.4}$$

where M_N is the nugget mass and m_B is the mean mass per baryon within the nuggets. The estimates to be made below are generally confined to the galactic centre. In this region it will be assumed that the dark matter forms a relatively constant density, spherically symmetric, core with a mean mass density comparable to that of the visible matter.

Detailed estimations of the consequences of this model for the galactic spectrum have been worked out in a series of previous papers [96], [128], [80], [42], [40], [43] and [74]. In each of these works a particular source of diffuse galactic emission, centred on the galactic centre, was considered and found to be consistent with emission generated by a galactic population of quark nugget dark matter, provided that the nuggets carry a baryonic charge greater than $\sim 10^{23}$. It is not the purpose of the present work to fully repeat these estimates, but rather to reproduce only the basic arguments necessary to motivate the further analysis which follows. For this discussion I will begin with the lowest frequency contributions to the galactic spectrum and move from there to the highest. Several independent observations of apparent excesses in diffuse emission are relevant here:

1. WMAP has observed a possible excess in microwave radiation associated with the galactic centre [36]. This so called "WMAP haze" seems to require an additional diffuse microwave source or a harder than predicted galactic synchrotron spectrum.

2. The Chandra X-ray Observatory has measured diffuse keV emission from the galactic centre [93]. This emission has been modeled as originating from a hot diffuse plasma, but the temperature of such a plasma would exceed the energy thought to be available.

3. SPI/INTEGRAL show a strong 511 keV line associated with the galactic centre [60, 70]. This line indicates the rate of low momentum electron-positron annihilations is higher than had been previously estimated and more strongly spherical than anticipated based on known positron sources and propagation models.

4. COMPTEL detects diffuse emission across the 1-20 MeV range that exceeds the previous estimates based on cosmic ray interactions and the decay of radionuclides [112].

Each of the following four sections will describe the features of a particular band of observed diffuse emission. These features are then mapped onto the properties of the nuggets discussed above. The resulting spectra, and their relative strengths, are uniquely predicted within the model with the only free parameter being the size of the nuggets. The spectral properties of the emission are largely independent of this parameter which is responsible only for the overall normalization of the emission spectrum[14]. As such the limits on any possible excess in each of the four emission bands discussed above may be translated into constraints on the minimum size of the nuggets.

3.2 Thermal emission : the WMAP "haze"

The Wilkinson Microwave Anisotropy Probe (WMAP) has produced full sky temperature maps across the microwave band [30]. Of particular importance to this work are observations made by WMAP of the galactic plane in the tens of GHz range[15][49]. These observations show an excess of diffuse emission across the galactic centre above what would be expected from extrapolating the synchrotron emission measured at lower energies [36]. This apparent excess has been dubbed the "WMAP haze." Subsequent observations by the Planck satellite, across a similar frequency band, have supported the existence of this diffuse hard spectral component. Analysis of the Planck data has found that the haze follows an approximate power law spectrum with a spectral index of $\beta_h = -2.55 \pm 0.05$, such that $T \propto \nu^{\beta_h}$[9]. This is a significantly harder spectrum than was expected for galactic synchrotron emission based on extrapolation from earlier measurements at 408MHz [54] which predict an index of $\beta_s = -3.1$ from all synchrotron sources in this energy range [16]. This implies the existence of a non-thermal component to the galactic spectrum with a spectral index considerably higher ($\beta_h - \beta_s \approx 0.5$) than is observed from typical galactic synchrotron emission. The strength

[14] As the total baryon number of the nuggets may range over several orders of magnitude we are not able to directly estimate the scale of emission in any particular band. However, it is possible to calculate the relative scales of the different bands, this will be demonstrated in chapter 4.

[15] The CMB measurements, which were the primary purpose of WMAP, will be important in a radically different context to be discussed in chapter 5.

[16] The relative strength and distinct spectral index may clearly be seen in figure 7 of the Planck Collaboration's investigation of the haze [9]

of this feature, its spectral index, and possibly its very existence are, however, highly dependent on the galactic model used. The galactic spectrum also contains contributions from other diffuse interstellar medium components, such as dust and the free-free emission of hot plasma, in addition to the galactic synchrotron emission, and the degree to which these may contribute to the haze remains an open question. Several physical mechanisms which may be responsible for producing the haze have been proposed. It was originally modeled as either a hard synchrotron component [29] or free-free emission from a hot ($10^4 K < T < 10^6 K$) gas [36]. However, the first of these explanations requires a much harder synchrotron component than is observed at lower energies, while the second should necessarily produce an associated Hα line which is not observed. The haze has also been interpreted as evidence for dark matter annihilations [58], a larger than expected pulsar contribution [63, 66] or the result of a modified dust spectrum [18]. It has also been argued that the galactic synchrotron emission may evolve with energy, more than is allowed by a power-law extrapolation from lower energy measurements, and that the uncertainty inherent in this extrapolation is on the same level as the observed haze [89]. However, at this time, none of these explanations is strongly preferred over the others, and the nature of the haze remains an open research question. I will argue that, if the dark matter is in the form of quark nuggets, it will necessarily produce microwave emission which could produce all, or a significant fraction, of this apparent haze effect. Before discussing the means by which this emission arises in the quark nugget model I will offer a brief review of the association of the haze with potential dark matter sources. This discussion is, of course, contingent on the uncertainties listed above and is necessarily somewhat speculative.

It has been argued that the haze has a roughly spherical morphology with an approximate $1/r$ fall off in intensity with distance from the galactic centre [58]. The haze may also be described as a hard synchrotron component on top of the expected, relatively soft, galactic synchrotron emission. This combination of morphology and spectrum lead to speculation that the haze could be produced by a distinct population of electron-positron pairs, injected into the galactic centre at high energies by the annihilation or decay of galactic dark matter [37]. In this model the spectral index of the haze is determined by the decay or annihilation spectrum of the dark matter particles, which may be chosen to match the spectrum of the haze. This interpretation is challenged by the apparent lack of polarization in the haze signal, as would be expected from synchrotron radiation [49]. However, any polarization of the signal could be masked if the galactic magnetic fields generating the synchrotron radiation heavily tangled [114]. It has also been argued that the electron injection spectra expected from standard dark matter candidates will generate significant emission at higher energies that should also be detectable. Dark matter which undergoes hadronic decays will produce a γ-ray signal through subsequent pion decays, such a signal would very closely trace the dark matter distribution. The same is true for decays or annihilations which directly produce photon pairs. Even if the dark matter decays or annihilates exclusively to electrons and positrons these will be injected into the interstellar medium at high energies ($E > 1$GeV) and will inverse Compton scatter off interstellar photons. This higher energy spectrum should be present along with the microwave range synchrotron emission at a magnitude which should be visible to the Fermi Large Area Telescope, but which is not observed[17][7]. It has also been argued that the production of high energy electron-positron pairs in dark matter decays or annihilations could explain the growth in the cosmic ray positron fraction with energy, as observed by the PAMELA satellite [10] and the Alpha Magnetic Spectrometer (AMS) experiment on board the International Space Station [98]. While possible, there seems to be some tension between the dark matter interaction cross section required by the different experimental results [7].

With this background in place I will now illustrate how a diffuse microwave component of the galactic spectrum is required within the dark matter model under consideration. Much of this discussion will rely on the thermodynamic properties of the nuggets as discussed in appendix C. The annihilation of visible matter within an antiquark nugget causes its temperature to increase. This thermal energy must then be radiated from the layer of the nugget where the electrosphere becomes transparent to low energy photons. The temperature of the nuggets in a given environment is thus determined by the flux of visible matter onto the nugget, and the fraction of the energy released in the subsequent annihilations which is thermalized within the quark matter. This fraction, which is important in determining the temperature of the nuggets and in estimating the relative strength of thermal and non-thermal components of their emission spectrum, will be called f_T in the following discussions. While the fraction of annihilation energy thermalized is determined purely by the physical properties of the nuggets, the flux of matter is set by the visible matter distribution through

[17]It has been argued that the Fermi constraints may be avoided if the large galactic latitude component of the diffuse γ-ray sources know as the "Fermi Bubbles" [114] is generated by the required inverse Compton scatterings [58]. However, this argument is disfavored by the morphology of the bubbles [114].

which the nugget moves[18]. The nugget temperature will be largest in environments where the visible matter density is relatively high, and where the average velocity is large.

If the nuggets are in thermodynamical equilibrium with the surrounding matter, then the total thermal emission, as given by equation C.5, must be balanced by the rate at which annihilations deposit energy within the nugget. This will result in a temperature as given by expression C.7. In the galactic centre, where the matter density is estimated as $\rho_{vis} \approx 300\text{GeV}/\text{cm}^3$ and the velocity as $v \approx 10^{-3}c$, the antiquark nuggets[19] carry a temperature of $T \sim 1\text{eV}$.

The thermal spectrum of the nuggets, as given in equation C.4, runs up to energies near or slightly above the temperature of the nugget (the eV band in the case considered here) but at lower energies, displays only a weak, logarithmic, dependence on emission frequency. By contrast, a typical blackbody spectrum falls off as the second power of frequency below the thermal peak. For this reason, thermal radiation emitted by the nuggets is distributed over a much wider range of frequencies below the eV scale. Radiation emitted in the eV band will easily be lost in the background of radiation from visible matter which is many orders of magnitude brighter in this range. But, at much lower energies, the relatively slow fall off in emission from the nuggets means that their contribution to the diffuse background may become competitive with that of the visible matter[20].

In [43] the thermal emission of the nuggets was applied to the distribution of dark matter across the galactic centre. At that time the more detailed observational data from Planck was not yet available and only the basic scale of the haze emission was known:

$$\frac{dE}{dt\ dA\ d\omega\ d\Omega} \approx (3-6)\times 10^{-20}\frac{\text{erg}}{\text{s cm}^2\text{ Hz sr}}. \tag{3.5}$$

In the case where we assume that quark nuggets near the galactic centre carry an average temperature of 1eV it is possible to estimate the total nugget contribution to the haze[21]. This is done by integrating the individual

[18] The rate of annihilations is also partially dependent on the charge of the nuggets, as noted in section 2.3.

[19] Nuggets composed of quarks rather than antiquarks do not annihilate incident matter and have a much lower radiating temperature, thus they do not make a significant contribution to the total diffuse thermal emission.

[20] A similar argument will be made in chapter 5 where the same considerations are applied in a very different context.

[21] A calculation in which the nugget temperature is allowed to vary with the properties of the surrounding visible matter is also possible, however the resulting temperature variation is relatively small and such a calculation adds more complexity than is currently warented.

nugget contributions along a given line of sight,

$$\frac{dE}{dt\ dA\ d\omega\ d\Omega} \approx \int \frac{dr}{4\pi} n_{\bar{N}} \frac{dE}{dt\ d\omega}, \tag{3.6}$$

where $n_{\bar{N}}$ is the number density of antiquark nuggets, and the integral sums the spectral contribution from each nugget (as given by equation C.4) along the line of sight through the galactic centre. Uncertainty in the distribution of nuggets makes this integral impossible to evaluate exactly. However, if we assume an approximately uniform dark matter distribution across the galactic centre and that emission is dominated by the inner few kpc of the galaxy we arrive at the approximation,

$$\frac{dE}{dt\ dA\ d\omega\ d\Omega} \sim \left(\frac{10^4}{B}\right) \frac{\text{erg}}{\text{s cm}^2\ \text{Hz sr}}. \tag{3.7}$$

Comparing this estimation with the observed intensity suggests that the haze emission could be entirely produced by a population of quark nuggets with a mean baryonic charge of $B \sim 10^{24}$. While this crude estimation is subject to large uncertainties the suggested baryonic charge falls within the allowed parameter space. This implies that the nuggets are at least capable of providing some or all of the required haze. In chapter 4 a scaling argument will be made that the intensity of the haze is also fully consistent with its coproduction with the other diffuse emission mechanisms discussed below.

The spectral index of the haze as measured by Planck was not available at the time of the publication of [43]. As such, that work simply pointed out that the spectrum of the haze component would be relatively hard. However, a simple estimate of of the index may be made from basic physical considerations. When one attempts to determine a background temperature by fitting a non-thermal spectrum to a blackbody radiation curve it leads to an frequency dependent temperature. In the case of a constant intensity across a range of wavelengths one has,

$$\frac{8\pi h\nu^3}{c^2} \frac{1}{e^{h\nu/T} - 1} = \Phi_0. \tag{3.8}$$

In the case where $h\nu < T$ it is easy to see that the temperature must scale as $T \sim \omega^{-2}$. Similarly, a spectrum that is inversely proportional to frequency will have a temperature scaling $T \sim \omega^{-3}$. The emission spectrum of the nuggets has a logarithmic decrease in intensity with wave length (as seen in equation A.6) and must fall between these two cases. As such, one expects a spectral index of,

$$-2 > \beta_N > -3. \tag{3.9}$$

Which is the range in which the spectral index of the haze falls. The spectral index of the low energy emission from the nuggets will be discussed in more detail in chapter 5, where the same considerations are applied in a very different physical scenario.

With further study of the spectrum and distribution of the haze, observations may come to favor any of the other proposed sources for this diffuse emission. For example, if the haze is found to be more strongly polarized than is presently believed thermal emission from the quark nuggets would be strongly disfavored. However, it is important to point out that the emission strength from the nuggets could easily have been much larger than observed if either the matter distribution, or the thermal emission spectrum from the nuggets had been dramatically different than their estimated values. There is no way to avoid the basic physics which goes into the flux approximated in [43], making it difficult to avoid these constraints. It is thus non-trivial that this model, which was proposed to explain very different phenomena, not only avoids the constraints imposed by WMAP and Planck, but may offer an explanation for an observed spectral feature.

3.3 Surface proton annihilations : the Chandra x-ray background

Imaging of the galactic centre by the Chandra X-ray Observatory has shown evidence of diffuse emission in the x-ray band, even following the subtraction of the contribution of known point sources [93]. This radiation has been fit by assuming the presence of a two component thermal plasma, with the cooler component having a temperature $T_{cool} \approx 0.8$keV and the hot component an order of magnitude warmer with $T_{hot} \approx 8$keV. The analysis leading to this model was performed by a best fit to specific regions of the galactic centre and, consequently, provides little information on the spatial distribution of these two components apart from their general association with the galactic centre. The cool component is consistent with being produced by supernova occurring in this region. An energy budget analysis suggests that the supernova rate is sufficient to provide the required energy input, and observations have confirmed that supernova do, in fact, heat the interstellar medium up to the 1keV scale [93]. The spatial distribution of the cool plasma is also relatively patchy, consistent with supernova heating. The hot component is, however, more difficult to understand. Its temperature is greater than the gas typically observed surrounding supernova or clusters of young stars, making its origin uncertain. While its morphology is not well constrained the emission from the hot component appears to be more homogeneous than the cool component with an observed surface brightness of

$$\Phi_{hot} = (1.5 - 2.6) \times 10^{13} \frac{\text{erg}}{\text{cm}^2 \text{ s arcmin}^2}. \tag{3.10}$$

The higher temperature also implies that the plasma should expand outward and cool more rapidly than the low temperature plasma. Consequently, the power required to sustain the hot plasma is several orders of magnitude larger than that required by the cool component. This power requirement seems beyond the level provided by mechanisms, such as supernova and stellar winds, known to heat the interstellar medium.

It has been suggested that some of the problems of gas expansion may be solved if the hot plasma has a higher than expected helium content as the heavier helium ions would be more strongly gravitationally bound to the galaxy than hydrogen [27]. This scenario could be realized by the preferential evaporation of the hydrogen component. This would lower the overall power requirements of the plasma, but does not provide an actual heating mechanism.

In addition to the continuum emission the observed hot plasma contains a number of emission lines, indicating that the plasma must be optically thin. These lines include contributions from Hydrogen like and Helium like ions of Mg, Si, S, and Fe. An analysis of the relative strength of these lines is consistent with production in a two component plasma and also finds that the spectrum is similar to that associated with point sources in the region of the galactic centre [93]. This analysis also suggests that, even after point source subtraction, there may remain some contribution to the diffuse emission spectrum from point sources below the detection threshold of Chandra [92, 93]. The contribution of these objects does not however, seem sufficient to explain the total emission from the galactic centre region, particularly in the case of the hot emission component. The most promising candidates considered were cataclysmic variables, but even these provide an x-ray contribution an order of magnitude below what is observed. If this is the case then a new source of diffuse emission in the x-ray band may be required to produce this apparent hot plasma component. I will argue that quark nugget dark matter may provide just such a source. In this picture the emission lines arise from conventional diffuse astrophysical processes and the point source contribution, while the nuggets contribute a significant portion of the observed x-ray continuum.

The previous section dealt with the fraction of energy, produced in nuclear annihilations, which is thermalized within the nuggets. However, these annihilations occur relatively near the surface, and we must also consider emission resulting from annihilation products that escape the nugget before thermalizing. This requires a more detailed description of the dynamics of the annihilation process. Within the quark matter, individual quarks are not bound in colour singlet hadronic states, but exist as Cooper pairs. The wave functions of these spatially extended pair states have only a small overlap with the proton wave function. Thus, in order for a galactic proton to annihilate within the quark matter, these two wave functions must first become aligned. The alignment process requires a longer time than in the case of proton-antiproton annihilation and the galactic protons, therefore, have time to penetrate deeply into the nugget, with respect to the QCD scale. If annihilation rates maintained their vacuum value the incoming proton would survive for roughly 2fm/c. However, it has been estimated that even in ordinary nuclear matter this lifetime could easily be an order of magnitude larger [90], resulting in a correspondingly longer penetration depth for the incident proton.

The annihilation of a galactic proton within the nugget typically produces a pair of back to back jets (as observed in standard proton-antiproton annihilations.) These jets then rapidly cascade down to the lightest modes of the colour superconductor. The exact decay chain of these hadronic processes will be very complicated, and will depend on the quark matter phase realized within the nugget. However, near the quark surface the lightest modes are quite generically the positrons which are only electromagnetically coupled to the quark matter. The result of a near surface proton annihilation will, therefore, be a stream of energetic positrons crossing the quark surface into the electrosphere. As with most electromagnetic processes, the transfer of energy from the initial hadronic jets to the positrons will be dominated by exchanges of the lowest possible energy photons. Within the Fermi gas of positrons near the quark surface, electromagnetic effects are screened by the presence of background charges. The plasma frequency in a Fermi gas with chemical potential μ is given by,

$$\omega_p \approx \sqrt{\frac{4\alpha}{3\pi}}\mu. \tag{3.11}$$

with the chemical potential at typical QCD scales, $\mu \sim 100$ MeV, in this case. This gives a plasma frequency $\omega_p \sim 5$MeV and photon exchange at lower energies is then strongly suppressed. Consequently, the majority of excited positrons will carry energies at this scale.

These excited positrons will be the primary source of non-thermal emission generated by nuclear annihilations. As such they carry a fraction $1 - f_T$

of the total energy released in a typical nuclear annihilation[22]. As only annihilation products directed towards the quark surface have any possibility of escaping the nugget we require $1 - f_T < 1/2$. Taking each positron to carry a momentum near the plasma frequency in expression 3.11, a single proton annihilation will produce, at most, roughly a hundred relativistic positrons crossing the quark matter surface.

As the positrons move through the strong electric field at the quark surface (as described by equation 2.10), they will be decelerated and emit bremsstrahlung radiation. The momentum of these positrons is sufficient that they penetrate upwards in the electrosphere to a regime where the positron chemical potential has dropped to the keV scale. As the excited positrons cross this region of the electrosphere, the bremsstrahlung photons must be emitted above the local plasma frequency. Across the electrosphere the plasma frequency falls from the MeV scale down to below a keV. This, combined with the growth of the electron-photon scattering cross section at low energies produces emission primarily at 1-10keV [42]. As with thermal emission, the observational consequences of near surface annihilation, x-ray emission will be strongest towards the galactic centre, where both the visible and dark matter densities are largest.

As the emission from a hot dilute plasma is primarily through thermal bremsstrahlung, it should not be surprising that the spectrum of photons emitted by an ejected positron is similar to that of a hot plasma. This spectrum tends to be relatively flat up to a sudden exponential cutoff. In the thermal case this cutoff is determined by the temperature of the plasma as the production of photons with energies above the average interaction energy of the plasma components is strongly disfavored. Near the cutoff the emission spectrum will scale as,

$$\frac{dE}{dt\ d\omega} \sim e^{-\omega/T}. \tag{3.12}$$

Estimating the high energy cutoff in the case of emission from the nuggets is more complicated as it involves many body interactions rather than the collective effect of many interactions between independent plasma components. At any given depth in the electrosphere the emission of a photon with an energy below the plasma frequency, as given in equation 3.11 is strongly suppressed. Once the positron reaches a regime of the electrosphere where the plasma frequency is well below the positron's momentum the nugget's

[22]Recall that f_T was introduced in section 3.2 and represents the fraction of energy thermalized within the nugget, $1 - f_T$ is then the fraction emitted through non-thermal processes.

electric field will be unscreened and the emission of bremsstrahlung radiation will quickly slow the positron.

An analysis of the classical path of a positron in the near surface electric field, as given by expression 2.10, was performed in [42]. That analysis suggested that the response time of the system could be approximated as,

$$\tau \approx \frac{\mu_0 + \epsilon_0}{eE} \approx \sqrt{\frac{3\pi}{2\alpha}} \left(\frac{z + z_0}{z_0}\right)^2 \frac{\mu_0 + \epsilon_0}{\mu_0^2} \tag{3.13}$$

where z should be taken as the height above the quark surface from which the majority of bremsstrahlung radiation is emitted and $\epsilon_0 \approx \omega_p$ is the positron injection energy. As this timescale limits the emission of radiation we should expect that the bremsstrahlung spectrum should be cut off at frequencies of $\omega_c \sim \tau^{-1}$. Numerically, if we take $\mu_0 = 10$MeV, $\epsilon_0 = 5$MeV and $z \sim z_0$ we obtain $\omega_c \approx 30$keV. This estimation (which is accurate only at the order of magnitude level) turns out to be quite close to the spectral cutoff $\omega_c \approx 10$keV suggested by the Chandra data. This ten keV scale arises from the basic physical properties of the nuggets and is in no way tuned to fit the observed emission. Near the point of maximum positron energy loss the emission spectrum may be given in terms of the modified Bessel function, $K_{5/3}$:

$$\frac{dE}{dt\ d\omega} \sim \frac{\omega}{\omega_c} \int_{\omega/\omega_c}^{\infty} K_{5/3}(x) dx, \tag{3.14}$$

$$\frac{dE}{dt\ d\omega} \sim e^{-\omega/\omega_c}, \quad \frac{\omega}{\omega_c} > 1. \tag{3.15}$$

The similar scaling of equations 3.12 and 3.14, with $T \sim \omega_c \sim 10$keV, implies that the basic continuum shape of the bremsstrahlung spectrum generated in these two very different physical scenarios may be indistinguishable[23].

In this framework, the heated plasma observed by Chandra is actually the localized hot spots , generated by the annihilation of galactic protons, on the surface of many individual antiquark nuggets. In this case, there is no need to explain how the plasma remains bound to the galaxy, as the positrons involved in each annihilation event remain bound to the nugget by the strong electric fields at the surface of the quark matter.

While the basic form of the spectrum generated by x-ray emission from the quark nuggets is consistent with the spectral shape observed by Chandra

[23] The actual spectra observed by Chandra, as well at the two component plasma fits to the data, may be seen in figure 6 of [93]. From that figure it is clear that a hot plasma component is required to fit the spectrum, as significant x-ray emission is observed across the entire 1-8keV range observable with Chandra.

the overall scale of the nugget contribution is not yet established. This emission strength is dependent on the details of the matter and dark matter distributions as well as the distribution of nugget masses. As with any other observational quantities the contribution of the nuggets to the galactic x-ray background will be lower if the nuggets have a larger average mass. In chapter 4 the scaling of the various emission features discussed here will be discussed allowing the total intensity to be estimated.

3.4 Low momentum electron annihilations : the galactic 511keV line

A strong 511 keV line, along with the associated three photon continuum, has been observed by the SPI spectrometer on board the INTEGRAL observatory [60, 70]. While this gamma ray source in the galactic centre has been known for four decades [62], the source of the roughly $10^{43}s^{-1}$ annihilating positrons remains an active research question (for a recent review of the situation see, for example, [100].)

The observed e^+e^- annihilation spectrum at 511keV is modeled as a two component spectral line, combined with the associated ortho-positronium continuum. The spectral line displays a broad component with a width of 5.4 ± 1.2 keV FWHM and a narrow component with width 1.3 ± 1.2 keV FWHM [61]. The narrow line is consistent with the low momentum annihilation of a positron with a free electron while the broad component has a width typical of annihilation through charge exchange with neutral hydrogen. This width is also entirely consistent with formation within the electrosphere of a quark nugget. In the latter case, the additional broadening comes from annihilations involving slightly higher momentum positrons closer to the quark surface as well as the capture of electrons from incident neutral hydrogen.

Morphologically, the 511 keV emission is strongly associated with the galactic centre and the galactic bulge [118], displaying only a much fainter disk component [70], [119]. However, the exact spatial distribution of the emission strength remains model dependent in that one may always introduction additional components (beyond disk and bulge) to obtain a better fit to the data. This is particularly true of components with low surface brightness and a large spatial extent [117]. A contribution of this form can represent a large total number of positrons but make only a small contribution to the observed spectrum. While the exact ratio is strongly dependent on the model employed, the bulge to disk ratio of the 511keV emission is generally found to be ≥ 1. This is a stronger spherical component than is seen in most astrophysical sources, and seems to require more complicated propagation of cosmic rays through the galaxy than had previously been assumed. This in turn generated interest in dark matter models capable of producing the requisite number of positrons through either decays or annihilations. The reasoning being that, as the dark matter is generally taken to have a spherically symmetric distribution, any associated emission should be dominantly in the spheroid component of the galactic centre, rather than being associated with the disk. These models, however, tend to produce positrons with sufficient energy that they will produce a significant inflight annihilation spectral component rather than just a clean 511 keV line [26]. As further observations revealed greater detail in the spatial distribution of the 511 keV emission it became clear that dark matter models involving the production of relativistic positrons would generally overproduce the high energy γ-ray background. As such, rather than naturally explaining the morphology, these models require modifications of the cosmic ray propagation models similar to those that they sought to avoid [83].

The difficulty in explaining the 511 keV line lies not in producing the required number of positrons, but in concentrating them so strongly in the galactic centre and at low momentum. The observed morphology does not seem to trace the spatial distribution of known positron sources, and the narrow width of the spectral line suggests that the positrons must slow dramatically between production and annihilation. As such, an understanding of the contribution of known positron sources to the observed 511 keV line requires extensive modeling of positron propagation. This remains an open research question and I will give only a brief overview here.

The main astrophysical source of positrons is thought to be supernovae. These produce a large number of radionuclei which may then β-decay and emit a positron, generally with an MeV scale energy. The supernova rate in the galaxy is believed to be sufficient to provide the required number of positrons. However, many of the relevant radionuclei have a short half life, which may lead to a large number of the positron produced being annihilated before they escape from the supernova remnant itself. This source also requires rather complicated transport of the resulting positrons as supernovae occur primarily in the disk while the majority of annihilations are observed to occur in the galactic bulge [101].

The disk component of the 511 keV emission may, however, be underestimated as the positron annihilation is likely to be more spatially dilute. This could result in sections of he disk having a surface brightness below the sensitivity of SPI/INTEGRAL. If this is the case the number of disk positrons could be much larger than is observed. In fact, the AMS [98] has measured the electron to positron ratio in the cosmic ray spectrum at energies up to 500 GeV. This spectrum shows a rise in the positron fraction above ~ 10 GeV, indicating the presence of more positrons in the local disk than would be extrapolated from lower energy measurements [33] and supports the possibility of an extended disk component. However, these positrons are at energies well above where they could contribute to the 511 keV line and there have not been convincing models put forward as to how they may be slowed and transported to the galactic bulge.

Several other potential astrophysical sources have been put forward such as pulsars or stellar winds These may increase the number of positrons available but do not solve the problems of distribution and energy discussed above. Keeping in mind this underlying uncertainty in the nature of the 511keV emission I will now discuss how such emission will arise in the quark nugget dark matter model.

In addition to protons, we may also consider the contribution made to the diffuse galactic spectrum by electrons annihilating on an antiquark nugget. The properties of these annihilations, and the related emission, will be governed by the properties of the nugget's electrosphere which were outlined in section 2.2. When a galactic electron strikes a nugget, it first moves through the low density "Boltzmann" region of the electrosphere, where the positron densities and momenta are at typical atomic scales. Under these conditions, the dominant annihilation channel is through the resonance formation of a positronium bound state (an "atom" consisting of a bound e^+e^- pair.) The positronium state subsequently decays, to either a pair of back to back 511 keV photons, or a three photon continuum, depending on its initial spin configuration[24]. Unlike the emission mechanisms, related to proton annihilation, considered in the previous two sections, the decay of a $^1S_0$ positronium state results in a narrow spectral line, rather than continuum emission extending over a wide frequency range. This relatively clean signal, independent of the nuclear physics of the quark matter, is a particularly attractive observational target. The line width is determined by the fact that positronium formation is strongest in the region of the electrosphere just above the atomic scale. This may be seen in figure 2.2 which shows the rapid increase in positronium annihilations where the electrosphere density

[24]One quarter of the time the electron-positron pair will form a positronium atom in the spin zero $^1S_0$ state which can decay to a pair of back to back photons with opposite helicities. The remainder of the time the positronium will decay from the $^3S_1$ state. As this state carries a half integer spin the state must decay to three photons in order to conserve angular momentum.

approaches a_B^{-3}. In this background the positronium is likely to form with an atomic scale momentum, well below its rest energy. The resulting line will then be Doppler broadened at the keV scale [128]. This diffuse emission source should track the matter and dark matter distributions as described by equation 3.2 and, as such, will be strongly peaked towards the galactic centre with a fainter disk component. This is not necessarily true of models in which the positrons are produced by astrophysical processes which are strongly associated with the disk or of models involving exclusively dark matter interactions which are purely spherical.

Finally, we may make a rough estimate of the number of positronium annihilations expected from the galactic core. The rate at which positronium is formed in the galactic bulge may be expressed as,

$$\Gamma_{Ps} = f_{Ps} n_e n_{\bar{N}} \sigma_n v_e V_B, \tag{3.16}$$

where $f_{Ps} \approx 0.9$ is the fraction of annihilating electrons expected to produce a 511 keV photon, n_e and $n_{\bar{N}}$ are the electron and antiquark nugget densities, v_e is the average electron speed and V_B is the volume of the galactic bulge. If we take the same matter distribution as was used in the estimation of the total haze contribution and take the observed bulge radius to be a few kpc then we arrive at the approximation,

$$\Gamma_{Ps} \approx 10^{51} s^{-1} B^{-1/3}. \tag{3.17}$$

Comparing this to the observed rate of 10^{43} s^{-1} implies that nuggets with a mean baryonic charge of 10^{24} could easily produce the required number of positronium decays. This approximation is very approximate, and may be affected by the charge of the nuggets in various environments, by gives a basic feel for the scale involved.

At present the source of the positrons responsible for the galactic 511 keV line remains ambiguous without a definite preferred origin. As such, it is possible that a considerable fraction of them could be associated with quark nugget dark matter without any contradictions with observation. In this case the positrons are naturally present at low energies and do not need to be produced in high energy astrophysical processes and then decelerated before undergoing low energy annihilation through the positronium channel. The morphology is also consistent with the mixed bulge/disk distribution as the emission will track the product of the matter and dark matter distributions.

As the 511 keV line is the cleanest, and best known, of the diffuse emission excesses discussed here it will be used to estimate the total rate of annihilation events involving quark nuggets in chapter 4. Once this basic rate has been established the scale of all other forms of diffuse emission may be estimated in a more detailed way than has been done here.

3.5 Near surface electron annihilations : the COMPTEL MeV excess

The galactic MeV background is dominated by nuclear decays and cosmic ray interactions. These processes require extensive modeling to compare astrophysical predictions to observational data. As in the case of the galactic 511 keV line there are many complications, relating to production and diffusion models which may dramatically change the scale of the predicted astrophysical background. Several attempts have been made to fit the galactic γ-ray spectrum based on known astrophysical emission mechanisms [112]. In each case, these calculations have produced a good fit to both the spectrum and the spatial distribution of the observed diffuse γ-ray background, except in the MeV band in the galactic centre region. In this region the models predict MeV band emission significantly below what is observed. The observational data for this analysis was taken from the COMPTEL telescope for energies from 1-30 MeV [113], while the data from 30MeV up to 50GeV comes from the Energetic Gamma Ray Experiment Telescope (EGRET) using the data set described in [111]. As with the other diffuse backgrounds discussed above it is difficult to extract an exact morphology from the COMPTEL excess. However, of the regions considered in [112] only the inner galaxy ($l = 330^o - 30^o, |b| = 0^o - 5^o$) show signs of this excess, indicating that whatever mechanism is responsible is strongly concentrated towards the galactic centre. Unfortunately the MeV scale excess cannot be verified with follow up with higher resolution observations by the Fermi gamma-ray telescope which is not sensitive to photons below 30MeV.

Several proposals have been made to fit this excess in diffuse emission by modifying the emission spectrum of known astrophysical objects, introducing a new class of unresolved point sources, or through dark matter interactions. In each of these cases, the modification to known physical processes must be very carefully chosen, so as not to ruin the good fit to the galactic spectrum at other energies or outside of the higher density galactic centre.

In the case of quark nugget dark matter this MeV excess must necessarily be coproduced with the 511keV line. It was demonstrated in [80] that this high energy component of the nugget spectrum could provide the additional source, necessary to explain the observed MeV galactic background. This is possible as the spectrum expected from the annihilation of galactic electrons, passing through the high density regime of the electrosphere, maps neatly onto the MeV background observed by COMPTEL [113].

A fraction of the galactic electrons incident on the quark nugget will avoid annihilation in the low density outer layers, these will penetrate through to the high density region of the electrosphere near the quark surface. Once there the annihilation energy scale becomes significantly larger, and emission cannot be treated as in the nonrelativistic positronium formation case considered above. The positronium resonance favours annihilation of the incident electron with the lowest momentum positrons available. This is because the probability of forming a positronium bound state scales as,

$$P_{Ps} = | < \psi_{Ps} | \psi_{e+e-} > |^2 \approx \left(\frac{1}{1 + a_B^2 q^2} \right)^2 \qquad (3.18)$$

where a_B is the Bohr radius and q is the centre of mass momentum. Thus, once the positron carries a momentum above the atomic scale, the formation rate falls with the fourth power of momentum. However, the density of states of a Fermi gas scales as $\frac{dn}{dk} \sim k^2$, so that the integrated number of high energy positrons will grow as $N_{k>>m} \sim k^3$. This effect will dominate over the decrease in scattering cross section which falls only as $\sigma \sim k^{-2}$. The density of low momentum positron states remains fixed with increasing chemical potential and thus the positronium formation rate saturates quite high in the electrosphere. Nearer to the quark matter surface the growth of the density of states at large momenta favors the off resonance, direct $e^+e^- \rightarrow 2\gamma$ channel despite its smaller cross-section. The relative scale of resonant and direct annihilation processes, as a function of height in the electrosphere, are shown at the top of figure 2.2. The exact relation between these two processes will be the primary focus of chapter 4.

Near the quark surface the positrons carry momenta on the order of $p_F \sim e\Lambda_{QCD} \sim 10$MeV. The photons produced in these annihilations will carry energies up to this scale. Some forms of quark matter are predicted to support a larger lepton density at their surface, and thus allow a larger maximum possible annihilation energy. However, electrons passing through a medium of this density have only a very low probability of reaching a depth at which the chemical potential is much greater than ~ 10 MeV. Consequently, these annihilations represent the highest energy emission from the nuggets produced in significant quantities, and no signature will be produced above this scale. As such, this model is not subject to the strong constraints imposed by the Fermi gamma-ray telescope [7, 8].

The details of this spectrum can be made more explicit through arguments based on some simple QED based calculations [80]. Consider an electron in a Fermi gas of positrons with chemical potential $\mu >> m_e$. The differential cross section for a positron of momentum p to annihilate with a stationary electron and produce a final state containing a photon of momentum k may be found, at tree level, by a standard QED calculation:

$$\begin{aligned}\frac{d\sigma}{dk} &= \frac{\pi\alpha^2}{mp^2}\left[\frac{-(3m+E)(E+m)}{(E+m-k)^2} - 2\right] \\ &+ \frac{\pi\alpha^2}{mp^2}\left[\frac{(3m+E)(E+m)^2/k - (m/k)^2(E+m)^2}{(E+m-k)^2}\right]. \qquad (3.19)\end{aligned}$$

Here $E = \sqrt{p^2+m^2}$ is the positron energy. From this we may calculate the rate at which photons of momentum k will be produced by integrating the cross section over the distribution of positron momenta in the Fermi gas, this gives

$$\frac{dN_\gamma(k,\mu)}{dk\ dt} = \int \frac{p^2}{\pi^2}\frac{d\sigma}{dk}dE, \qquad (3.20)$$

with the differential cross section as given in expression 3.19. The integration in this expression should run from the threshold positron energy required to produce a photon of momentum k up to the chemical potential of the Fermi gas. This integral may be evaluated explicitly and the result is given in [80], however, the exact form of this solution is rather cumbersome and is beyond the level required here. Near the peak of the spectrum, when both k and μ are much larger than the electron mass it has the approximate form,

$$\frac{dN_\gamma}{dk\ dt} \approx \frac{\alpha^2 k}{\pi m}\left(\frac{1}{2} + \ln\left[\frac{2(\mu-k)}{m}\right]\right) \qquad (3.21)$$

which is valid up to photon energies where $\mu - k \sim m$. Above these energies the spectrum quickly falls to zero as kinematic constraints require that $k < \mu + 2m$. In the limit where the chemical potential is well above the electron mass, $\mu >> m$, the total annihilation rate has a relatively simple form:

$$\Gamma_{an}(\mu) \equiv \frac{dN_\gamma}{dt} = \int \frac{dN_\gamma}{dk\ dt}dk \approx \frac{\alpha^2 m}{2\pi}\left(\frac{\mu}{m}\right)^2 \ln\left(\frac{\mu}{m}\right). \qquad (3.22)$$

This rate may then be used to estimate the fraction of electrons annihilating at a specific height through direct annihilation. This fraction is given by,

$$\mathcal{F}(z) = \exp\left(-\int_{z_0}^{z} \Gamma_{an}(\mu(z))\frac{dz}{v_e}\right). \qquad (3.23)$$

In this expression v_e is the velocity of the electron incident on the nugget and is assumed to be at the galactic scale. The lower limit for the integration may be taken as the beginning of the ultrarelativistic regime in the electrosphere where the evolution of the chemical potential is as given in expression 2.9. We may get a feel for the rate of this exponential fall off by noting that, from equation 2.9 we find, $\mu^2 dz = \sqrt{3\pi/2\alpha}\, d\mu$. Using this substitution and the form of the total rate given in equation 3.22 gives a survival fraction

$$\mathcal{F} \approx \exp\left[-\frac{\mu}{\bar{\mu}}\left(1+\ln\left(\frac{\mu}{m}\right)\right)\right], \quad \bar{\mu} \approx \frac{2\pi m v_e}{\alpha^2}\sqrt{\frac{2\alpha}{3\pi}}. \tag{3.24}$$

Here I have defined $\bar{\mu}$ as an energy scale that sets the rate of the exponential decay. If I take the electron velocity to be at a typical galactic scale of $v_e = 10^{-3}c$, then the decay energy scale is $\bar{\mu} \approx 3$MeV. This decay rate becomes relevant at chemical potentials above roughly an MeV, as discussed above.

The spectrum given in equation 3.21, combined with the weighting factor in expression 3.24, determines the spectral contribution of the quark nuggets from the ultrarelativistic limit regime of the electrosphere. The uncertainties in dark matter distribution, and the distribution of nugget masses, prevents an explicit calculation of the overall scale we should expect for this diffuse emission source. However, following the estimations made in [80], we may assume that high energy emission from the ultrarelativistic regime is co-produced with the galactic 511keV line, and that nugget emission dominates the 511keV signal. This procedure packages all the uncertainties in the estimated emission strength in a single parameter, here called f_{ur}, which sets the fraction of annihilating electrons able to penetrate into the ultrarelativistic regime (and thus contributing to the galactic diffuse emission above 1MeV.) Using this scaling procedure it is possible to estimate the nugget contribution to the galactic spectrum. The result for a typical value of $f_{ur} = 0.1$, along with observational data and the predicted galactic diffuse emission, may be seen in figure 3.1. The diffuse spectrum, taken from [91], provides a good fit to the observed spectrum over much of the γ-ray range, but is predicted to fall too rapidly below 100MeV to be able to fit the COMPTEL data. It is precisely in this range that the nuggets provide an additional contribution to the galactic γ-ray spectrum.

The introduction of the scaling parameter f_{ur} allows us to treat the overall normalization of the spectrum in a relatively simple way. However, it is possible to go beyond this very approximate treatment by using the detailed modeling of the electrosphere presented in section 2.2. This will be done in

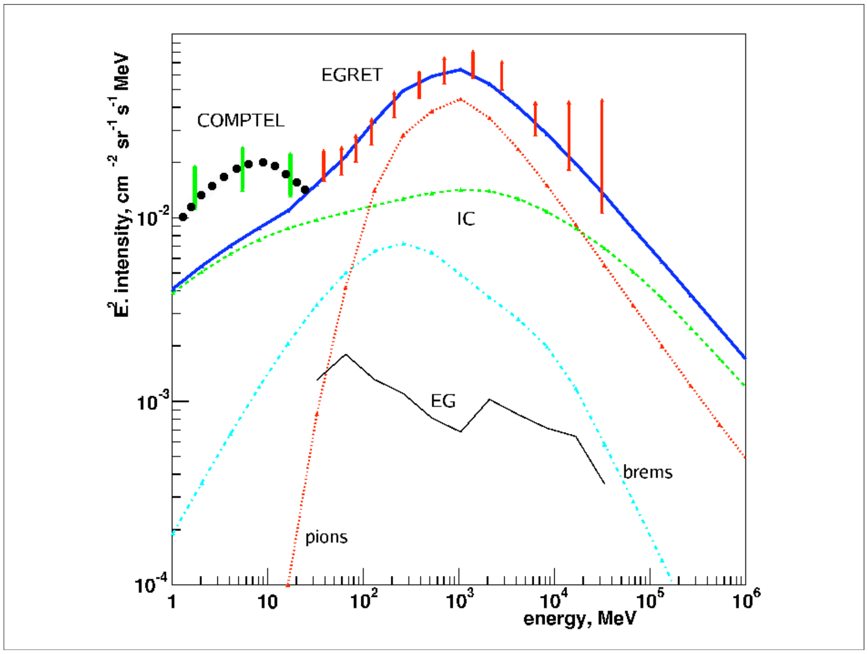

Figure 3.1: The diffuse γ-ray spectrum of the inner galaxy as observed by COMPTEL (Green bars) and EGRET (red bars). Also shown are the contributions from expected backgrounds including; inverse Compton scattering, bremsstrahlung and pion decay as well as the extragalactic background. The solid blue line gives the predicted total γ-ray intensity and the black dots show the effect of adding a quark nugget contribution as described in the text. Figure taken from [80] where it was adapted from [91].

chapter 4, where the exact rates of positronium formation and direct annihilation will be calculated and a precise electron annihilation spectrum will be determined without the necessity of introducing the phenomenological parameter f_{ur}. A more version of figure 3.1 based on this calculation is presented in figure 4.2.

Some important aspects of the spectral properties outlined here should be highlighted. The emission falls in the band between approximately 1MeV, the chemical potential at which direct annihilation first becomes important and the chemical potential at the nugget's surface. As mentioned above, the lepton chemical potential should be expected to be a few tens of MeV. However, emission from increasing depths are suppressed by the exponential decay of the number of galactic electrons penetrating to a given depth. It may be estimated that this effect will limit the emission spectrum to a few times $\bar{\mu}$. These features are consistent with generating a diffuse excess in the MeV range while not contributing strongly to the well fit diffuse background at higher energies.

It is also important to note that, had the MeV spectrum from the galactic centre been more tightly constrained, the quark nugget model could not serve as a source for the galactic 511 keV line. The two components must both be present if the nuggets are to be invoked to explain the galactic diffuse γ-ray background. The fact that these two spectral components are produced through exactly the same physical process will be exploited in the following chapter to predict the exact ratio between the 511keV line and the MeV diffuse emission. That analysis will demonstrate that this ratio must be close to that which is observed.

3.6 Conclusions

This chapter has argued that the presence of quark nugget dark matter is not ruled out by observations of the galactic centre, where the contribution of the nuggets to the diffuse background should be largest. In fact, their contribution to the galactic spectrum may help to explain some apparent anomalies in galactic observations from the microwave band up to γ-rays. Taken together these observations span more than ten orders of magnitude in energy, but may all be understood in terms of a single emission model. Improved constraints on any one of the spectral bands discussed above, whether through further observations or improved modeling of astrophysical backgrounds, must necessarily lower any potential nugget contribution to all the others. This correlation will be the subject of the following chapter where more precise estimations of the relative strengths of different components of the nugget spectrum will be calculated.

Chapter 4

Relative Emission Strengths

In this chapter I will estimate the relative emission strength of the various components of the nugget emission spectrum outlined in the previous chapter. As the baryonic charge of the nuggets is unknown the line of sight integral, from expression 3.2, cannot be directly evaluated. Thus, we cannot fix the absolute emission strength of the various spectral components. However, once this overall scaling is fixed it must be identical for all the forms of emission. As such, if we assume that the galactic 511keV line is dominated by annihilations involving positrons in the electrosphere of an antiquark nugget, then we may estimate the relative strengths of all the other spectral components. The discussion of the relative strength of the two electron-positron annihilation processes (those which we associate with the 511keV line and the diffuse MeV continuum observed by COMPTEL) is derived from original research conducted as part of this thesis [40]. The following discussion of the relation of the nuclear annihilation processes is based on previous work [42, 43] and, as such, only briefly reviewed here.

4.1 Electron-positron annihilation

Both the 511keV line and the MeV continuum discussed above arise from the same physical process; the impact of a galactic electron on an antiquark nugget and its subsequent annihilation with a positron. The relative scale of emission expected from these two processes is, therefore, directly calculable. As discussed in section 3.5 the ratio between the two spectral components is essentially determined by the fraction of low momentum galactic electrons penetrating deeply into the electrosphere to a point where the Fermi momentum of the positron gas is large.

The survival fraction of electrons depends on the annihilation rate at each depth (through both the positronium and direct annihilation channels) and this is, in turn, depends on how the positron density grows with depth. The structure of the electrosphere was discussed in section 2.2, and many of its specifics have been established in detail in [40].

The rate at which a galactic electron of velocity v_e binds to a positron to form a positronium may be estimated as

$$\Gamma_{Ps}(z) = \int_{p<m\alpha} v_e \ \sigma_{Ps} \frac{d^3\vec{p}}{(2\pi)^3} \ \sim \ 4\pi v_e a_b^2 n_{e+}, \quad p_F < m\alpha \tag{4.1}$$

$$\sim \ \frac{4v_e}{3\pi a_b}, \quad p_F > m\alpha. \tag{4.2}$$

Here the integral runs over the local density of states with momenta small enough to sit within the positronium resonance. Far from the quark surface, where the density is below the atomic scale, the positrons carry only small momenta and they all contribute to positronium formation. This gives the factor of the positron density, n_{e+}, appearing in the expression for Γ_{Ps} at low densities. Above the atomic scale, the low energy positron states are fully occupied, and any additional positrons must be added in momentum states large enough to be off of the positronium resonance. At these densities, only the low lying states contribute to positronium formation, and the formation rate saturates. This saturation effect, and the radial distance at which it occurs are plotted at the top of figure 2.2.

The cross section for an electron-positron pair to scatter to a pair of photons is easily calculated within the framework of QED, an approximate version of this rate was given in expression 3.22 while the exact form may be obtained by performing the integration in expression 3.20 and then integrating the result over the final state photon momenta, as was done in [80]. Within the dense region of the electrosphere scattering is limited to cases where the emitted photons are above the local plasma frequency so that the phase space for annihilation is partially restricted by the kinematic constraints on the final state photons. The resulting annihilation rate was calculated analytically in the zero temperature limit in [80] and numerically for non-zero temperatures in [40]. Within the context of this full numerical solution, it is possible to calculate directly the fraction of incident electrons that survive to a given depth in the electrosphere. This survival fraction is plotted in figure 4.1. Two important features of the annihilation rate are immediately obvious from figure 4.1. First, the rapid drop in the survival fraction at Fermi momenta in the keV range is almost entirely due to positronium formation, and accounts for the majority of annihilation events. The steepening of the decay curve beginning at $p_F \sim 1$MeV is due to the growth of the direct annihilation rate, and accounts for roughly a tenth of the total annihilation events. Second, at very large positron densities, annihilations occur at an ever increasing rate, to the point where there is

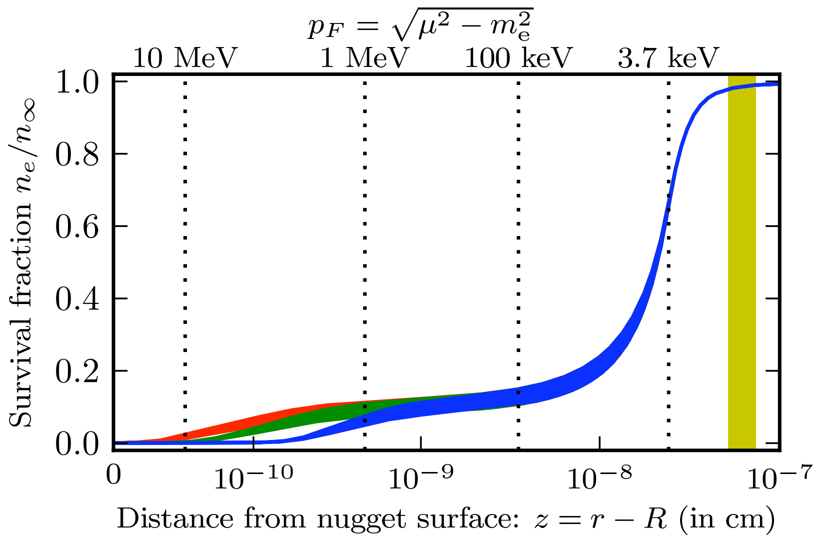

Figure 4.1: The fraction of incident electrons which survive to a given depth within the electrosphere of an antiquark nugget. The three different curves represent different initial electron velocities: v=0.01c (red), v=0.005c (green) and v=0.001c (blue). The thickness of the curves represents a 10% variation in the positronium formation rate. The yellow band indicates the region of the electrosphere well modeled by the Boltzmann approximations as discussed in section 2.2. Figure taken from [40].

virtually no chance of an electron penetrating to a depth where its annihilation produces a photon with an energy of more than a few tens of MeV. In [80] these features were built into the emission model, in a phenomenological way, to demonstrate that the presence of quark nuggets in the galactic centre was entirely compatible with the COMPTEL measurements. In the full treatment of the annihilation rates presented in [40], these values were derived from a precise microscopic modeling of the properties of the electrosphere. In that analysis, it was found that the MeV excess and the 511keV line must, not only both be present, but must be present in the ratio in which they seem to be observed.

To further establish the importance of this correlation between the 511keV line and the MeV continuum, I will now repeat the estimations of [40] used in determining the ratio between the two spectral features. From the annihilation rates presented in figure 4.1 it is possible to determine the fraction of galactic electrons which annihilate through the positronium channel. These represent roughly 90% of all annihilations, and must account for the observed 511keV line and its associated three photon continuum. The strength of the 511keV line from the galactic centre, as observed by SPI/INTEGRAL, is ~ 0.025 photons cm^{-2} s^{-1}sr^{-1}, coming from a circle of half angle 6^o centred on the galactic centre [60]. The majority of this emission does not have a well established origin and, for present purposes, will be assumed to be produced in annihilations within a quark nugget. Under this assumption the flux of 511keV photons essentially fixes the value of the line of sight integral in equation 3.2. Fixing this emission rate allows us to scale all of the other emission mechanisms, without adopting a particular matter density profile or nugget size distribution.

An exact comparison between the SPI/INTEGRAL data at 511keV and the COMPTEL data in the 1-30 MeV range is made difficult by the complicated background subtraction required to extract the MeV continuum. The diffuse background contribution, due to known astrophysical processes in the interstellar medium, was modeled in [112] which provides a detailed spectrum across the relevant energy range, but averages emission over a somewhat larger angular extent than the SPI/INTEGRAL data, covering galactic longitudes in the range $l = 330^o - 30^o$ and latitudes $|b| = 0^o - 5^o$. Across this region the average strength in the MeV band, as measured by COMPTEL, is approximately $k^2 \frac{d\Phi}{dk} \sim 10^{-2} MeV s^{-1} cm^{-2} sr^{-1}$, where I have given the spectral density flattened by the energy squared following the original work in [112]. Directly scaling the MeV continuum, such that the total number of photons involved (i.e. $\int \frac{d\Phi}{dk} dk$) matches the annihilation rate set by the strength of the 511keV line results in the spectrum shown in figure 4.2. Even neglecting the difference in the angular distributions in [60] and [112], and ignoring the very complicated distribution of matter densities and velocities across the galactic centre, it can be seen that the spectrum generated by quark nugget dark matter will fall in precisely the range where COMPTEL observes an excess above the predicted galactic background both in terms of energy and intensity.

4.2 Nuclear annihilations

A similar analysis may be applied to the WMAP and Chandra data both of which are, in this model, associated with the annihilation of a galactic proton within an antiquark nugget. There is, however, a complication in that the division of energy, between thermal emission and surface bremsstrahlung from accelerated positrons, is highly dependent on the depth in the quark

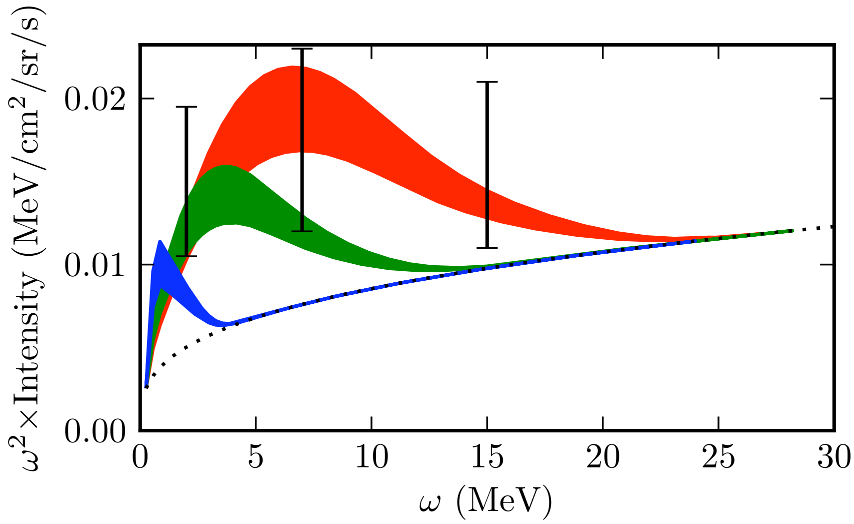

Figure 4.2: Spectral density scaled by ω^2 emitted by electrons annihilating on an antiquark nugget. The three curves assume incident electron temperatures v=0.01c (red), v=0.005c (green) and v=0.001c blue). The thickness of the bands assumes a 10% variation in the positronium formation rate as in figure 4.1. The overall normalization of the curves is obtained from the galactic 511keV line as discussed in the text. The vertical bars are the COMPTEL data points [113] and the dashed line is the predicted astrophysical background calculated in [112]. Figure taken from [40].

matter at which the annihilation occurs, and on the efficiency with which energy is distributed between the various light modes of the colour superconductor. These are difficult problems to address theoretically and have little experimental input. The structure of interactions, and even the nature of the light modes of the superconductor, are also highly dependent on the particular phase of quark matter realized in the nuggets. As such, the relative scale of the various emission mechanisms cannot be extracted as cleanly as was the case with electron-positron annihilations. Instead I will introduce a pair of phenomenological parameters which parameterize the uncertainty inherent in this process. The values of these parameters will then be extracted from observation and it will be argued that their values are reasonable based on the generic properties of quark matter. Much of this analysis follows previous work done in [42] and [43].

The first parameter to be introduced is the fraction of energy, produced in a nuclear annihilation, that is thermalized within the nugget. This parameter, which will be called f_T, was previously referred to in estimating the nuggets' temperature in the discussion of the WMAP haze in section 3.2. As all thermalized energy is emitted in the thermal spectrum while the dominant non-thermal emission process is x-ray bremsstrahlung from excited positrons this fraction sets the relative scaling of the microwave band "haze" component and the diffuse x-ray background. As the physics of this ratio is entirely determined by the internal properties of the nuggets it should be independent of the environment in which the nuggets are found.

The second parameter is related to the relative rate of electron and proton annihilations, it will be labeled f_{ep}. This will set the relative scale of electron annihilation processes (positronium decay and the direct annihilation MeV continuum) and those associated with nuclear annihilation (microwave band thermal emission and x-ray bremsstrahlung.) The value of f_{ep} will be dependent on the relative rates of charge exchange processes and inelastic collisions with the nugget as discussed in section 2.3. As these properties may depend on the nugget temperature and ionization, as well as the ionization of the surrounding interstellar medium, this parameter may show more spatial variation than is expected for f_T.

As was demonstrated in the discussion of electron-positron annihilation in section 4.1 the photon flux from all these events is,

$$\Phi_{e^+e^-} \approx 0.1 \frac{\text{photons}}{\text{cm}^2 \text{ s sr}}. \tag{4.3}$$

This is related to the total energy flux from proton annihilations by the parameter f_{ep}, such that,

$$I_{p\bar{p}} = I_{therm} + I_{brem} = 2 m_p f_{ep} \Phi_{e^+e^-}. \tag{4.4}$$

Here I_{therm} is the intensity generated by thermal emission from the nuggets (which I will associate with the WMAP haze) and I_{brem} is the non-thermal bremsstrahlung emission from the nugget surface (which I associate with the diffuse x-ray background.) The fraction of energy thermalized in the nugget may be expressed in terms of the same parameters,

$$f_T = \frac{I_{therm}}{I_{p\bar{p}}} = \frac{I_{therm}}{2 m_p f_{ep} \Phi_{e^+e^-}}, \tag{4.5}$$

so that, by extracting the total intensities associated with the two spectral components, it is possible to determine observational values for f_T and f_{ep}.

The Planck analysis gives the haze contribution in the 23GHz channel as $\Delta T = 0.1$mK, which translates to an intensity of $\frac{dI}{d\nu} \approx 10^{-9} \frac{\text{eV}}{\text{cm}^2 \text{ s sr Hz}}$.

If I want to associate this with the thermal emission from a distribution of quark nuggets then the frequency dependence must be as given in equation C.4 so that I may generally write

$$\frac{dI(\nu)}{d\nu} = I_0 \left(1 + \frac{h\nu}{T_N}\right) e^{-h\nu/T_N} F\left(\frac{h\nu}{T_N}\right) \tag{4.6}$$

with the function F as defined in expression C.2. Evaluating this expression at 23GHz and equating it with the flux, measured by Planck at this frequency, gives $I_0 = 7 \times 10^{-11} \frac{\text{eV}}{\text{cm}^2\ \text{s sr Hz}}$. This normalization must hold across the entire thermal emission spectrum so that,

$$\begin{aligned} I_{therm} &= \int I_0 \left(1 + \frac{h\nu}{T_N}\right) e^{-h\nu/T_N} F\left(\frac{h\nu}{T_N}\right) d\nu \\ &= \frac{I_0 T}{h} \int (1+x)\, e^x F(x) \\ &\approx 10^6 \frac{\text{eV}}{\text{cm}^2\ \text{s sr}}. \end{aligned} \tag{4.7}$$

This gives the total energy flux to be expected from thermal emission from the nuggets.

The case of the diffuse x-ray background is somewhat simpler as the majority of emission falls in the 2-8 keV range which is observed. As such the observed surface brightness may be taken to be approximately equal to the total intensity and $I_{brem} \approx 4 \times 10^5 \frac{\text{eV}}{\text{cm}^2\ \text{s sr}}$. These intensities allow for an estimation of the parameters f_T and f_{ep} so that,

$$f_T \approx 0.7, \quad f_{ep} \approx 10^{-2} \tag{4.8}$$

The remainder of this chapter will be devoted to arguing that these, observationally derived, values are well motivated by the physical properties of the nuggets.

As argued above any annihilation products directed downward into the nugget will necessarily be thermalized. This means that we require $f_T > 1/2$. Any inefficiency in the energy transfer from the initial hadronic annihilation will act to further lower the value of f_T. Some energy loss must be expected in the cascade of secondary particles down to the positrons which actually produce the x-ray bremsstrahlung emission. However, these energy losses should be expected to remove only a fraction of the total cascade energy as the annihilation occurs at a depth to which the incident proton was able to penetrate unimpeded. These considerations make the value of $f_T \approx 0.7$ perfectly reasonable within the context of the quark nugget model. It should also be noticed that the actual value must be larger than stated here as at least some of the diffuse x-ray background must come from sources capable of producing the observed spectral lines.

An estimation of the factor f_{ep} is more complicated. As suggested above the probability that a proton will scatter inelastically off the quark surface is much greater than for it to penetrate into the quark matter. However, if the nuggets are sufficiently charged, a reflected proton will remain bound to the nugget. As discussed in section 2.3, the bound proton will then remain bound to the nugget until it either annihilates or undergoes a charge exchange reaction, either through induced beta decay or direct charge exchange with the quark matter. As the net rate of charge deposition on the nugget must be near zero the relative rate of electron and proton annihilations will be set by the probability of these charge exchange interactions.

In all the cases discussed above, there remains much uncertainty related to the distribution of matter across the galactic centre, and to the nature of the astrophysical backgrounds contributing to the galactic spectrum at the same frequencies as the quark nuggets. It is compelling that estimations of the energy scales and spectra expected from the nuggets, which are all based on well known physics, predict an excess of diffuse emission at precisely the frequencies where the galactic spectrum seems to require a larger than anticipated set of sources. These excesses are also found to occur in a ratio very much like that anticipated by the quark nugget dark matter model. In order to further test this model, it would be beneficial to explore its consequences in a regime in which the physical processes, backgrounds, and overall scales involved are dramatically different from the galactic data discussed above. To this end, the following chapter will be devoted to applying many of the considerations we have just dealt with to much larger scale cosmological observations.

Chapter 5

Cosmological Consequences

As argued in the previous chapter, antimatter nuggets, in an environment with a matter density comparable to that of the galactic centre, will produce thermal radiation across the microwave band up to the eV scale. The other emission mechanisms discussed above will also occur, but here we are concerned only with the thermal component which represents the majority of the energy involved. At present, these densities are reached only in regions where gravitational collapse has produced an over-density of matter, well above the cosmological average[25]. However, the expansion of the universe implies that, in the distant past, the matter density must have been at this scale even in the highly isotropic early universe. We may then ask if the collective thermal contribution of these quark nuggets at large distances make a significant contribution to the isotropic radio background. The following section, which addresses this question, is based on original research first published in collaboration with Ariel Zhitnitsky [81].

At microwave wavelengths the isotropic background is saturated by the CMB radiation, a blackbody spectrum with a temperature of 2.7K (up to well known anisotropies below the mK scale.) As should be expected from thermal radiation, the spectral intensity of this background falls off as essentially the second power of frequency below its peak. Conversely, as discussed in appendix C and section 3.2, the thermal spectrum of emission from the electrosphere displays only a relatively weak, logarithmic, dependence on frequency. As a result of this relatively flat spectrum, the nugget contribution to the radio background may come to exceed the CMB contribution at frequencies well below the thermal peak of the CMB. If this is the case there may be a window in the radio band, below the CMB peak but above the low frequency cut off in the nugget spectrum, in which the nuggets have observational consequences.

Recent observations by the Arcade 2 experiment show just such a low energy excess over the isotropic background of the CMB [39]. In the context of these observations, it has been suggested that several earlier observations

[25]The galactic centre has a density of $\rho \sim 100\text{GeV cm}^{-3}$, roughly eight orders of magnitude above the average matter density in the universe today.

[54, 87, 103, 104] may show evidence for a similar excess at even lower frequencies [39, 46]. The ARCADE 2 analysis suggests that their data is consistent with a power law rise with a spectral index of ~ 2.6. When combined with the earlier radio data the best fit power law obtained is,

$$T(\nu) = T_0 + T_R \left(\frac{\nu}{\nu_0} \right)^{\beta} \tag{5.1}$$

with the CMB temperature $T_0 = 2.729 \pm 0.004$K, and with the fit parameters $T_R = 1.19 \pm 0.14$K and $\beta = -2.62 \pm 0.04$ for the reference frequency $\nu_0 = 1$GHz[26]. According to the ARCADE analysis, the total magnitude and the spectral index observed seem to require an additional spectral component beyond that expected based on a range of complementary observations. At these wavelengths and angular scales the primary astrophysical contributions (apart from the CMB) are galactic foreground emission and the contribution of distant point sources below the resolution of ARCADE 2. The treatment of these galactic and extragalactic contributions is discussed extensively in the original ARCADE papers [39, 72, 106] and will only be briefly reviewed here.

The galactic contribution to the ARCADE 2 data in the 3-10GHz range was analyzed in [72]. In this frequency band galactic emission is dominated by synchrotron emission but also includes smaller contributions from bremsstrahlung emission from ionized particles and discrete radio sources. Determination of the extragalactic background requires the removal of the foreground galactic component. This process is rather complicated and involves introducing various models for galactic emission determined by both the ARCADE 2 data and earlier radio sky maps[27]. However, the subtraction process performed in [72] is not believed to contribute to uncertainties above 5mK in the 3GHz channel, well below the ~ 60mK excess observed. The ARCADE 2 data plotted in figure 5.1 has had the galactic contribution subtracted and the error bars include the cited uncertainty level in this subtraction. To extract an extragalactic radio background, data from the earlier radio surveys [54, 87, 103, 104] incorporated into the analysis of the

[26] It should be noted that the spectral index of the ARCADE 2 excess is suggestively similar to that which the Planck results suggest for the WMAP haze as discussed in section 3.2. This must be the case if both are to arise from the same thermal emission process.

[27] In particular the ARCADE 2 analysis uses a galactic emission map derived either from a simple plane parallel galactic model or a more complicated map constructed from a survey at 408 MHz [54] and the CII line map made by COBE/FIRAS [38]. Both models produce a similar result in terms of the extragalactic background extracted.

ARCADE 2 results in [106] were subjected to the same galactic foreground subtraction procedure as the ARCADE 2 data.

The contribution of various background sources was analyzed in [106]. That analysis used deep surveys of radio sources in the 1-10GHz range and far-IR surveys, which may be correlated with radio band emission, to estimate the total discrete source contribution to the observed isotropic background. It was concluded that the 58mK excess observed in the ARCADE 2 data at 3GHz would require an implausibly large source density, and that even optimistic estimates are likely to provide a temperature increase of only 5-10mK above the CMB. A separate assessment of the radio background was made in [48] based on previous radio surveys. That work extracted the contribution from potential unresolved extragalactic sources from source counts in the 150MHz to 10GHz range, modeled by a two component power law background allowing for populations of both hard and soft radio emitters. In this case the observed contribution to sky temperature from unresolved sources take the form,

$$\Delta T = T_0 \left(\frac{\nu}{\nu_0}\right)^{\gamma_0} + T_1 \left(\frac{\nu}{\nu_0}\right)^{\gamma_1} \tag{5.2}$$

with the reference frequency taken as $\nu_0 = 610$MHz. The best fit was obtained for $T_0 = 876 \pm 22$ mK, $T_1 = 18.9 \pm 0.2$ mK and $\gamma_0 = -2.707 \pm 0.027$, $\gamma_1 = -2.0$. This implies a relatively weak flat component and a steep component that exceeds the CMB emission only below the ARCADE 2 data but with steeper slope than observed. This implies the existence of an additional, highly isotropic radio source which provides the ARCADE 2 excess. Subsequent to the publication of the ARCADE 2 results several reanalyses of the astrophysical contribution to the radio background (through large low surface brightness regions, radio supernova, quasars and distant star forming galaxies) have found that these sources seem able to account for, at most, a small fraction of the observed excess [110, 123].

Since its detection the ARCADE 2 radio excess has motivated a number of dark matter models in which processes involving dark matter contribute to the radio background [44, 45, 57, 125][28]. In the dark matter model considered here, the radio excess is explained in exactly the same way as the galactic backgrounds discussed in the previous chapter. As such, the scale of the cosmological background in this model is directly predicted, with no

[28]Direct annihilation of the $\chi\bar{\chi} \to 2\gamma$ occurring at a rate sufficient to produce the observed excess are excluded by other constraints, so these models generally assume that the dark matter must annihilate to pairs of leptons. These then emit radio band radiation as they are deflected by the magnetic fields of early galaxies.

tunable parameters, based on the strength of the diffuse galactic emission. The following sections will argue that, if the galactic backgrounds discussed above are due to a quark nugget dark matter contribution, then the isotropic radio background generated by the nuggets must occur at exactly the scale and energies which are observed by ARCADE 2.

5.1 Temperature evolution

The temperature of an antiquark nugget in a given environment is determined by the flux of matter onto the nugget. When matter annihilates within the nugget much of the released energy is thermalized, raising the nugget's temperature. In a gas of hydrogen atoms, with temperature T, this flux may be estimated as,

$$\frac{dE}{dt\ dA} = \rho c^2 v = \rho c \sqrt{\frac{2T}{m_H}}. \tag{5.3}$$

Here ρ is the background density and v is the mean velocity of the hydrogen atoms (which scales with the square root of the temperature) and m_H is the mass of a hydrogen atom. As the universe expands both the matter density and the temperature of the matter fall, resulting in a lower flux onto the nuggets. In a matter dominated universe the temperature drops with the square of scale factor while density falls as the third power. The matter flux at redshift z may then be expressed as

$$\frac{dE}{dt\ dA} = \rho_0 c^2 v_0 (1+z)^4. \tag{5.4}$$

The transport of thermal energy across the nuggets occurs rapidly in comparison to the Hubble time, so it may safely be assumed that the nuggets will remain in thermal equilibrium as the universe expands. The total thermal emissivity of the nuggets, as a function of temperature, is given in appendix C, equation C.5. Under the assumption of thermal equilibrium, this emission rate must be directly proportional to the flux of energy into the nuggets, as given in equation 5.4. The exact proportionality will depend on the efficiency with which the background matter is converted to thermal energy. This, in turn, depends on the thermal properties of the nuggets as well as the physics of the early universe plasma. Rather than introducing this constant of proportionality as a phenomenological parameter, it is more intuitive to note that, once its value is fixed at any point in the cosmological history, the subsequent evolution of temperature, as a function of redshift, is given by expression 5.4. As such, we may equivalently take the temperature of the nuggets at the time of last scattering as a phenomenological parameter to be estimated from observed data. In this case, the temperature evolution is given by,

$$T(z) = T_{LS}\left(\frac{1+z}{1+z_{LS}}\right)^{17/4} \tag{5.5}$$

where the subscript LS denotes values at the surface of last scattering. The effective radiating temperature of the nuggets at the time of last scattering is, in principle, calculable from first principles within the context of a specific quark matter model. However, the inherent uncertainties in such a calculation make it unjustified at the present level of analysis. Instead, I will use a comparison with microwave emission from the galactic centre (which was argued in section 3.2 to be attributable to the same thermal emission process) to make a consistency argument that, if the microwave excess observed from the galactic centre arises through the interaction of the interstellar plasma with nuggets of quark antimatter, then the same process will necessarily produce a cosmological background at the observed scale.

The similarity in temperature in the galactic centre and at the time of last scattering may be seen by estimating the energy flux onto the nuggets in these two different environments. The estimation of the nugget contribution to the galactic spectrum made in [43] adopted a typical visible matter number density, in the galactic centre, of $n_{vm} \sim 150\text{cm}^{-3}$ and assumed an interstellar medium dominated by hydrogen, and a velocity at typical galactic scales of $v \sim 200\text{km/s}$. In this environment the energy flux onto the nuggets will scale as

$$\rho v \approx \left(150\frac{\text{GeV}}{\text{cm}^3}\right)\left(2\times 10^7\text{cm/s}\right) = 3\times 10^9\frac{\text{GeV}}{\text{cm}^2\text{s}}. \tag{5.6}$$

At the time of last scattering the photons decouple from the baryonic matter. Up until this moment the photons are thermally abundant, afterwards the photon number density dilutes with the expansion in the same way as the baryon density, so that the baryon to photon ratio, η given in equation 1.1, remains fixed. At last scattering the motion of the baryonic matter is primarily thermal. Under these conditions the matter flux onto the nugget must scale as,

$$\rho v \approx \eta n_\gamma\sqrt{\frac{2T}{m_p}} \approx 3\times 10^8\frac{\text{GeV}}{\text{cm}^2\text{s}}. \tag{5.7}$$

Noting the similar scales of equations 5.6 and 5.7, as well as the fact that the temperature scales as only a weak $(\sim 4/17)^{29}$ power of the energy flux, we should anticipate that the temperature reached by the nuggets in the early universe should be similar to, if slightly lower than, that reached in the galactic centre where they were estimated to have a temperature of $T \sim 1\text{eV}$ [43].

5.2 The isotropic radio background

Combining the emission spectrum of a quark nugget at a given temperature, from expression C.4, with the redshift evolution of nugget temperature, from expression 5.5, allows us to determine the contribution of quark nugget dark matter to the isotropic radio background. This may be done by integrating each individual nugget's contribution over the entire dark matter distribution back to the time of CMB formation. A full treatment of this process would include the reheating of the nuggets, as a result of structure formation at late times. While technically possible, such a calculation would be computationally expensive, and would detract from the simplicity of the basic ideas presented here. Instead, I will neglect the effects of structure formation and consider an isotropic universe, in which the nuggets' temperature falls with the universe's expansion precisely as given in expression 5.5[30].

In the limit in which the universe remains homogeneous, the dark matter contribution to the radio background is given by the line of sight integral, through the increasingly dense dark matter distribution, of the spectral contribution from each distance. This intensity must then be redshifted to the wavelength at which it will appear today. The line of sight integral through the dark matter background is discussed in appendix A.3, and results in an isotropic background intensity given by,

$$I(\nu) = \int \frac{c\ dz}{(1+z)H(z)} \frac{\rho_{DM}}{M_N} \frac{dE}{d\nu\ dt} \left[\nu(1+z), T(z)\right]. \tag{5.8}$$

[29] This scaling differs from the typical fourth root as the nuggets do not emit a standard blackbody spectrum. See appendix C for details.

[30] While this may seem a dramatic simplification it is, to some extent, justified by the fact that the total radio background is strongly dominated by early time emission. Even if the calculations are modified to allow a tenth of the dark matter to reheat to 1eV (the present temperature in the galactic centre) it is found to result in variations in the radio background at only the few percent level. As such, reheating will make little contribution to the scale of the radio background though it may result in slight anisotropies, an analysis of which is beyond the scope of this work and is not strongly motivated by the resolution of present data.

Here H is the Hubble constant and M_N is the average mass of a nugget so that $n_{DM} = \rho_{DM}/M_N$ is the dark matter number density. The emission spectrum, $\frac{dE}{d\nu\, dt}$, is as given in equation C.4 and is to be evaluated at the temperature of the nuggets at redshift z, and at the frequency $\nu(1+z)$ that is redshifted to the present day observed value ν. The low energy cutoff, as given in expression C.3, will also be redshifted to lower energies so that we should expect little or no spectral contribution below $\sim$ 6MHz, the observed frequency today of a photon emitted at the minimum allowed frequency in the early universe.

Rather than dealing directly with the measured intensity this discussion will follow the analysis of Arcade 2 [39] and convert the measured intensity into an apparent sky temperature. This is done by assuming that the sky acts as a blackbody emitter (as it does in the case of the CMB) and inverting the Planck spectrum to find the temperature which would account for the intensity at a given wavelength. In this representation a universe with no radio background apart from the CMB contribution would have an observed sky temperature of 2.7K across all frequencies. The presence of any type of cosmological radio sources will then produce sky temperatures above this value across the frequencies over which they emit.

Figure 5.1 shows the sky temperature values reported by Arcade 2 as well as those extracted from earlier radio maps by the Arcade group. The best fit power spectrum determined in [39] is then plotted over this data. The strong rise in the isotropic radio background above the CMB contribution, after subtraction of the galactic foreground, can clearly be seen[31].

Having established the basic properties of the observed isotropic radio background it is now possible to assess the contribution which quark nugget dark matter could make to this spectrum. Based on the arguments of section 5.1 the initial temperature of the nuggets should be expected to fall in the range 0.1eV $< T_{LS} <$ 1eV. As the baryon number of the nuggets increases the spectral contribution falls, due to the decreasing dark matter number density, as can be seen in equation 5.8. Demanding that the nugget contribution to the isotropic radio background does not exceed the Arcade 2 data, while also having an initial temperature in the physically acceptable range, requires that the nuggets have a baryon number larger than $B \sim 10^{24}$ but does not produce an upper limit on the baryonic charge. However, to associate the Arcade 2 excess with emission from the nuggets,

[31] As this plot shows measured temperature as a function of frequency a CMB dominated spectrum would remain flat at T=2.7K across all frequencies as opposed to the power law rise in temperature at low frequencies.

while constraining the initial temperature to be less than 1eV, requires a baryon number less than $B \sim 10^{28}$. Obviously, a larger nugget size cannot be ruled out, but these objects would have no observational consequences at the frequencies covered by ARCADE 2[32]. Within the range of mean baryon numbers from 10^{24} to 10^{28} the nuggets may produce some or all of the excess radio band emission observed by ARCADE 2. A representative spectrum for nuggets (with $B = 10^{25}$ and initial temperature $T_0 = 0.2$eV) is included in figure 5.1 and, as can be seen, is able to match the observed rise in sky temperature across the ARCADE 2 range.

For the background sky temperature extracted from the pre-existing sky maps of [54, 87, 103, 104]. The resulting temperature estimates are likely to contain at least some contamination from the galactic foregrounds, but certainly set an upper limit on any extragalactic contribution. The trend of increasing effective sky temperature at lower frequencies, observed in the ARCADE 2 data, is seen to continue down to the $\sim$ 10MHz scale.

It should be noted that the low energy cutoff in the spectrum, discussed in appendix C, is likely to be considerably more complicated than the hard cutoff imposed here. As such, the spectrum should be considered only a rough estimate near its low energy peak. A more complete treatment of the finite size effects that lead to this cutoff could alter the details of spectrum at low energies. Even given these uncertainties, it may be seen that the contribution of quark nugget dark matter to the isotropic background fall below the constraints imposed by low frequency observations, and may contribute, in part, to the radio excess argued for in [39] and [46].

5.3 Conclusions

The consequences of quark nugget dark matter have now been investigated in a range of environments, both galactic and cosmological, and across a wide range of energies, from MHz radio emission up to γ-rays in the tens of MeV range. In each case, the predicted diffuse emission associated with the nuggets has been found to be entirely consistent with observational data. In fact, this dark matter model may offer a single mechanism capable of explaining the origin of several observed emission features. These were previously thought to be unrelated, and each requires substantial modifications to predicted astrophysical spectra to explain.

[32]For nuggets with $B > 10^{30}$ the nugget contribution to the radio background remains well below the CMB contribution down to the cut off frequency of the spectrum. As such these objects would remain unobservable for the foreseeable future.

It is important to note that this model was not introduced in order to explain any of these observed sources of diffuse emission, but was instead proposed as a solution to cosmologically motivated questions about the nature of dark matter and baryogenesis. The only unknown parameter within this model is the mean baryonic charge of the nuggets, and thus their number density. This unknown factor will scale the total strength of each of the emission mechanisms discussed above, but will not alter the shape of the actual spectrum. Once the scale of one emission source, for example the strength of the galactic 511keV line, is established the relative scales of all other spectral contributions are also fixed.

Possible future experiments may more tightly constrain the strength and morphology of the various diffuse emission sources discussed here. This experimental progress will, necessarily, have to be accompanied by a deeper understanding of the contribution of known astrophysical sources to the various diffuse backgrounds. However, it is difficult at present to take these signals as more than suggestive of particular models or ideas. The uncertainty remaining in both the measurements themselves, and particularly in the astrophysical backgrounds, means that attributing any particular observation to dark matter is necessarily speculative. Even in well studied examples of a known diffuse excess, such as the galactic 511keV line, numerous explanations have been offered. Most of these are subject to large enough uncertainties that they would be difficult to distinguish, even with significantly improved observational data.

Given the inherent difficulties of this sort of analysis, it makes sense that it be complemented by direct searches for dark matter. The prospects for applying this type of detection to quark nugget dark matter will be the subject of the remainder of this work.

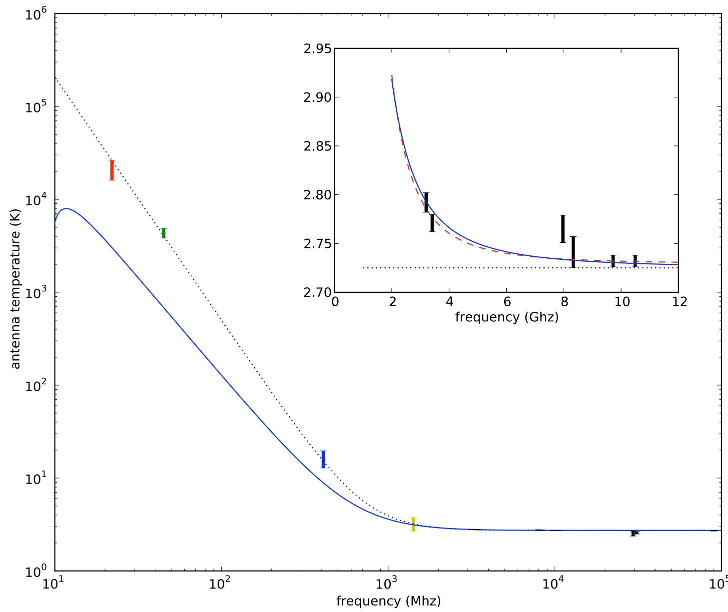

Figure 5.1: Antenna temperature as extracted from Rogers and Bowman [104] (red), Maeda *et al.* [87] (green), Haslam *et al.* [54] (blue), Reich and Reich [103] (yellow) and the ARCADE2 data [39] (black). The data is overlaid with spectra calculated from equation 5.8 for nuggets of baryonic charge $B = 10^{25}$ and an initial temperature $T = 0.2$eV chosen for a best fit to the high frequency ARCADE2 data. The dotted line is the best fit obtained in the ARCADE analysis, as given in equation 5.1.
Insert: The background temperature, as a function of frequency, measured by ARCADE 2 [39] showing the reported GHz scale excess. This data is overlaid with spectra calculated from equation 5.8 for nuggets with baryon number $B = 10^{25}$ (blue) and the best fit curve of equation 5.1 (red). A variation of this plot was originally published in [81].

Chapter 6

Direct Detection

6.1 Introduction

The indirect detection techniques discussed in previous chapters may offer hints as to the nature of the dark matter, and the observations behind them have certainly inspired a wide range of dark matter models apart from the one discussed here. However, while these unexpected excesses in diffuse emission are difficult to explain through known astrophysical processes, particularly when considered collectively, it remains possible to fit this data through significant modification of the background astrophysics. As the exact nature of the relevant astrophysical processes remains an open research question, it is difficult to know to what degree, if any, dark matter must be invoked to explain the galactic and cosmic diffuse backgrounds. Even if the contributions of conventional astrophysical sources were known precisely, it is possible that any remaining dark matter signature could be fit by a variety of alternative models. This is particularly true of models with an extended dark sector involving a large number of tunable parameters[33]. As such, indirect dark matter searches are strongly complemented by parallel direct searches. These involve contact between a detector and the dark matter itself, rather than the light produced by its interactions, and may provide a cleaner detection signal and a greater ability to distinguish between alternate dark matter models. The following discussion is based on original research conducted as a component of this thesis and closely follows the results first published in [73, 77].

There are, at present, many dark matter searches underway around the world [11, 22, 31]. There have been several intriguing results from this

[33]It is generally assumed that the dark matter consists of a single particle type, left as a relic from the early universe. In this case its self interactions would be limited to the annihilation of particle antiparticle pairs. However, in attempts to explain observations such as the diffuse emission discussed here, the DAMA annual modulation [31] and the apparent positron excess observed by PAMELA [10] and AMS [12], dark matter models involving an extended dark sector involving many particle types have been introduced to allow for a richer phenomenology than is possible with a single dark matter particle species.

search program, for example the DAMA experiment [31] at the Gran Sasso laboratory has observed an unexplained seasonal variation in particles hits. This type of seasonal variation is expected as the earth's velocity relative to the dark matter distribution varies with motion around the sun. This was assumed to be a signal clearly attributable to dark matter interactions and its detection over many years and with the correct phase for a dark matter signal, would seem strong evidence for dark matter detection. This strong detection signal is, however, problematic. The DAMA result favors a light ($M \sim 10$GeV) dark matter particle mass and a nucleon scattering cross section at the $\sigma \sim 10^{-40}\text{cm}^2$ level. However, much of the allowed parameter space is excluded by non-detection in collider searches and by higher sensitivity direct dark matter searches, such as CDMS [13] and XENON [21]. Conversely, the CoGeNT experiment reports an excess of low energy, single-hit detector events which may be consistent with a light dark matter particle with similar properties to those required to explain the DAMA oscillation [2]. The CoGeNT signal also seems to show a seasonal variation with a phase similar, though not identical, to that of DAMA [1]. In light of their confusing, and partially contradictory, observations the results of these various underground cryogenic experiments will be taken as interesting, though far from conclusive.

The main focus of the underground direct detection search program is the rare interactions of WIMP scale dark matter passing through a detector. Given the relatively large flux, as expressed in equation 1.2, and the small interaction cross section of WIMP dark matter, these experiments attempt to push the sensitivity limit in as large a detection mass as possible. However, even the largest present or proposed dark matter searches do not have the multiple square kilometer detector dimensions capable of placing meaningful limits on the presence of very high mass dark matter such as the model considered here. Instead, this work will focus on the largest area particle physics detectors available and their prospects for detecting this class of heavy dark matter.

The most important experiments in this context are those designed to study ultrahigh energy cosmic rays[34]. In recent years there has been significant interest in the study of the origin and propagation of cosmic rays at the highest energies. Experiments targeting these ultrahigh energy cosmic rays are particularly interested in gathering statistically significant numbers of

[34]There have previously been several searches for a flux of high mass neutral objects such as strangelets or monopoles but none impose serious constraints in the mass range considered here. A review of several of these experiments and the resulting mass and flux bounds are given in [23].

events at or above the Greisen-Zatsepin-Kuzmin (GZK) cutoff in the cosmic ray spectrum[35]. The flux of cosmic rays falls with energy as a simple power law over many orders of magnitude up to the GZK cutoff which occurs near a flux of roughly one per square kilometer per year and steepens the spectrum significantly at higher energies. Consequently, the detectors intended to study these events must have areas at or above the square kilometer scale if they hope to provide statistically significant data on cosmic rays at relevant energies. This scale is of interest not only for cosmic rays physics but also, I will argue, may prove useful in the search for quark nugget dark matter.

Ultrahigh energy cosmic rays are detected via the extensive air shower they initiate through the particle cascade extending downward from the first collision between the ultrahigh energy primary and the molecules of the upper atmosphere. The developing air shower may be detected by particle detectors on the ground, which directly observe any secondary particles reaching the earth's surface, through atmospheric fluorescence generated as the passage of charged particles excites UV band transitions in the surrounding nitrogen molecules or, through the radio emission generated by the large number of secondary charged particles moving through the earth's magnetic field.

In order to extract meaningful limits on the flux of quark nugget dark matter from cosmic ray observatories it is necessary that their passage through the atmosphere initiate a large scale air shower, which may be detected, rather than a highly concentrated energy release which, while possibly quite intense, would not lend itself to this type of detection. The remainder of this work will be devoted to the phenomenology of the air shower associated with the passage of a quark nugget through the atmosphere and will argue that the rate of these events may be strongly constrained with data from the current generation of cosmic ray experiments.

A nugget of quark matter passing through the atmosphere at galactic velocities will interact primarily through the elastic scattering of atmospheric molecules, possibly generating some amount of ionization. As the scattered particles remain at relatively low energies, the trail of accelerated molecules will be limited to roughly the cross section of the nugget rather than triggering a much larger air shower. If we assume that every molecule along the nugget's path is accelerated to a typical galactic velocity of $v_N \sim 200$km/s

[35]The GZK cutoff is a feature in the cosmic ray spectrum above 10^{19}eV originally predicted in 1966 [52, 124] and only recently observed [3, 4]. It is due to the limiting of the cosmic ray horizon by the scattering of cosmic rays off the CMB above the threshold for photo-pion production.

then the total deposited energy will be on the order of a few joules[36]. These events will release most of their energy low in the atmosphere, and at difficult to observe thermal levels. Consequently, they will have little or no detectable signature for a detector whose primary target is high energy cosmic rays. Conversely, a nugget composed of antiquarks will annihilate much of the atmospheric material in its path and the products of these annihilations, many of which will be produced at nuclear scale energies, may be capable of initiating a much larger shower of high energy secondary particles. The maximum total energy generated by a quark nugget can be estimated by assuming that all the matter lying in its path is annihilated and that the energy released is twice the energy equivalent of this atmospheric mass:

$$\Delta E \approx 2\pi R_N^2 X_{at} c^2 \approx 10^7 \mathrm{J} \left(\frac{R_N}{10^{-5}\mathrm{cm}} \right)^2 . \tag{6.1}$$

Here $X_{at} \approx 1\mathrm{kg/cm}^2$ is the total atmospheric depth and R_N is the radial size of the nugget. This is obviously a substantial amount of energy and, though much of it will be thermalized within the nugget or emitted in difficult to detect channels, it is easily capable of producing a signal which may be observed with a range of present experiments. The following sections will discuss the physics of the passage of a quark nugget through the earth's atmosphere and extract the basic observable properties of such an event.

6.2 Air shower production and scale

The primary interaction of a nugget of quark matter will be nuclear annihilations involving atmospheric molecules. Any initial imbalance between the rate at which molecular electrons and nuclei annihilate will quickly be compensated by a net charge developed by the nugget. As such, it is safe to assume that electron and proton annihilations proceed at essentially the same rate.

Electron annihilations will proceed in much the same way they do in the much lower density environment of the interstellar medium, so much of the analysis of the previous chapter is directly applicable. The majority of these

[36]The nuggets carry substantial momentum relative to the much lower density atmosphere so that their velocity is essentially unaltered as they travel downwards. Assuming that the entire atmospheric column swept out is accelerated to the velocity of the incoming nugget then the kinetic energy loss is simply given by the ratio of the mass of this air column to that of the nugget. Using typical nugget parameters the fractional change in kinetic energy is $\Delta T/T \sim 10^{13}/B$ which is negligible across the allowed range of nugget baryon number.

annihilations will result in the production of photons in the energy range 0.1-10MeV. These photons contribute to the electromagnetic component of the shower.

Tracing the energy generated by nuclear annihilations is a more complicated problem. As previously discussed, the majority of the energy generated will be thermalized within the nugget, to eventually be emitted as thermal photons with a spectrum as given in equation C.4. Annihilations happening near the nugget's quark surface produce hadronic jets, which cascade down to lighter modes of the quark matter. Much of this energy will be dissipated as the charged components pass through the electrosphere, resulting in x-ray emission as discussed in section 3.3. Hadronic components of the annihilation jets are likely to remain bound to the nugget, while electrons and positrons will either annihilate or be captured within the high density layers of the electrosphere. The only components to escape the nugget are likely to be secondary muons generated in annihilations very near the quark surface. All other particles are likely to eventually transfer their energy to some form of photon emission from the nugget electrosphere.

First, consider the thermal evolution of the nugget as it passes through the atmosphere. Before entering the atmosphere the nugget will have a temperature of $\sim$ 1eV as discussed in section 3.2. As it annihilates atmospheric material some fraction (which I label f_T as in section 3.2) of the released energy will thermalize within the quark matter. The thermalization process will occur on QCD timescales, much shorter than the evolution of the atmospheric density along the nugget's path, so we may safely assume that the nugget will remain in radiative equilibrium as it crosses the atmosphere. That is, the rate at which energy is deposited in the nugget should be balanced by its net thermal radiation as given by expression C.5. This can be translated into a temperature evolution in terms of the surrounding atmospheric density:

$$\left(\frac{T}{10keV}\right)^{17/4} = \left(\frac{\rho_{at}(h)}{5 \times 10^{-2}\mathrm{kg/m}^3}\right)\left(\frac{v_N}{200\mathrm{km/s}}\right) f_T. \tag{6.2}$$

Given that the atmospheric density at ground level is $\rho_{at} \approx 1.2$ kg/m^3, this implies a maximum nugget temperature of roughly 20keV provided that all matter swept up by the nugget fully annihilates.

There is, however, an upper limit to the rate at which atomic scale matter can be forced onto the quark surface. As the flux of matter onto the surface increases, so must the flow of energy away from the surface. Independent of the exact mechanism of outward energy transfer it must, at some level, impede the inward flow of matter, setting up a feedback mechanism by which a maximum annihilation rate is established. The temperature at which the annihilation rate saturates was estimated in [73] based on the rate of inelastic scattering of positrons off of an incoming molecule. This analysis suggested $T_{max} \sim 10$keV. However, as pointed out in [50] this analysis did not consider the photoionization of surrounding matter, an effect which may increase the maximum temperature by an order of magnitude. A more precise estimation of the maximum temperature reached by the quark nugget while it crosses the atmosphere requires a detailed treatment of the plasma surrounding the nugget by the time it reaches the lower atmosphere. As the evolution of this plasma will influence the emission spectrum of the nuggets its development remains an important open question. Despite this remaining uncertainty it is possible to extract a rough phenomenological description of the air shower's development based on a simplified set of energetic constraints.

One crucial feature of the development of a quark nugget induced air shower is the timescale over which it will develop. In a conventional air shower, initiated by a single ultrahigh energy proton or nucleus, all of the shower components are ultrarelativistic and move at essentially the speed of light. The resulting shower thus crosses the entire atmosphere on a $\sim 10\mu s$ timescale. All observables related to the shower should occur over timescales shorter than this. In the case of a quark nugget initiated shower, the secondary particles emitted by the nugget will move at the speed of light but the nugget itself, which sources the surrounding shower, moves at galactic scale velocities, some three orders of magnitude slower. Consequently, the air shower initiated by a quark nugget will develop on a much slower $\sim$ ms timescale.

Beginning with this qualitative picture of air shower development, it is possible to estimate some of the most important observable properties of a quark nugget induced air shower relevant for cosmic ray observatories.

The scale of an air shower, generated by an antiquark nugget passing through the atmosphere, will depend on the rate of nuclear annihilations within the nugget. As this rate increases with atmospheric density, rather than depth, the shower develops deep in the atmosphere where the density is well modeled as an exponential decay with height

$$n_{at}(h) = n_0 e^{-h/H} \tag{6.3}$$

with a typical scale height $H \approx 7.5$km and a surface nucleon density of $n_0 = \rho_0/m_N \approx 7\times10^{20}$ cm^{-3}. If we neglect the thermal saturation effect discussed in the previous section the rate of nuclear annihilations is simply given by the product of the nugget cross section and velocity with the atmospheric density:

$$\Gamma_{an} = \pi R_N^2 v_N n_{at}(h). \tag{6.4}$$

This would result in an annihilation rate $\sim 10^{18} s^{-1}$ near the surface. If, however, the annihilation rate saturates at a temperature T_{max} then the maximum annihilation rate may be obtained by solving expression C.5 for the rate at which annihilating material must deposit energy :

$$\Gamma_{an} = \frac{1}{m_N c^2}\frac{dE}{dT} = \frac{64}{3}\alpha^{5/2}\frac{R_N^2 T_{max}^4}{m_N}\sqrt[4]{\frac{T_{max}}{10\text{keV}}} \tag{6.5}$$

$$\approx 2\times 10^{17} s^{-1}\left(\frac{R_n}{10^{-5}\text{cm}}\right)^2\left(\frac{T_{max}}{10\text{keV}}\right)^{17/4}. \tag{6.6}$$

Figure 6.1 shows the annihilation rate as a function of height in the atmosphere.

This analysis of the annihilation rate sets the energy scale available to drive air shower development at a given height. Having established this scale it is now necessary to determine how efficiently this energy can propagate out from the nugget and create the type of large scale events to which cosmic ray detectors are sensitive.

As stated above, the annihilation of electrons results in the production of high energy photons across the x-ray and γ-ray bands. The majority of the energy released in nuclear annihilations is thermalized within the nugget and subsequently radiated according to the thermal spectrum given in equation C.4. Of the energy emitted directly from the annihilation point without thermalizing the majority is transferred to surface positrons which then radiate in the x-ray band as discussed in section 3.3. Finally, some small fraction arising from annihilations very near the surface will release high energy particles with near the GeV scale.

Hadronic particles are strongly coupled to the quark matter, and are unlikely to escape the nugget. Electrons and positrons created in nuclear annihilations are unlikely to be able to penetrate through the high density electrosphere, with the electrons rapidly annihilating as was discussed in section 3.5 and the positrons being rapidly decelerated as discussed in section 3.3. As such, the only charged particles likely to be able to escape from the nugget and propagate through the atmosphere in significant numbers are high energy muons produced in nuclear annihilations very near the quark surface. Thermal photons will be readily emitted from the outer regions of the electrosphere and higher energy photons may escape from deeper within the nugget where they are generated by either nuclear of electron-positron

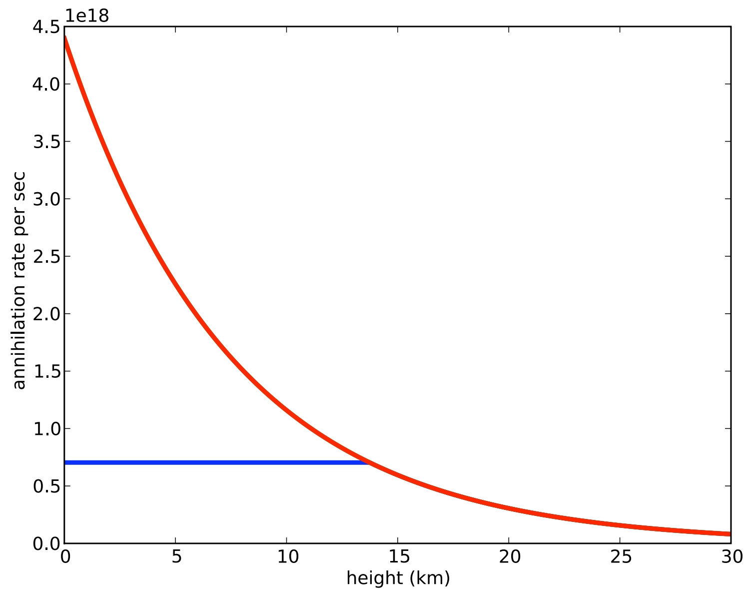

Figure 6.1: The total rate of nuclear annihilation as a function of height in the earth's atmosphere. The red curve assumes no saturation of this rate and exactly follows expression 6.4. The blue curve assumes a thermal saturation effect that switches on at a nugget temperature of T = 15eV.

annihilations. As the temperature of the nuggets in the lower atmosphere may be as high as a few tens of keV, the majority of the radiation emitted by the nuggets will be in the form of x-rays. There will also be a much smaller component of higher energy photons with energies up to about 1GeV. At lower energies the very flat thermal spectrum means that there will also be non-negligible emission right down to radio frequencies.

The atmosphere is relatively opaque to high energy photons, so that the majority of emitted radiation will be absorbed quite close to the nugget. This will produce a localized ionization trail, but will not lead to emission on a large enough scale to present a clear target for large cosmic ray detectors. For present purposes, I will focus on the high energy muons and the long wavelength radiation which is capable of propagating over long distances in the atmosphere.

The production of low energy photons is governed by the thermal spectrum in expression C.4, and the nugget's temperature evolution is as given in equation 6.2. The production of muons is more difficult to estimate. A relativistic muon may be produced directly in a nuclear annihilation, but this process is disfavored relative to the production of strongly coupled mesons or other light superconductor modes. As a rough estimate of the scale of this process we may assume that the production of electromagnetically coupled particles is suppressed by a factor of $(\alpha/\alpha_s)^2$ where $\alpha = 1/137$ is the fine structure constant and α_s is its order one strong force equivalent. This suppression factor would imply that the probability of producing a muon is smaller than annihilation to more strongly coupled modes by a factor of at least 10^4. Assuming that high energy muons are produced at this level we would expect roughly one muon to be produced in every 10^4 events involving non-thermal emission which in turn represent roughly a tenth of all annihilation events. Assuming that this is the only mode of muon production, the rate of muon production will be given in terms of the total annihilation rate by approximately $10^{-5}\Gamma_{an}$. There are, however, other processes which are capable of producing high energy muons such as the decay of a meson-like excitation very near the quark surface. The range of mechanisms which may lead to emission of a relativistic muon is large and rather complicated, and will depend on the form of quark matter realized near the nugget's surface. For the purposes of this analysis I will comress all of this information into a single muon production factor f_μ defined so that the rate of muon production is given by

$$\Gamma_\mu = f_\mu \Gamma_{an}, \tag{6.7}$$

where I will assume $f_\mu \geq 10^{-5}$ though it is not likely to greatly exceed this value. Taking f_μ at this scale would give a production rate of $10^{12}s^{-1}$ deep in the atmosphere. While muon production may be strongly suppressed the sheer number of annihilations leads to the production of a large number of relativistic charged particles surrounding the nugget.

6.3 Atmospheric fluorescence

One of the primary detection techniques for high energy cosmic rays is through the observation of atmospheric fluorescence generated as charged particles move through the atmosphere. A relativistic particle dissipates energy along its path through the excitation and ionization of stationary background molecules. For nitrogen molecules, which constitute the majority of the atmosphere, excitation by a charged particle is followed by radiative de-excitation emitting light in the UV band with wavelengths $\lambda \sim 300 - 430$

nm. As the atmosphere is relatively transparent to UV radiation this fluorescence light may be used for detection of cosmic rays of sufficient energy to produce a large number of secondary particles. This radiation is emitted isotropically from the track of excited nitrogen molecules left in the shower's wake so that it may be observed from positions well off the shower axis (as opposed to Cherenkov radiation, for example, which is also produced by relativistic particles moving through a medium, but which is emitted in a forward directed cone.) The total fluorescence yield is proportional to the total number of charged particles in the shower so that its intensity directly traces shower development. The main drawback of this detection technique is that the fluorescence light is relatively faint and can only be observed on clear moonless nights. These restrictions give fluorescence detection a duty cycle of only about 10%.

There are currently several large experiments which use this technique to detect high energy cosmic rays including the Pierre Auger Observatory [5] and the Telescope Array [115].

As discussed above, the air shower initiated by an antiquark nugget will be dominated by ultrarelativistic muons emitted in annihilations near the quark matter surface. These are generated at a rate given by expression 6.7 and, from this estimate of muons production at a given height, it is possible to predict the fluorescence yield of these muons. The motion of charged particles through the atmosphere is rather complicated and, as such, the details of their treatment have been relegated to appendix D to better concentrate this discussion on the most fundamental properties of the shower.

The rate at which muons are produced will scale with the atmospheric density, becoming quite large near the surface. However higher atmospheric density also reduces the average distance that each muon travels. As argued in appendix D, the drop in scattering cross-section with energy implies that high energy muons lose very little of their total energy before they decay. As such, this length scale is independent of the height at which the muon is initially produced. However, muons at lower energies may lose enough energy to be stopped by collisions with surrounding matter in the lower atmosphere. This means that the average path length of a muon is dependent on the energy spectrum with which the muons are emitted.

If we consider a model in which all muons are injected at typical QCD scales with about a GeV of energy, the energy loss to the atmosphere slows the muons only negligibly and the total number simply decays exponentially over the muon decay length ($l_d \approx 7$km in this case.) In this case the number density of particles as a function of radial distance from the nugget and the angle between the observer and the direction of nugget motion is,

$$n_\mu(r, \phi) = \frac{\Gamma_\mu}{2\pi r^2 c} \cos\phi \; e^{-r/l_d}. \tag{6.8}$$

This expression uses the radial dependence of muon emission given in equation D.7. For demonstrative purposes, consider the case of a nugget whose motion is vertically downwards as this will allow us to discuss the shower properties in a relatively simply geometric case. More general cases may be dealt with using an identical procedure, a more complicated geometry would simple obscures the basic arguments on which I want to focus. In the vertical geometry we may parameterize the muon distribution purely in terms of height (h) and distance from the shower core (b):

$$n_\mu(\Delta h, b) = \frac{\Gamma_\mu}{2\pi c} \frac{\Delta h}{(b^2 + \Delta h^2)^{3/2}} \exp\left(-\frac{\sqrt{b^2 + \Delta h^2}}{l_d} \right). \tag{6.9}$$

Here I have defined $\Delta h = h_N - h$ as the difference between the height of the nugget and the height at which muon density is being evaluated. We may then integrate this expression over all b values to get the area integrated flux of particles at a given height :

$$\frac{dN_\mu}{dt} = 2\pi c \int_0^\infty n_\mu(\Delta h, b) \cos\phi \; b \; db = \frac{\Gamma_\mu \Delta h^2}{l_d^2} \int_{\Delta h/l_d}^\infty \frac{e^{-x} dx}{x^4}. \tag{6.10}$$

The exponential integral is easily evaluated numerically and the resulting integrated flux, as given by expression 6.10 assuming that the annihilation rate does not saturate at large atmospheric densities, is shown in figure 6.2.

We may also use this expression to find the total number of particles which will move past a given height over the course of the entire shower. To do this one simply integrates the muon flux at a given height over the entire time that the nugget spends above that height in the atmosphere:

$$N_\mu = \int_h^\infty \left(\frac{dN_\mu}{dt} \right) \frac{dh_N}{v_N} \tag{6.11}$$

where the integrated flux $\frac{dN_\mu}{dt}$ is as given in equation 6.10. This expression gives a scale for the total number of charged particles contributing to atmospheric fluorescence over the entire duration of the shower. The results of this integration are shown in figure 6.3.

This gives a basic idea of the scale of the shower, but we may also consider geometries more complex than in this simple estimate. Consider, for

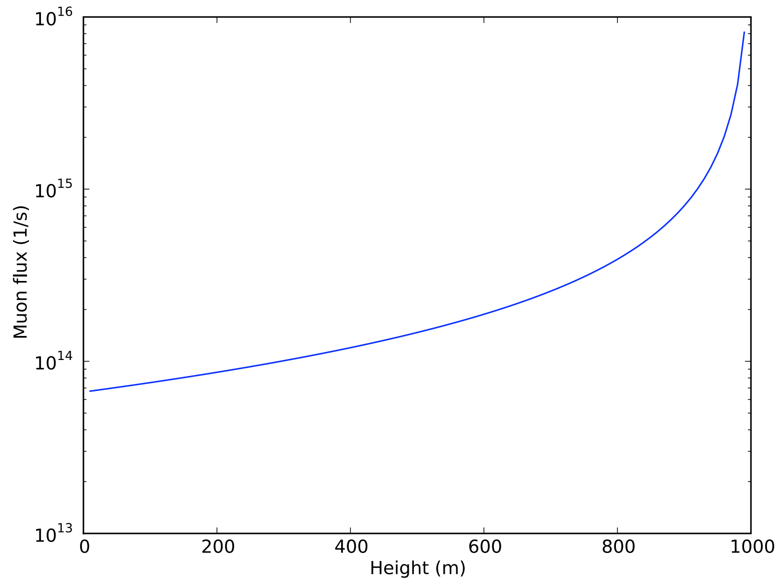

Figure 6.2: Laterally integrated particle flux as a function of height when the antiquark nugget is at a height of 1km. This example uses a constant muon injection energy $E_\mu = 1\text{GeV}$ and takes the thermal maximum to occur below the earth's surface.

example, a case in which the annihilation rate saturates at some height above the earth's surface. If all the shower components are highly energetic then their path length is set by the decay time and the profile simply levels out at a constant particle number after saturation. Less energetic muons may however have their path length limited by energy loses to the atmosphere. If the shower involves a sufficient number of marginally relativistic muons their decreasing path length near the surface will cause the total shower size to shrink near the surface much as it does in a conventional cosmic ray shower. For example [73] considered a model in which the muons rapidly lose energy to the surrounding positrons as they pass through the electrosphere. In this case the energy spectrum is peaked near the plasma frequency of the high density regime of the electrosphere but includes a high energy tail :

$$\frac{dn_\mu}{dk} = \frac{1}{\omega_p} e^{(\omega_p - k)/\omega_p}, \quad m_p > k > \omega_p. \tag{6.12}$$

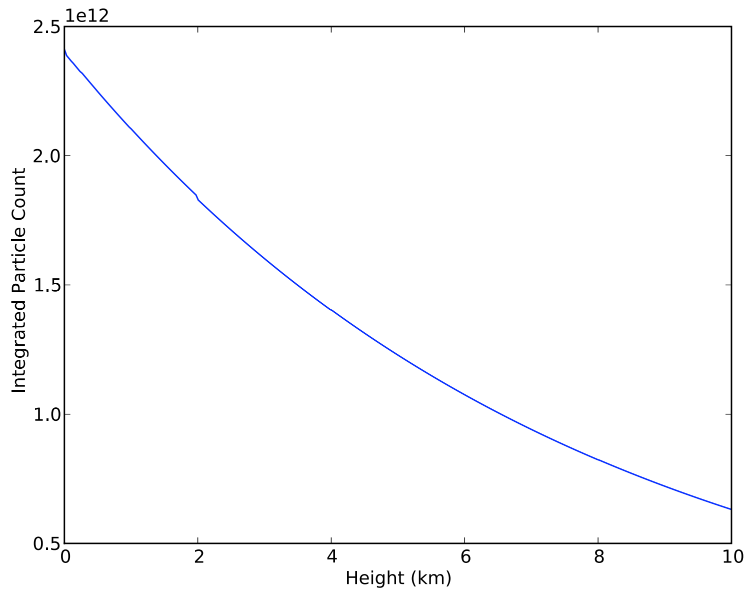

Figure 6.3: Total integrated particle flux as a function of height. This example uses a constant muon injection energy $E_\mu = 1\text{GeV}$ and takes the thermal maximum to occur below the earth's surface and is the total shower integrated counterpart to figure 6.2.

In this case many of the muons are rapidly slowed in the dense lower atmosphere and the shower size begins to decline as shown in figure 6.4.

For comparison a large cosmic ray shower may have a maximum particle content on the order of 10^{10} or more. As can be seen in figures 6.3 and 6.4 the air shower initiated by an antiquark nugget can easily have a particle content at or above this level. Consequently, the total fluorescence yield should be at levels observable to cosmic ray fluorescence detectors.

The complication in this basic analysis comes in the cuts made to the data based on timing. As the fluorescence light generated by a quark nugget persists over a timescale much longer than that associated with a cosmic ray, it is possible that data cuts made to avoid backgrounds such as meteors or distant lightning may limit the ability of some experiments to detect this type of long duration air shower. The chances of making a detection will be increased if the fluorescence signal is accompanied by a signal in an

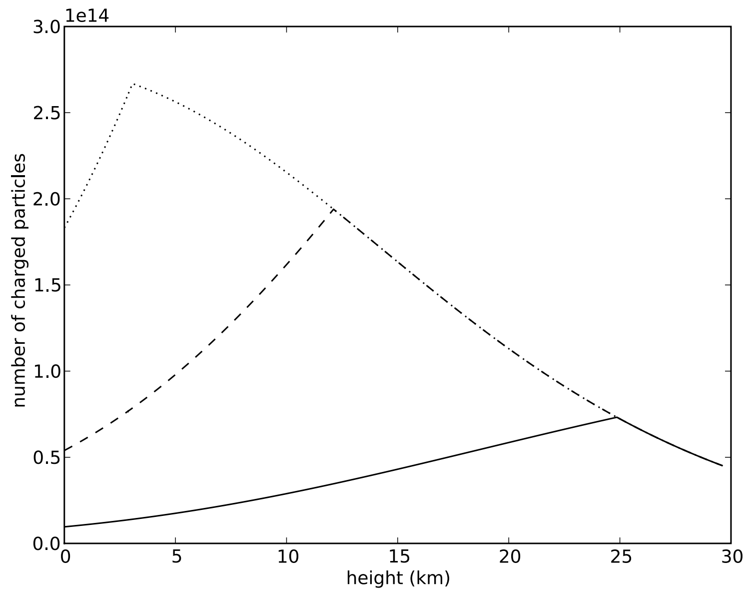

Figure 6.4: Total integrated particle flux as a function of height. This example uses the muon energy spectrum 6.12 and results in a reduction of the total particle count near the surface as low energy muons are lost from the shower. The curves shown are for saturation temperatures of 10keV (solid), 15keV(dashed) and 20keV (dotted). This model also uses a muon production factor of $f_\mu \sim 10^{-3}$ thus the larger overall shower scale. Figure taken from [73].

associated surface detector array. To this end, I will now turn to the surface particle flux associated with an antiquark nugget.

6.4 Lateral surface profile

A complementary cosmic ray detection technique to the fluorescence detection discussed in the previous section involves the use of ground based particle detectors, and is generally referred to as surface detection. An air shower initiated by a cosmic ray of sufficiently high energy will produce a large number of secondary particles as it cascades down towards the earth's surface. Pions produced in the cascade decay before they are able to reach the surface and electrons are quickly slowed by energy loss to the surrounding atmosphere. However, if they are produced at sufficiently large energies, muons produced in the air shower are able to reach the surface in significant numbers [37]. On reaching the surface these particles may be detected using a grid of particle detectors, the properties of the initial cosmic ray may then be reconstructed from the number of particle counts at each station and the arrival time of the particles at different stations. While this procedure gives less information about shower evolution, and requires more extensive modeling to reconstruct the properties of the initial cosmic ray, it has the advantage over fluorescence detection of operating day and night and under most weather conditions and thus has a duty cycle of nearly 100%. For this reason surface detectors gather statistics at roughly ten times the rate of the fluorescence detectors.

On reaching the earth's surface the secondary air shower components are spread into a flat disk with a thickness of 1-10 m depending on the amount of atmosphere through which the shower has passed. This implies that all of the relativistic components of the shower will strike the surface within approximately 10^{-7}s with some electromagnetic shower components trickling in at later times.

Both the Pierre Auger Observatory [19] and the Telescope Array Project [6] have large scale surface detector grids. Auger employs Cherenkov detectors consisting of photomultiplier tubes submersed in tanks of water and spread across 3000 km^2 while Telescope Array uses an array of plastic scintillation panels spread over roughly 700 km^2. The array spacing for Auger is 1.5km while the Telescope Array has a grid spacing of 1.2 km. In order for either of these observatories to trigger on a surface detection event adjacent surface detectors must record particle hits at the same time, thus the surface arrays are only sensitive to events spread over multiple square kilometers[38].

As surface particle detectors are primarily sensitive to relativistic particles distributed across multiple square kilometers they will only detect the muonic component of a quark matter induced air shower [39]. In these show-

[37] The muon has a lifetime of 2.2×10^{-6}s. Most are produced high in the atmosphere where the shower components are energetic enough for pair production to occur and they will be able to travel the tens of kilometers to the surface provided that they are produced with a boost factor of $\gamma \sim 10 - 20$

[38] Both projects have smaller sections of the array where the spacing between surface detectors is smaller, thus allowing for the detection of lower energy showers. These however represent only a small fraction of the total array and, for the purpose of a search for quark nugget dark matter, I am interested mainly in the detection capability of the entire area covered by surface detectors.

[39] Obviously if an antiquark nugget were to directly strike a surface detector it would

ers the nugget emits muons with energies of up to about 1GeV which are capable of traveling a few kilometers before they decay. The nugget producing these relativistic muons has a speed of only about 200km/s and the presence of this slower moving primary extends the timescale over which particles will arrive at the surface. The first particle counts in a surface detector will occur when the nugget is still several kilometers above the surface when the highest energy muons it emits are first able to reach the ground. Surface detection will end when the nugget strikes the surface of the earth. Therefore, the difference between the arrival time of the first and last shower components may be as large as a few tens of milliseconds. This timescale is considerably longer than that of a cosmic ray induced air shower and may present difficulties in the triggering of detectors built with the specific parameters of a cosmic ray air shower in mind.

The surface detection of particles emitted from a quark nugget may be studied in much the same way as particle motion through the atmosphere was treated in section 6.3. In particular the approximations leading to the expressions for the charge density in equation 6.9 and integrated flux 6.10 may be directly applied to the case where $h = 0$. It is also useful to know the total number of particle hits received at a detector a given distance from the shower core. I can define a local muon flux as $n_\mu \vec{v}_\mu$ and then take the dot product of this with the surface to get the local flux along the surface as a function of the nugget's height. The total flux over the course of the shower is then given by integrating this expression back along the nugget's path through the atmosphere. If we again work in the simplified geometry where the nugget moves vertically downwards this gives a total particle count of

$$\frac{dN_\mu}{dA}(b) = \int_0^\infty \frac{dh_N}{v_N} c \; n_\mu(h_N, b) \; \frac{\Delta h}{\sqrt{b^2 + h_N^2}}. \tag{6.13}$$

This expression gives the surface flux as a function of radial distance from the shower core, the lateral profile produced is shown in figure 6.5 and the integrated flux arriving at the earth's surface as a function of time during the shower is shown in figure 6.6.

The most important feature of figure 6.5 is its lateral extent. The particles of the air shower arrive at the earth's surface distributed over a multiple kilometer radius. This is of particular importance for the relatively sparse

observe a very large deposit of energy. However, the individual surface detectors have cross sections of only a few square meters so the probability of a direct hit is very small. It is only when taken collectively that the surface array of a cosmic ray detector has a sufficient collection area to impose useful constraints on the flux of quark nuggets.

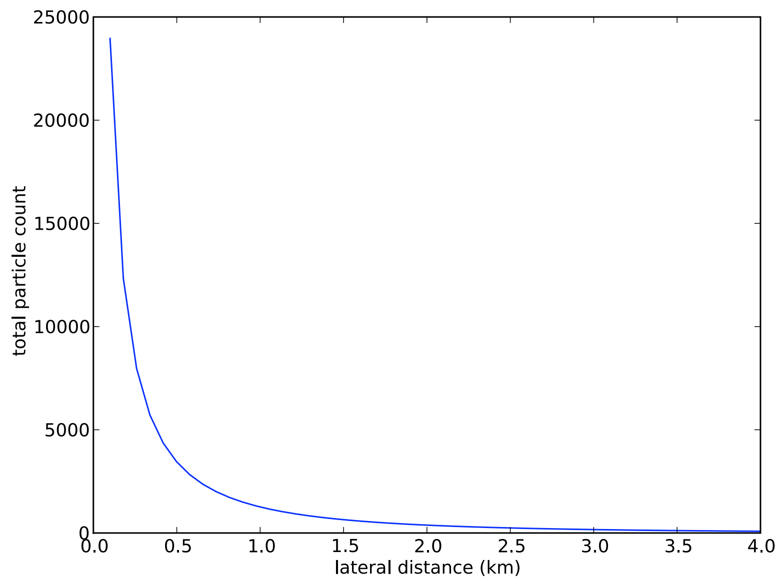

Figure 6.5: Total particle flux received over the entire air shower as a function of radial distance from the shower core.

surface detector grids employed at large scale cosmic ray detectors. If the lateral scale of the shower had been less than a kilometer across it would be unlikely to cause coincidental particle hits in adjacent detectors and, consequently, would not be able to trigger a shower detection. While the timescale involved in the shower is longer than that of a typical ultra high energy cosmic ray initiated shower the particle flux is steeply peaked at late times, as may be seen from figure 6.6.

6.5 Geosynchrotron emission

The same relativistic particles responsible for generating atmospheric fluorescence and triggering surface detectors will also produce a contribution to the radio band emission of the nugget. This occurs as charged particles are deflected by the earth's magnetic field resulting in the emission of synchrotron radiation. A similar effect occurs with the secondary particles of an air shower induced by an ultrahigh energy cosmic ray. Radio detection

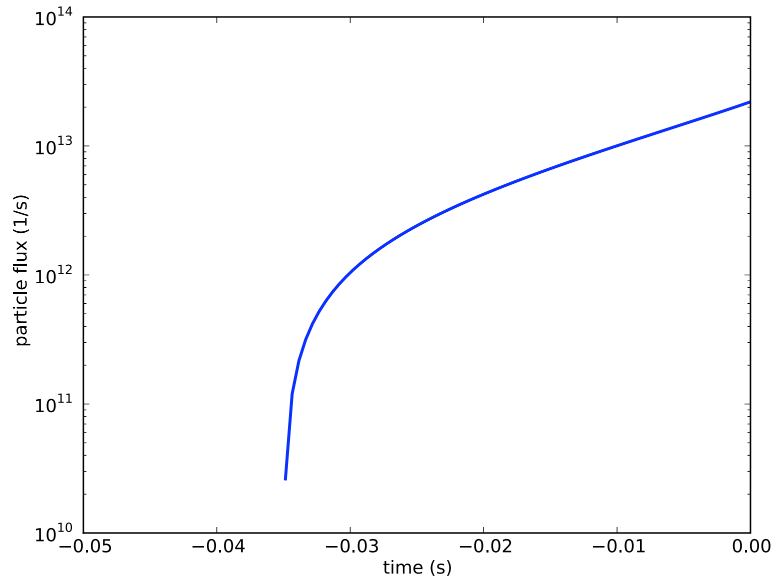

Figure 6.6: Laterally integrated flux of particles recorded at the earth's surface as a function of time. Here the nugget is taken to strike the surface at $t = 0$.

is a promising addition to hybrid detectors as it can operate with a much higher duty cycle than fluorescence detection, which requires clear moonless nights, and is sensitive to many of the same air shower properties. As such, there are several experiments currently operating which use radio detection to study cosmic ray showers [24, 59, 65]. As with the case of fluorescence and surface detection, large scale radio detection arrays also have the ability to set strong constraints on the flux of quark nuggets. This section will outline the basic mechanisms by which the radio band signal is generated, and then use those properties to extract the basic observable quantities associated with such a shower. The results presented here are based on original research published in [77].

The earth's magnetic field near the surface has a strength in the range of a few times 10μT. For this field strength a muon will undergo circular motion with a frequency $\omega_B = eB_0/m_\mu \sim 10^4$ s^{-1}. The muon will only follow this path until it decays, and since the product of this frequency with the muon life time is small $\omega_B \tau_\mu \approx 5 \times 10^{-2}$ we can simplify the problem considerably by taking the limit in which moving charges separate in a linear way within the magnetic field,

$$\vec{v}(t) \approx \vec{v}_0 + \dot{\vec{v}}_0 t \approx \vec{v}_0 + \left(\frac{q}{m\gamma}\right) \vec{v}_0 \times \vec{B}_0, \tag{6.14}$$

where $\vec{v}_0$ is the initial velocity of the charged particle emitted from the nugget. The velocity distribution will generally be rather complicated as the muons are produced in complex many body annihilations and subsequently lose energy as they propagate through the quark matter and surrounding electrosphere. Rather than attempting to estimate the initial energy spectrum with which muons are produced and then tracking the energy loss as they escape from the nugget I will simply consider all muons capable of escaping the nugget to carry nuclear scale energies, so that they have a boost factor of $\beta \sim 0.9$. While this may be a serious simplification of a rather complex physical process it allows much of the shower evolution to be treated in a relatively transparent way and elucidates some of its basic properties.

The acceleration term in 6.14 leads to the emission of synchrotron radiation. The electric field produced by an accelerating particle is given by

$$\vec{E}(\vec{r}, t) = \frac{q}{4\pi\epsilon_0} \frac{\mathcal{R}}{\left(\vec{\mathcal{R}} \cdot \vec{u}\right)^3} \left[\left(c^2 - v^2\right) \vec{u} + \vec{\mathcal{R}} \times (\vec{u} \times \vec{a})\right] \tag{6.15}$$

with

$$\vec{u}(t) \equiv c\hat{\mathcal{R}} - \vec{v}(t_R), \tag{6.16}$$

where $\vec{\mathcal{R}}$ points from the charged particle to the observation point and $t_R = t - \mathcal{R}/c$ is the retarded time. While the emitted muons do not arise through pair production the emission process is essentially charge independent, so we can assume that μ^+ and μ^- production proceeds at the same rate. Applying 6.15 to a net neutral $\mu^+\mu^-$ pair and keeping only leading order terms we arrive at the electric field strength

$$|\vec{E}(\vec{r}, t)| = \frac{q}{2\pi\epsilon_0} \frac{\omega_B}{cR(t)} \frac{\beta_0 \sin\theta_{vB}}{\gamma(1-\beta_0)^2}, \tag{6.17}$$

where $\sin\theta_{vB}$ is the angle between the initial muon velocity and the earth's magnetic field and $R(t)$ is the distance between the muon and the observation point. Integrating this expression over the muons' entire path we obtain the frequency space representation

$$|\vec{\mathcal{E}}(\vec{r}, \omega)| = \frac{q}{(2\pi)^{3/2}\epsilon_0} \frac{\omega_B \sin\theta_{vB}}{c^2\gamma(1-\beta_0)^2} |\mathcal{I}(R, \omega)|, \tag{6.18}$$

where, for notational convenience, I have defined the integral

$$
\begin{aligned}
|\mathcal{I}(R,\omega)|^2 &= \left(\int_{\Delta R/R_0}^{1} \frac{dx}{x}\cos\left(\frac{R_0\omega}{c\beta_0}x\right)\right)^2 \\
&+ \left(\int_{\Delta R/R_0}^{1} \frac{dx}{x}\sin\left(\frac{R_0\omega}{c\beta_0}x\right)\right)^2 \qquad (6.19)
\end{aligned}
$$

with R_0 being the nugget to observer distance and ΔR the smallest separation between the emitting muon and the observer. Note that in cases where $\Delta R \to 0$ (i.e. cases where the muon pairs reach the observer) the integral 6.19 diverges. In order to regulate this divergence the integral will be cut off at distance scales where ΔR becomes comparable to the separation distance between the $\mu^+\mu^-$ pair. All of the geometry of the shower is carried by the sine function and the unitless integral. Writing 6.19 in a form that makes the scale of the emission clear we have,

$$
|\vec{\mathcal{E}}(\vec{r},\omega)| \approx (5\times 10^{-10}\mu\text{V m}^{-1}\ \text{MHz}^{-1})\left(\frac{\text{B}}{0.5\text{G}}\right)\frac{\sin\theta_{\text{vB}}|\mathcal{I}|}{\gamma(1-\beta)^2}. \qquad (6.20)
$$

As should be expected, the contribution of each muon pair is relatively small. The total field strength is then obtained by scaling this expression up by the total number of particles involved in the shower at a given time.

The total number of relativistic particles was estimated in section 6.2 so it remains to estimate which fraction of these contribute to the synchrotron emission along a given line of sight. I will assume that the angular dependence of particle emission is scaled by the forward directed surface area as in equation D.7 and once again focus on the geometrically simple case of a quark nugget with a purely vertical trajectory.

Following the analysis in [77] I will begin by noting that the radiation from a relativistic particle is sharply peaked along the direction of particle motion with the intensity showing an angular dependence of $I \sim (1-\beta\cos\theta)^4$. For the order of magnitude estimates here it will serve to consider contributions to the radio flux across the angular distribution over which the intensity falls to half its maximum value. This scale may be estimated as

$$
\left(\frac{1-\beta}{1-\beta\cos\theta_{1/2}}\right) = \frac{1}{2} \qquad (6.21)
$$

$$
\theta_{1/2}^2 \approx 0.38\left(\frac{1-\beta}{\beta}\right). \qquad (6.22)
$$

The second equation here uses the small angle approximation for the cosine. The solid angle of the nugget's surface from which emitted particles contribute to the radio flux will be estimated as $d\Omega \approx \theta_{1/2}^2$. This gives a total rate of muons contributing to the geosynchrotron flux of

$$\frac{dN_\mu}{dt} = \Gamma_\mu \frac{\theta_{1/2}^2}{2\pi} \frac{h_N}{\sqrt{h_N^2 + b^2}} \tag{6.23}$$

with Γ_μ as given in 6.7. Finally I need to evaluate the timescale over which the particles are contributing to the emission. This, as with many shower properties, is dependent on the energy loss rate of the particles as they move through the atmosphere and a full treatment of the problem would involve large scale numerical simulations. However, for the demonstrative purposes of this work I will assume that muon propagation may be treated in the simple model presented in appendix D. Furthermore I will assume that the muons are injected at sufficiently large energies that their total path length in the atmosphere is limited by their decay rate so that the timescale for emission is roughly $\Delta t \sim \gamma\tau_\mu$. Combining this with the emission rate, expression 6.23 gives the total number of particles contributing to the synchrotron flux,

$$N_\mu = \Gamma_\mu \gamma \tau_\mu \frac{\theta_{1/2}^2}{2\pi} \frac{h_N}{\sqrt{h_N^2 + b^2}}. \tag{6.24}$$

This factor allows us to scale the field strength for a single muon pair given in equation 6.20 to give an estimate of the radio contribution from the entire shower. This will depend on the height of the nugget in the atmosphere and the observer's distance from the shower core (or, in a more general non-vertical shower it will depend on the observer's orientation with respect to the plane of the nugget's motion. The electric field strength as a function of frequency across the radio MHz band is shown in figure 6.7. Figure 6.8 gives the field intensity as a function of distance from the shower core across multiple radio frequency bins.

It should be noted that the oscillations appearing in figure 6.7 are unphysical and arise from the assumption that all muons are emitted with identical energies. Even a small spread in emission energy will smooth out this effect which is related to the cutoff imposed on the integral 6.19.

Finally, I will work out the total intensity produced by geosynchrotron emission. This is given by the Poynting vector:

$$|\vec{S}| = \frac{dE}{dt\, dA} = \frac{|\vec{E}|^2}{\mu_0 c} \tag{6.25}$$

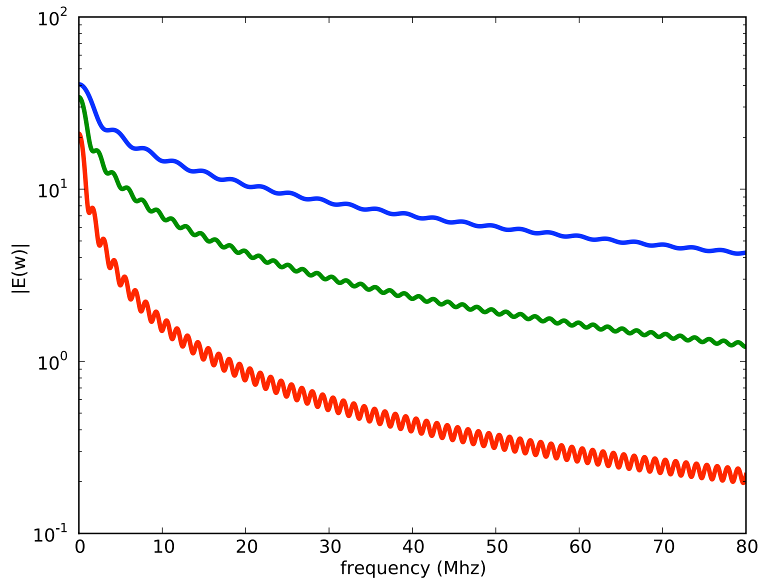

Figure 6.7: Total electric field strength generated by geosynchrotron emission in units of (μV m^{-1} MHz^{-1}) as received 250m from the shower core when the nugget is at heights of h=500m (blue), h=1000m (green) and h=1500m (red). Figure taken from [77].

$$|\vec{\mathcal{S}}| = \frac{dE}{d\omega\ dA} = \frac{|\vec{\mathcal{E}}(\omega)|^2}{\mu_0 c} \tag{6.26}$$

where the second expression is formulated in frequency space. As argued above this energy will be deposited over the lifetime of the boosted muon so that the total flux along a given line of sight is given by,

$$\begin{aligned} \frac{dE}{d\omega\ dt\ dA} &= \frac{1}{\gamma\tau_\mu}\frac{|N_\mu \mathcal{E}|^2}{\mu_0 c} \qquad (6.27)\\ &= \left(10^{-16}\text{J m}^{-2}\text{s}^{-1}\text{MHz}^{-1}\right)\left(\frac{\Gamma_{an} f_\mu}{10^{16}\text{s}^{-1}}\right)^2\left(\frac{B}{0.5\text{G}}\right)^2 \\ &\times \frac{\gamma\ |\mathcal{I}|^2}{\beta^2(1-\beta)^2}\ \left(\frac{h_N^2}{b^2+h_N^2}\right)\sin^2\theta_{vB}. \end{aligned}$$

This expression gives the total geosynchrotron intensity as a function of position on the earth's surface. I want to add to this the contribution from

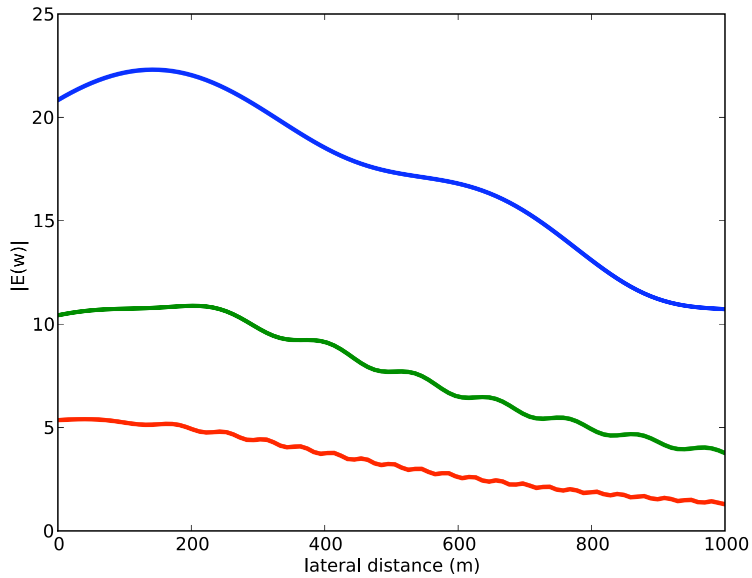

Figure 6.8: Total electric field strength generated by geosynchrotron emission in units of (μV m^{-1} MHz^{-1}) as a function of radial distance from the shower core. The individual curves are the field strength as measured at $\omega = 5$MHz (blue), $\omega = 20$MHz (green) and $\omega = 20$MHz (red). Figure taken from [77].

thermal emission in the radio band. This has the relatively simple form,

$$\frac{dE}{d\omega\ dt\ dA} = \frac{1}{4\pi(b^2 + h_N^2)} \frac{dE}{d\omega\ dt}. \tag{6.28}$$

To give a feel for the scales involved the thermal and geosynchrotron flux as a function of frequency are plotted in figure 6.9. It is also possible to use expressions 6.27 and 6.28 to extract the intensity received as a function of time. This time dependence is shown in figure 6.10.

As may be seen from figure 6.8 the radio signal produced by an antiquark nugget crossing the atmosphere will extend over a few square kilometers. This makes the radio signal a potentially valuable search channel, particularly at radio facilities designed to look for the radio signal from high energy cosmic rays. As in the case of fluorescence detection, the simultaneous arrival of a millisecond duration radio pulse with a particle shower

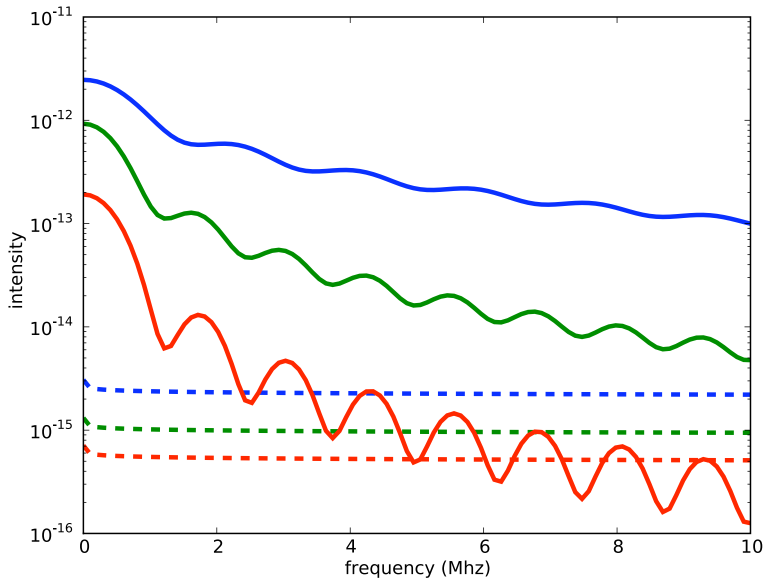

Figure 6.9: Total radio band electromagnetic intensity (J $s^{-1}m^{-2}MHz^{-1}$) received on the shower axis when the nugget is at heights of h=1km (blue), h=1.5km (green) and h=2km (red). The solid curves are the geosynchrotron contribution while the dashed lines are the thermal contribution. Figure taken from [77].

detected by a surface array would be a strong signal of a quark nugget initiated shower as conventional mechanisms producing a large number of high energy secondary particles evolve over much shorter timescales.

Of particular interest in this context are experiments such as the Auger Engineering Radio Array (AERA) [65], LOPES [59] at the KASCADE-Grande array and CODALEMA [24]. Each of these radio detection experiments have sufficient spatial extents to observe square kilometer scale events and a sufficient sensitivity in the MHz range to detect radio signals at the scale relevant for a quark nugget search.

This work was originally intended to allow constraints to be made on the flux of antiquark nuggets based on ground based radio detection programs. It has since been pointed out in [50] that suborbital observations by the Antarctic Impulsive Transient Antenna (ANITA) ballon borne experi-

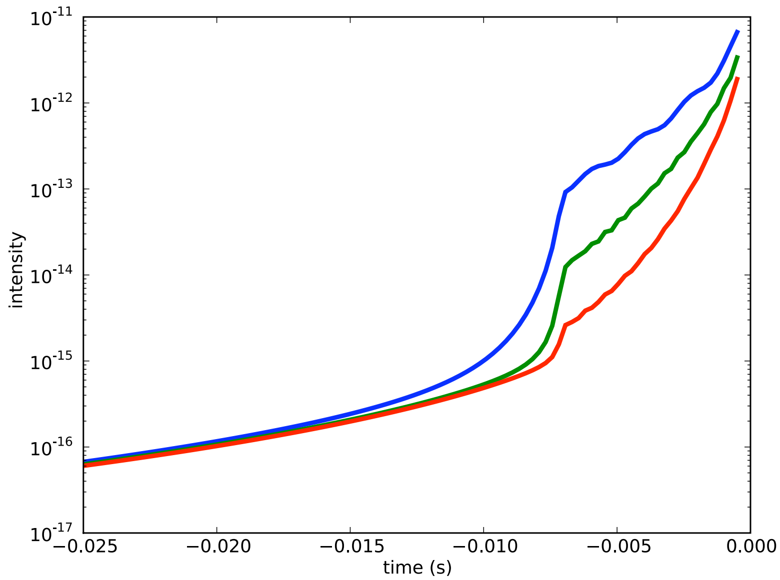

Figure 6.10: Total radio band electromagnetic intensity (J $s^{-1}m^{-2}MHz^{-1}$) as a function of time received on the shower axis from both thermal and geosynchrotron emission. Here the nugget is taken to hit the surface at t=0 after which the radio intensity will drop to zero. Intensity profiles are shown at 5MHz (blue), 20MHz (green) and 60MHz (red). Figure taken from [77].

ment [51] will also be sensitive to this radio signal. The ANITA detector is intended to detect radio signals produced by ultrahigh energy cosmic rays scattering in the radio transparent antarctic ice. The detector views the ice out to the horizon at a radius of approximately 600km, and has the directional sensitivity to use the nugget velocity to discriminate an antiquark nugget from many of the backgrounds. The ANITA project involves three flights ANITA-1 (2006-2007), ANITA-2 (2009-2010) and ANITA-3 which is planned for future flight. ANITA-2 does not have the sampling rate to track the entire evolution of a nugget induced radio pulse, however, it records data in multiple independent channels, allowing the nugget signal to be detected through a coincidence signal in all channels. The ANITA-3 experiment will increase the integration time of the detectors and thus have an even higher sensitivity. The ANITA-2 data is currently available and is being analyzed to look for events characteristic of an antiquark produced radio signal. The anticipated sensitivity range of ANITA is shown in figure 6.11 (taken from[50]) and can been seen to cover several decades of the allowed mass range. Figure 6.11 also shows the limits which may be derived from earlier searches conducted by the Gyrlanda array at lake Baikal [28], the analysis of lunar seismology [55], and the IceCube detector in its 22 and 80 string configurations [64].

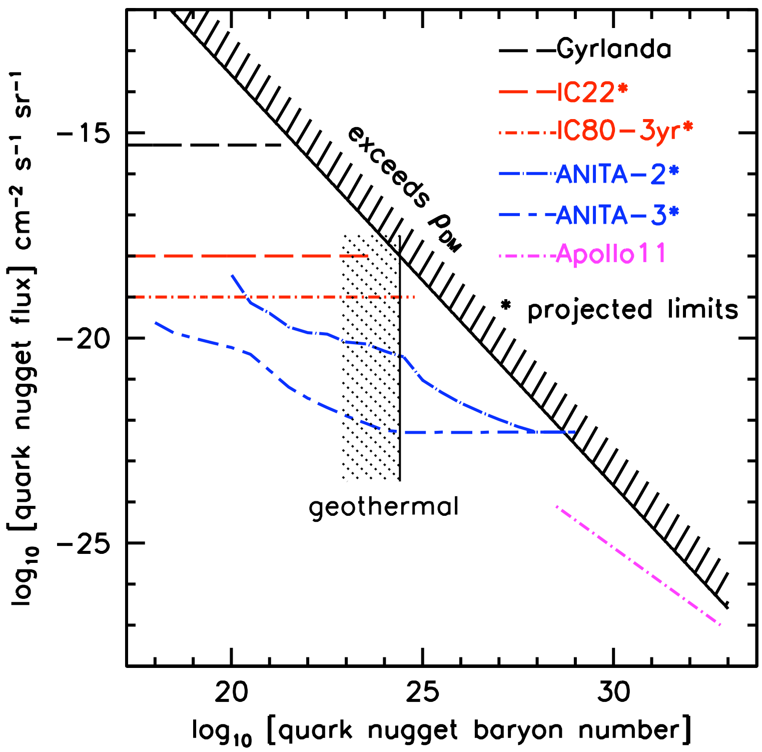

Figure 6.11: Projected ANITA constraints on the flux of antiquark nuggets. If the quark nuggets do comprise all of the dark matter then they must sit somewhere on the solid black line. The geothermal exclusion line is derived based on a limit to the amount of thermal energy that annihilating nuggets can add to the earth's temperature. All limits other than those from ANITA (shown here in blue) are based on completed analysis. The ANITA-2 data is currently under analysis while the ANITA-3 experiment has not yet been conducted. Figure taken from [50].

Chapter 7

Conclusions

The fundamental nature of the dark matter is one of the most important open questions in physics today. We have had strong evidence of its existence, through gravitational effects, for a long time but, currently, we have no clear picture of its origins or physical properties. In this absence of direct observational evidence many dark matter models have been proposed. Most of these models introduce a new fundamental particle (or particles) with their mass and interaction strength chosen to match the known properties of the dark matter.

This work has attempted to take a different approach, asking whether the dark matter can be composed of known Standard Model particles in a novel configuration. While the possibility that heavy nuggets of quark matter form in the early universe remains conjectural, the physical properties of these objects are strongly constrained by the well tested theories of QCD and QED. Beginning with the established properties of any form of high density quark matter from which the nuggets may be composed, I have attempted to extract their basic, unavoidable observational consequences.

If the galactic dark matter does consist of heavy quark nuggets, then it will necessarily have an observable signature in the high density galactic centre. In this environment the nuggets will emit thermal radiation, x-rays from hot spots near the site of proton annihilations and high energy photons from the annihilation of galactic electrons. All of these forms of radiation, spread across vastly different scales, must necessarily be generated by the nuggets. Furthermore, once we fix the emission scale from a single spectral feature (for example the galactic 511keV line) the scale is fixed across the rest of the emission spectrum. Following this procedure it has been found that emission from nuggets in the preferred mass range of this model is entirely compatible with observations. These possible diffuse excess features include the WMAP haze, the Chandra x-ray background, the galactic 511keV line and its associated three photon positronium decay continuum and the MeV band galactic excess observed by COMPTEL. Individually none of these features provides a smoking gun signature for quark nugget dark matter but, if any of these apparent excesses had been dramatically smaller than measured, the model could have been strongly constrained. Future observations may well reduce the “excess” of emission in any one of these channels and pose a serious challenge to quark nugget dark matter. But, at present, it is non-trivial that all of these correlated emissions, across ten orders of magnitude in energy, are simultaneously allowed, and that the dark matter model considered here may explain them all with only a single parameter.

The consequences of this model may be extrapolated from the galaxy up to a vastly larger scale. The matter density at the time the universe became transparent is only slightly below that in the galactic centre today. As the nugget temperature is determined by the background matter density, thermal emission from the nuggets at the time of CMB formation must have been similar to that from the galactic centre today. The redshift of these thermal photons implies that they will now fall primarily in the MHz radio band. This is an unavoidable consequence of the quark nugget dark matter model once the emission scale from the galactic centre is fixed. As such, it is highly non-trivial that the isotropic radio background shows an increase in sky temperature at low frequencies, with the temperature growing inversely with the third power of frequency, as predicted by the thermal spectrum of the nuggets which was originally computed to compare to a very different set of data.

Given the intriguing, if inconclusive, evidence offered by these galactic and cosmological observations, it is worthwhile to ask whether any current or planned experiments may be directly sensitive to the flux of quark nuggets. In this context, I have examined the observable consequences of the passage of a nugget through the earth’s atmosphere. In particular, I have focused on the extensive air shower that will surround an antiquark nugget. These air showers have been demonstrated to extend over a multiple kilometer scale and, consequently, may prove observable by large scale cosmic ray detectors. I have given a qualitative description of the basic properties of these air showers and highlighted their distinguishing features. The primary distinguishing feature in this context is the production of an air shower with a millisecond or longer duration. There are very few mechanisms, outside of this model, able to deposit enough energy to trigger a kilometer scale air shower without carrying a velocity well above the typical galactic scale. It is precisely this low velocity primary which allows for the production of a long duration air shower. With this main distinguishing feature in mind I have reviewed the prospect for nugget detection at cosmic ray detectors, whether through atmospheric fluorescence, surface detection or radio measurements. I have also pointed out the constraints which may be provided by data from the ANITA experiment which is currently under analysis.

It has been the basic purpose of this work to highlight that the quark nugget dark matter model has essentially one free parameter, the average mass of an individual nugget. While this quantity is, in principle, calculable in the theory of QCD, it is dependent on dynamics at the QCD phase transition, at $\theta \neq 0$, far from equilibrium and at strong coupling. As such, it is unlikely that significant theoretical progress will be made on this front in the near future. However, once the mass scale is set by a single observation it automatically fixes the scale of a highly diverse range of other consequences. These range from galactic scale astrophysics up to Hubble scale contributions to the isotropic background. Once this mass scale is established, it also determines the flux of nuggets through the earth. It is also possible to directly constrain this flux. The present interest in understanding the nature of ultrahigh energy cosmic rays has motivated the construction of several large scale detectors and this work has attempted to demonstrate how they may be able to constrain the quark nugget flux across much of the mass range allowed by astronomical observations. It is precisely this testability across a broad range of experiments and scales that makes the quark nugget dark matter model compelling.

Bibliography

[1] C.E. Aalseth, P.S. Barbeau, J. Colaresi, J.I. Collar, J. Diaz Leon, et al. Search for an annual modulation in a p-type point contact germanium dark matter detector. *Phys. Rev. Lett.*, 107:141301, 2011.

[2] C.E. Aalseth et al. Results from a search for light-mass dark matter with a p-type point contact germanium detector. *Phys. Rev. Lett.*, 106:131301, 2011.

[3] R.U. Abbasi et al. First observation of the greisen-zatsepin-kuzmin suppression. *Phys.Rev.Lett.*, 100:101101, 2008.

[4] J. Abraham et al. Observation of the suppression of the flux of cosmic rays above 4×10^{19}eV. *Phys. Rev. Lett.*, 101(6):061101, 2008.

[5] J. Abraham et al. The fluorescence detector of the pierre auger observatory. *Nucl. Instrum. Meth.*, A620:227–251, 2010.

[6] T. Abu-Zayyad et al. The surface detector array of the telescope array experiment. *Nucl. Instrum. Meth.*, A689:87–97, 2012.

[7] M. Ackermann et al. Constraints on the galactic halo dark matter from fermi-lat diffuse measurements. *Astrophys. J.*, 761:91, 2012.

[8] M. Ackermann et al. Fermi lat search for dark matter in gamma-ray lines and the inclusive photon spectrum. *Phys. Rev. D*, 86:022002, 2012.

[9] P.A.R. Ade and other. Planck intermediate results. ix. detection of the galactic haze with planck. *Astron. Astrophys. (submitted)*, 2012.

[10] Oscar Adriani et al. An anomalous positron abundance in cosmic rays with energies 1.5-100 gev. *Nature*, 458:607–609, 2009.

[11] R. Agnese et al. Dark matter search results using the silicon detectors of cdms ii. *Phys. Rev. Lett.*, 2013.

[12] M. Aguilar et al. Cosmic-ray positron fraction measurement from 1 to 30-gev with ams-01. *Phys. Lett. B.*, 646:145–154, 2007.

[13] Z. Ahmed et al. Results from a low-energy analysis of the cdms ii germanium data. *Phys.Rev.Lett.*, 106:131302, 2011.

[14] Z. Ahmed et al. Search for inelastic dark matter with the cdms ii experiment. *Phys. Rev. D*, 83:112002, 2011.

[15] Charles Alcock, Edward Farhi, and Angela Olinto. Strange stars. *Astrophys.J.*, 310:261–272, 1986.

[16] Mark Alford, Krishna Rajagopal, and Frank Wilczek. Color-flavor locking and chiral symmetry breaking in high density QCD. *Nucl. Phys. B*, 537:443–458, 1999.

[17] Mark G. Alford. Color superconducting quark matter. *Ann.Rev.Nucl.Part.Sci.*, 51:131–160, 2001.

[18] Y. Ali-Haimoud, C.M. Hirata, and C. Dickinson. A refined model for spinning dust radiation. *MNRAS*, 395:1055, 2009.

[19] I. Allekotte et al. The surface detector system of the pierre auger observatory. *Nucl. Instrum. Meth.*, A586:409–420, 2008.

[20] J. Allen et al. Air shower simulation and hadronic interactions. *EPJ Web Conf.*, 53:01007, 2013.

[21] J. Angle et al. A search for light dark matter in xenon10 data. *Phys. Rev. Lett.*, 107:051301, 2011.

[22] E. Aprile et al. The xenon100 dark matter experiment. *Astropart. Phys.*, 35:573–590, 2012.

[23] J. Arafune, T. Yoshida, S. Nakamura, and K. Ogure. Experimental bounds on masses and fluxes of nontopological solitons. *Phys. Rev. D*, 62:105013, 2000.

[24] D. Ardouin, A. Belletoile, C. Berat, D. Breton, D. Charrier, et al. Geomagnetic origin of the radio emission from cosmic ray induced air showers observed by codalema. *Astropart. Phys.*, 31:192–200, 2009.

[25] Stephen J. Asztalos, Leslie J. Rosenberg, Karl van Bibber, Pierre Sikivie, and Konstantin Zioutas. Searches for astrophysical and cosmological axions. *Ann.Rev.Nucl.Part.Sci.*, 56:293–326, 2006.

[26] John F. Beacom and Hasan Yuksel. Stringent constraint on galactic positron production. *Phys. Rev. Lett.*, 97:071102, 2006.

[27] Renaud Belmont, M. Tagger, M. Muno, M. Morris, and Steven Charles Cowley. A hot helium plasma in the galactic center region. *Astrophys.J.*, 631:L53–L56, 2005.

[28] I.A. Belolaptikov, Leonid B. Bezrukov, N.M. Budnev, E.V. Bugaev, Jan-Arys M. Dzhilkibaev, et al. The experimental limits on q ball flux with the baikal deep underwater array 'gyrlyanda'. *preprint*, 1998.

[29] C. Bennett et al. First year wilkinson microwave anisotropy probe (wmap) observations: Foreground emission. *Astrophys.J.Suppl.*, 148:97, 2003.

[30] C.L. Bennett et al. Nine-year wilkinson microwave anisotropy probe (wmap) observations: Final maps and results. *Astrophysical Journal Supplement Series*, 2012.

[31] R. Bernabei, P. Belli, S. d'Angelo, A. Di Marco, F. Montecchia, et al. Dark matter investigation by dama at gran sasso. *Int. J. Mod. Phys.*, A28:1330022, 2013.

[32] Sanghyeon Chang, C. Hagmann, and P. Sikivie. Studies of the motion and decay of axion walls bounded by strings. *Phys. Rev. D*, 59:023505, 1999.

[33] Claudio Corti. The cosmic ray electron and positron spectra measured by ams-02. *Proceedings of The 10th International Symposium on Cosmology and Particle Astrophysics*, 2013.

[34] Michael Dine, Willy Fischler, and Mark Srednicki. A simple solution to the strong cp problem with a harmless axion. *Phys.Lett.*, B104:199, 1981.

[35] Edward Farhi and R.L. Jaffe. Strange matter. *Phys. Rev. D*, 30:2379, 1984.

[36] Douglas P. Finkbeiner. Microwave ism emission observed by wmap. *Astrophys.J.*, 614:186–193, 2004.

[37] Douglas P. Finkbeiner. Wmap microwave emission interpreted as dark matter annihilation in the inner galaxy. *preprint, astro-ph/0409027*, 2004.

[38] Dale J. Fixsen, C.L. Bennett, and John C. Mather. Cobe-firas observations of galactic lines. *Astrophys. J.*, 526:207, 1999.

[39] D.J. Fixsen, A. Kogut, S. Levin, M. Limon, P. Lubin, et al. Arcade2 measurement of the absolute sky brightness at 3-90 ghz. *The Astrophysical Journal*, 734(1), 2011.

[40] Michael McNeil Forbes, Kyle Lawson, and Ariel R. Zhitnitsky. The electrosphere of macroscopic 'quark nuclei': A source for diffuse mev emissions from dark matter. *Phys. Rev. D*, 82:083510, 2010.

[41] Michael McNeil Forbes and Ariel R. Zhitnitsky. Domain walls in qcd. *JHEP*, 0110:013, 2001.

[42] Michael McNeil Forbes and Ariel R. Zhitnitsky. Diffuse x-rays: Directly observing dark matter? *JCAP*, 0801(01):023, 2008.

[43] Michael McNeil Forbes and Ariel R. Zhitnitsky. Wmap haze: Directly observing dark matter? *Phys. Rev. D*, 78(8):083505, 2008.

[44] N. Fornengo, R. Lineros, M. Regis, and M. Taoso. Possibility of a dark matter interpretation for the excess in isotropic radio emission reported by arcade. *Phys. Rev. Lett.*, 107:271302, 2011.

[45] N. Fornengo, R. Lineros, M. Regis, and M. Taoso. Cosmological radio emission induced by wimp dark matter. *JCAP*, 1203:033, 2012.

[46] Nicolao Fornengo, Roberto A. Lineros, Marco Regis, and Marco Taoso. The isotropic radio background revisited. *preprint, arXiv:1402.2218*, 2014.

[47] Gregory Gabadadze and Mikhail A. Shifman. Vacuum structure and the axion walls in gluodynamics and qcd with light quarks. *Phys. Rev. D*, 62:114003, 2000.

[48] M. Gervasi, A. Tartari, M. Zannoni, G. Boella, and G. Sironi. The contribution of the unresolved extragalactic radio sources to the brightness temperature of the sky. *Astrophys. J.*, 682:223, 2008.

[49] B. Gold, N. Odegard, J.L. Weiland, R.S. Hill, A. Kogut, et al. Seven-year wilkinson microwave anisotropy probe (wmap) observations: Galactic foreground emission. *Astrophysical Journal Supplement Series*, 192:15, 2011.

[50] Peter.W. Gorham. Antiquark nuggets as dark matter: New constraints and detection prospects. *Phys. Rev. D*, 86:123005, 2012.

[51] Peter.W. Gorham et al. The antarctic impulsive transient antenna ultra-high energy neutrino detector design, performance, and sensitivity for 2006-2007 balloon flight. *Astropart. Phys.*, 32:10–41, 2009.

[52] Kenneth Greisen. End to the cosmic ray spectrum? *Phys. Rev. Lett.*, 16:748–750, 1966.

[53] D.J. Gross and Frank Wilczek. Ultraviolet behavior of nonabelian gauge theories. *Phys. Rev. Lett.*, 30:1343–1346, 1973.

[54] C. G. T. Haslam, U. Klein, C. J. Salter, H. Stoffel, W. E. Wilson, M. N. Cleary, D. J. Cooke, and P. Thomasson. A 408 mhz all-sky continuum survey. i - observations at southern declinations and for the north polar region. *Astronomy and Astrophysics*, 100(2):209–219, July 1981.

[55] Eugene T. Herrin, Doris C. Rosenbaum, and Vigdor L. Teplitz. Seismic search for strange quark nuggets. *Phys. Rev. D*, 73:043511, 2006.

[56] G. Hinshaw et al. Nine-year wilkinson microwave anisotropy probe (wmap) observations: Cosmological parameter results. *Astrophysical Journal Supplement Series*, 2012.

[57] Dan Hooper, Alexander V. Belikov, Tesla E. Jeltema, Tim Linden, Stefano Profumo, et al. The isotropic radio background and annihilating dark matter. *Phys. Rev. D*, 86:103003, 2012.

[58] Dan Hooper, Douglas P. Finkbeiner, and Gregory Dobler. Possible evidence for dark matter annihilations from the excess microwave emission around the center of the galaxy seen by the wilkinson microwave anisotropy probe. *Phys. Rev. D*, 76:083012, 2007.

[59] T. Huege and Collaboration. The lopes experiment - recent results, status and perspectives. *Nucl. Instrum. Meth.*, A662:S72–S79, 2012.

[60] Pierre Jean et al. Early SPI/INTEGRAL measurements of galactic 511 keV line emission from positron annihilation. *Astron. Astrophys.*, 407:L55, 2003.

[61] Pierre Jean, J. Knodlseder, W. Gillard, N. Guessoum, K. Ferriere, et al. Spectral analysis of the galactic e+ e- annihilation emission. *Astron. Astrophys.*, 445:579–589, 2006.

[62] W.N. Johnson, F.R. Harnden, and R.C. Haymes. The spectrum of low-energy gamma radiation from the galactic-center region. *The Astrophysical Journal*, 172:L1, 1972.

[63] Manoj Kaplinghat, Daniel J. Phalen, and Kathryn M. Zurek. Pulsars as the source of the wmap haze. *JCAP*, 0912:010, 2009.

[64] A. Karle. Icecube - status and recent results. *Proceedings for the XVth Workshop on Neutrino Telescopes*, 2014.

[65] J.L. Kelley. Data acquisition, triggering, and filtering at the auger engineering radio array. *Nucl. Instrum. Meth.*, 2012.

[66] Christopher M. Kelso and Dan Hooper. Synchrotron emission from young and nearby pulsars. *JCAP*, 1005:039, 2010.

[67] C. Kettner, F. Weber, M.K. Weigel, and N.K. Glendenning. Structure and stability of strange and charm stars at finite temperatures. *Phys.Rev.*, D51:1440–1457, 1995.

[68] D. Kharzeev and A. Zhitnitsky. Charge separation induced by p-odd bubbles in qcd matter. *Nucl.Phys.*, A797:67–79, 2007.

[69] Jihn E. Kim. Weak interaction singlet and strong cp invariance. *Phys.Rev.Lett.*, 43:103, 1979.

[70] Jurgen Knödlseder, Pierre Jean, V. Lonjou, G. Weidenspointner, N. Guessoum, W. Gillard, G. Skinner, P. von Ballmoos, G. Vedrenne, J.-P. Roques, S. Schanne, B. Teegarden, V. Schönfelder, and C. Winkler. The all-sky distribution of 511-keV electron positron annihilation emission. *Astron. Astrophys.*, 441:513–532, 2005.

[71] Makoto Kobayashi and Toshihide Maskawa. Cp violation in the renormalizable theory of weak interaction. *Prog.Theor.Phys.*, 49:652–657, 1973.

[72] A. Kogut, D.J. Fixsen, S.M. Levin, M. Limon, P.M. Lubin, et al. Arcade 2 observations of galactic radio emission. *Astrophys.J.*, 734:4, 2011.

[73] K. Lawson. Quark matter induced extensive air showers. *Phys. Rev. D*, 83:103520, 2011.

[74] Kyle Lawson. Observing dark matter in the galactic spectrum? Master's thesis, UBC Departmet of Physics and Astronomy, 6224 Agricultural Road, Vancouver, BC, 2008.

[75] Kyle Lawson. A signature of colour-superconducting dark matter? *Proceedings of the Lake Louise Winter Institute 2009*, 2009.

[76] Kyle Lawson. 'cosmic rays' from quark matter. *Proceedings of the 2010 Lake Louise Winter Institute*, 2010.

[77] Kyle Lawson. Atmospheric radio signals from galactic dark matter. *Phys. Rev. D*, 88:043519, 2013.

[78] Kyle Lawson. A quark matter contribution to the cosmic ray spectrum. *EPJ Web Conf.*, 52:04008, 2013.

[79] Kyle Lawson. Limits on quark nugget dark matter from cosmic ray detectors. *Proceedings of the International Symposium on Very High Energy Cosmic Ray Interactions (in preparation)*, 2014.

[80] Kyle Lawson and Ariel R. Zhitnitsky. Diffuse cosmic gamma-rays at 1-20 MeV: A trace of the dark matter? *JCAP*, 0801(01), January 2008.

[81] Kyle Lawson and Ariel R. Zhitnitsky. Isotropic radio background from quark nugget dark matter. *Phys. Lett. B.*, 724:17–21, 2013.

[82] Kyle Lawson and Ariel R. Zhitnitsky. Quark (anti) nugget dark matter. *Snowmass 2013 e-Proceedings*, 2013.

[83] R.E. Lingenfelter, J.C. Higdon, and R.E. Rothschild. Is there a dark matter signal in the galactic positron annihilation radiation? *Phys.Rev.Lett.*, 103:031301, 2009.

[84] Jes Madsen. Color flavor locked strangelets. *Phys.Rev.Lett.*, 87:172003, 2001.

[85] Jes Madsen. Cosmic ray strangelets. *J.Phys. G*, pages S833–3S840, 2005.

[86] Jes Madsen. Strangelets, nuclearites, q-balls: A brief overview. *Invited talk at Workshop on Exotic Physics with Neutrino Telescopes*, 2006.

[87] K. Maeda, H. Alvarez, J. Aparici, J. May, and P. Reich. A 45-mhz continuum survey of the northern hemisphere. *Astronomy and Astrophysics Supplement*, 140:145–154, December 1999.

[88] Ziro Maki, Masami Nakagawa, and Shoichi Sakata. Remarks on the unified model of elementary particles. *Prog.Theor.Phys.*, 28:870–880, 1962.

[89] Philipp Mertsch and Subir Sarkar. Systematic effects in the extraction of the 'wmap haze'. *JCAP*, 1010:019, 2010.

[90] I.N. Mishustin, L.M. Satarov, T.J. Burvenich, Horst Stoecker, and W. Greiner. Antibaryons bound in nuclei. *Phys. Rev. C*, 71:035201, 2005.

[91] Igor V. Moskalenko, Andrew W. Strong, Seth W. Digel, and Troy A. Porter. Developing the galactic diffuse emission model for the glast large area telescope. *AIP Conf.Proc.*, 921:490–491, 2007.

[92] Michael P. Muno, F.K. Baganoff, M.W. Bautz, W.N. Brandt, P.S. Broos, et al. A deep chandra catalog of x-ray point sources toward the galactic center. *Astrophys. J.*, 589, 2003.

[93] Michael P. Muno, F.K. Baganoff, M.W. Bautz, E.D. Feigelson, G.P. Garmire, et al. Diffuse x-ray emission in a deep chandra image of the galactic center. *Astrophys. J.*, 613:326–342, 2004.

[94] Julio F. Navarro, Carlos S. Frenk, and Simon D.M. White. The structure of cold dark matter halos. *Astrophys.J.*, 462:563–575, 1996.

[95] David H. Oaknin and Ariel Zhitnitsky. Baryon asymmetry, dark matter and quantum chromodynamics. *Phys. Rev. D*, 71:023519, 2005.

[96] David H. Oaknin and Ariel R. Zhitnitsky. 511-kev photons from color superconducting dark matter. *Phys. Rev. D*, 94:101301, 2005.

[97] R.D. Peccei and Helen R. Quinn. Cp conservation in the presence of instantons. *Phys.Rev.Lett.*, 38:1440–1443, 1977.

[98] Rui Pereira. Astrophysics with the ams-02 experiment. *Proceedings of the 2005 Europhysics Conference on High Energy Physics*, 2007.

[99] H. David Politzer. Reliable perturbative results for strong interactions? *Phys. Rev. Lett.*, 30:1346–1349, 1973.

[100] N. Prantzos, C. Boehm, A.M. Bykov, R. Diehl, K. Ferriere, et al. The 511 kev emission from positron annihilation in the galaxy. *Rev. Mod. Phys.*, 83:1001–1056, 2011.

[101] Nikos Prantzos. On the intensity and spatial morphology of the 511-kev emission in the milky way. *Astron.Astrophys.*, 449:869–878, 2006.

[102] Krishna Rajagopal and Frank Wilczek. The condensed matter physics of qcd. *Frontier of Particle Physics Vol. 3*, 2000.

[103] P. Reich and W. Reich. A radio continuum survey of the northern sky at 1420 mhz. ii. *Astronomy and Astrophysics Supplement*, 63(2):205–288, February 1986.

[104] A.E.E. Rogers and J.D. Bowman. Spectral index of the diffuse radio background measured from 100 to 200 mhz. *The Astrophysical Journal*, 136:641–648, August 2008.

[105] A.D. Sakharov. Violation of cp invariance, c asymmetry, and baryon asymmetry of the universe. *Pisma Zh.Eksp.Teor.Fiz.*, 5:32–35, 1967.

[106] M. Seiffert, D.J. Fixsen, A. Kogut, S.M. Levin, M. Limon, et al. Interpretation of the extragalactic radio background. *arXiv:0901.0559*, 2009.

[107] Mikhail A. Shifman, A.I. Vainshtein, and Valentin I. Zakharov. Can confinement ensure natural cp invariance of strong interactions? *Nucl.Phys.*, B166:493, 1980.

[108] Edward V. Shuryak. Which chiral symmetry is restored in hot qcd? *Comments Nucl.Part.Phys.*, 21:235–248, 1994.

[109] P. Sikivie. Dark matter axions. *Int.J.Mod.Phys.*, pages 554–563, 2010.

[110] J. Singal, L. Stawarz, A. Lawrence, and V. Petrosian. Sources of the radio background considered. *MNRAS*, 409:1172–1182, 2010.

[111] Andrew W. Strong, Igor V. Moskalenko, and Olaf Reimer. Diffuse continuum gamma-rays from the galaxy. *Astrophys.J.*, 537, 2000.

[112] Andrew W. Strong, Igor V. Moskalenko, and Olaf Reimer. Diffuse galactic continuum gamma rays. a model compatible with egret data and cosmic-ray measurements. *Astrophys. J.*, 613:962–976, 2004.

[113] A.W. Strong, H. Bloemen, R. Diehl, W. Hermsen, and V. Schoenfelder. Comptel skymapping: A new approach using parallel computing. *Astrophys. Lett. Commun.*, 39:209, 1999.

[114] Meng Su, Tracy R. Slatyer, and Douglas P. Finkbeiner. Giant gamma-ray bubbles from fermi-lat: Agn activity or bipolar galactic wind? *Astrophys.J.*, 724:1044–1082, 2010.

[115] H. Tokuno, Y. Tameda, M. Takeda, K. Kadota, D. Ikeda, et al. New air fluorescence detectors employed in the telescope array experiment. *Nucl. Instrum. Meth.*, A676:54–65, 2012.

[116] K. van Bibber and L.J. Rosenberg. Ultrasensitive searches for the axion. *Phys.Today*, 59(8):30–35, 2006.

[117] G. Weidenspointner, G. Skinner, P. Jean, J. Knödlseder, P. von Ballmoos, R. Diehl, A.W. Strong, B. Cordier, S. Schanne, and C. Winkler. Positron astronomy with spi/integral. *New Astron. Rev.*, 52:454–456, 2008.

[118] Georg Weidenspointner, C.R. Shrader, J. Knoedlseder, P. Jean, V. Lonjou, et al. The sky distribution of positronium annihilation continuum emission measured with spi/integral. *Astron.Astrophys.*, 450:1012, 2006.

[119] Georg Weidenspointner, Gerry Skinner, Pierre Jean, Jurgen Knodlseder, Peter von Ballmoos, et al. An asymmetric distribution of positrons in the galactic disk revealed by gamma-rays. *Nature*, 451:159–162, 2008.

[120] Steven Weinberg. A new light boson? *Phys.Rev.Lett.*, 40:223–226, 1978.

[121] Frank Wilczek. Problem of strong p and t invariance in the presence of instantons. *Phys.Rev.Lett.*, 40:279–282, 1978.

[122] Edward Witten. Cosmic separation of phases. *Phys. Rev. D*, 30:272–285, 1984.

[123] Nathalie Ysard and Guilaine Lagache. Microwave and radio emission of dusty star-forming galaxies: Implication for the cosmic radio background. *Astron. Astrophys. (accepted)*, 2013.

[124] G. T. Zatsepin and V. A. Kuzmin. Upper limit of the spectrum of cosmic rays. *JETP Lett.*, 4:78–80, 1966.

[125] Le Zhang and Gunther Sigl. Dark matter signatures in the anisotropic radio sky. *JCAP*, 0809:027, 2008.

[126] Ariel Zhitnitsky. 'Nonbaryonic' dark matter as baryonic color superconductor. *JCAP*, 10:010, May 2003.

[127] Ariel Zhitnitsky. Cold dark matter as compact composite objects. *Phys. Rev. D*, 74:043515, 2006.

[128] Ariel Zhitnitsky. The width of the 511 kev line from the bulge of the galaxy. *Phys. Rev. D*, 76:103518, 2007.

[129] Ariel R. Zhitnitsky. On possible suppression of the axion hadron interactions. (in russian). *Sov.J.Nucl.Phys.*, 31:260, 1980.

Appendix A

Cosmology Review

This appendix is intended to provide a brief review of some basic concepts in cosmology relevant, but not directly related, to the main focus of this work. In addition to providing general background this material is particularly relevant to the discussion of the nugget contribution to the cosmic radio background presented in chapter 5.

A.1 The expanding universe

We live in an expanding universe that emerged from a hot big bang approximately 13.7 billion years ago. The expansion of the universe is governed by general relativity and may, in the isotropic and flat limit, be described by the Friedmann equations:

$$H^2 \equiv \left(\frac{\dot{a}}{a}\right)^2 = \frac{8\pi G\rho + \Lambda c^2}{3} \tag{A.1}$$

$$\frac{\ddot{a}}{a} = -\frac{4\pi G}{3}\left(\rho + \frac{3p}{c^2}\right) + \frac{\Lambda c^2}{3}. \tag{A.2}$$

Here a is the scale factor, a measure of the scale of the universe, and the rate of change of this scale (the Hubble parameter H) describes the expansion of the universe. This expansion rate is related to the energy density (ρ) and pressure (p) of the contents of the universe and is also sourced by the cosmological constant Λ. In terms of their impact on the dynamics of the expansion, the contents of the universe may be expressed by their equation of state, that is, the ratio between density and pressure ($w = p/\rho$.) Non-relativistic matter carries the majority of its energy as mass and exerts no pressure, thus $w_m = 0$. Radiation or ultrarelativistic matter has $w_r = 1/3$ and the cosmological constant has $w_\Lambda = -1$. From the Friedmann equations we can determine the rate at which different types of energy densities dilute:

$$\dot{\rho} = -3\frac{\dot{a}}{a}(p + \rho). \tag{A.3}$$

This expression can be solved for the various types of energy density to find their dependence on the scale factor. The energy of non-relativistic matter is mass dominated, thus, the energy content remains constant while the volume it occupies expands and $\rho_m \sim a^{-3}$. The expansion of spacetime causes a redshifting of radiation so that its energy density dilutes faster than that of matter, and $\rho_r \sim a^{-4}$. Finally, the cosmological constant is a form of vacuum energy, it scales in proportion to the size of the spacetime it occupies. That is to say, it does not dilute with the universe's expansion.

A useful parameterization of the contents of the universe is in terms of the fraction of the critical density that a given form of energy represents. The critical density is defined as the energy density for which, in the absence of a cosmological constant, the universe just avoids collapsing back on itself (analogous to the escape speed at which an object is no longer gravitationally bound to the earth.) This density may be found by inverting expression A.1 when $\Lambda = 0$

$$\rho_c = \frac{3H^2}{8\pi G}. \tag{A.4}$$

From this we may define the density parameter of a substance, of energy density ρ, as $\Omega = \rho/\rho_c$. This provides a simple way of characterizing the contents of the universe and, if we assume that the total energy density is equal to the critical density, allows us to write the first Friedmann equation as,

$$\left(\frac{\dot{a}}{a}\right)^2 = H_0^2 \left(\Omega_r a^{-4} + \Omega_{DM} a^{-3} + \Omega_{vis} a^{-3} + \Omega_\Lambda\right) \tag{A.5}$$

where H_0 is the Hubble constant as measured today and the present value of a is normalized to one. In this expression, I have separated the visible matter (Ω_{vis}) and the dark matter components, despite the fact that they display identical dynamics in terms of the expansion. In is only when we consider their microscopic properties that these two components display unique behaviours. From expression A.5, it is clear that at different times in the history of the universe the form of energy density which drives the dynamics of the expansion will be different. In the early universe there are many ultrarelativistic species, and their energy density is large, so that the universe is radiation dominated. As the universe expands the energy density of radiation drops relatively quickly and eventually the dynamics become matter driven. Finally, at relatively late times in the cosmic history, the other forms of energy have diluted away and the dynamics become dominated by the cosmological constant.

At present the universe is dominated by dark energy which, thus far, seems consistent with a cosmological constant. The dark matter and visible matter make secondary contributions with $\Omega_\Lambda = 0.7181, \Omega_{DM} = 0.236$ and $\Omega_B = 0.0461$ [56].

When we observe distant objects, we see the light they emit as having been redshifted by the expansion according to $\nu_{emit} a_{emit} = \nu_{obs} a_{obs}$. Here the subscripts *emit* and *obs* denote the values at the time of emission and observation respectively. Using this relation, and normalizing the present day scale factor to one, the scale factor at any given distance may be expressed in terms of the redshift of objects observed at that distance $a = 1/(1+z)$.

A.2 The cosmic microwave background

The cosmic microwave background (CMB) is one of the most important sources of our knowledge of the early universe, and it has also provided significant insight into the development of large scale structure. This review will give only a very brief discussion of the details of CMB formation and evolution as required for an understanding of the main discussion of this work.

The expansion of the universe has diluted and cooled the contents which, at earlier times, were much hotter and more dense. In the early universe the temperature was high enough that the matter existed as a highly ionized plasma which was fully coupled to the radiation. At this time the mean free path of a photon was short, and the number density of photons was set by the temperature of the plasma. As the plasma cooled its ionization fraction fell and the photons' mean free path increased until they could travel unimpeded across the universe. This transition represents the furthest distance in the universe from which electromagnetic radiation can reach us. In the time since it was emitted, this radiation has diluted and cooled to the point where it now represents a thermal bath of photons with a temperature of $T_{CMB} = 2.7$K. These photons carry too little energy to influence the dynamics of the expansion, but there are enough of them that they still dominate the thermodynamics of the universe. As a thermal collection of photons, the spectrum of the CMB is given by,

$$\frac{dE}{dt\ dA\ d\nu} = \frac{8\pi h\nu^3}{c^2} \frac{1}{e^{h\nu/T} - 1}. \tag{A.6}$$

Once the CMB has decoupled from the matter its temperature falls with the scale factor so that this expression holds at all later times with a radiation temperature given by $T = T_0(1+z)$, where $T_0 = 2.7$K is the present day photon temperature. The form of this spectrum will be important in the analysis of the isotropic radio background in chapter 5. The scattering of ultrahigh energy cosmic rays off this photon background determines the energy of the GZK cutoff as discussed in the introduction to chapter 6.

A.3 Radiation from distant objects

A photon emitted at a scale factor a will experience a redshift of $z = a_0/a-1$, where a_0 is the present day scale factor, generally normalized to one. In practice, it is easier to speak about a distant source as being at a particular redshift which, unlike the scale factor, is a directly observable quantity. In this case, the frequency of a photon observed today will be redshifted from its original value down to

$$\nu = \frac{\nu_{emit}}{1+z} \tag{A.7}$$

with the energy carried by the photon falling accordingly.

When observing a distant object the energy flux received is reduced by the redshift of the photons. We can write the intensity as

$$I(\nu) \equiv \frac{dE}{dt\ d\nu\ dA} = \frac{(1+z)}{4\pi d_L^2}\ \frac{dE}{dt\ d\nu}\,(\nu[1+z]) \tag{A.8}$$

where d_L is the luminosity distance of the object. A more complex case is that of emission from a distribution of sources extended over a range of different redshifts. This flux calculation is needed in determining cosmological backgrounds such as the isotropic cosmological background associated with dark matter (analyzed, for example in [125].) This may be formulated as an integral of the comoving source density over all redshifts back to the surface of last scattering:

$$I(\nu) \equiv \frac{dE}{dt\ d\nu\ dA} = \int \frac{c\ dz}{(1+z)H(z)} n_s(z)L(\nu(1+z), z) \tag{A.9}$$

where n_s is the number density of sources and $L(\nu(1+z), z)$ is the luminosity per frequency interval, evaluated at the frequency from which it will be redshifted down to ν in the present day universe. In evaluating this expression it is useful to invert expression A.5 and note that, over the cosmological history we are interested in, the radiation term is negligible so that,

$$H(z) = H_0\sqrt{\Omega_M(1+z)^3 + \Omega_\Lambda}. \tag{A.10}$$

Thus, if we know how sources evolve with redshift, we can integrate their combined intensity across the observable universe and determine their contribution to the cosmological background. This procedure is followed in section 5.2 to determine the isotropic radio background arising from a population of antiquark nuggets in the early universe.

Appendix B

QCD Review

This appendix will offer a brief review of some of the properties of quantum chromodynamics (QCD) as necessary background to the main body of this work. After a brief introduction, it will focus primarily on the strong CP problem, and its potential resolution through the introduction of the axion. Finally, these concepts will be applied, in a qualitative way, to the problem of nugget formation in the early universe.

B.1 Introduction

QCD is the theory governing the strong force interactions of hadronic matter. It is an SU(3) gauge symmetry in which the colour charge carrying quarks interact through the exchange of eight gauge bosons known as gluons. As the gluons also carry colour charge they couple to each other directly as well as to the quarks. In addition to the more complicated set of gauge interactions, QCD is differentiated from the U(1) gauge theory of quantum electrodynamics (QED) by the strength of the quark-gluon coupling. The strength of coupling between a photon and an electrically charged particle is indicated by the scale of the fine structure constant, $\alpha = 1/137$. The small value of this parameter ensures that processes involving additional interactions occur with significantly lower probability. This allows QED to be treated perturbatively, so that transition probabilities may be expanded in powers of α, corresponding to an expansion in the number of charge-photon interaction vertices. In QCD the strong force coupling constant, α_s, is of order one and, consequently, the theory is not suited to the type of perturbative treatment which has proved so useful in QED.

There is, however, a regime in which the above considerations do not apply. The values of the coupling constants, as given above, are measured in the zero momentum exchange limit, but these values run with increasing momentum. In the case of QED the coupling strength grows with momentum, as a result of vacuum polarization. In QCD the vacuum polarization, involving the non-abelian gauge fields, produces an antiscreening effect, rather than screening. As a result, the coupling strength in QCD falls with growing momentum exchange, an effect know as asymptotic freedom [53, 99] . This effect has been critical in the understanding of deep inelastic scattering experiments and, more germane to this work, has allowed for detailed studies of the QCD phase diagram at asymptotically large densities where the fermi surface quarks are in the asymptotically free regime, as discussed in section 2.1.

B.2 The QCD vacuum

The ground state of QCD is fully non-perturbative and is found to exhibit a complex phenomenology. This discussion will, however, limit itself to the introduction of some basic concepts, and the properties necessary to motivate the formulation of the strong CP problem. The basic QCD Lagrangian is,

$$\mathcal{L}_{QCD} = \bar{\psi}_j \left[i\gamma_\mu D^\mu - m \right] \psi_j - \frac{1}{4} G_{\mu\nu} G^{\mu\nu}, \tag{B.1}$$

which is the standard formulation for a gauge field (here the gluons, with field strength tensor $G_{\mu\nu}$) coupled to charged fermions (the quarks ψ_j, with the index j running over all the quark flavours.) This formulation of the Lagrangian uses a summation convention whereby repeated indices are to be summed over. In the limit where the quarks are massless the Lagrangian has a conformal symmetry and a symmetry under chiral rotations, both of these are spontaneously broken by the QCD vacuum. The breaking of conformal symmetry introduces the fundamental scale of the theory Λ_{QCD}, and establishes the mass scale of the baryons. Chiral symmetry is spontaneously broken by the non-vanishing vacuum expectation values of the quark condensates. The nine broken generators of the chiral-flavour symmetry correspond to the pseudoscalar meson nonet. The nonet may be broken down into an octet (the pions, kaons and the η) and a singlet (the η'.) An example of the impact of the vacuum may be seen in the mass splitting of the η and the η' meson, with the η' having a mass comparable to the proton, while the η has a mass roughly half this value despite having the same quark content. This mass splitting is traceable to the fact that the η' is associated with the axial $U(1)_A$ symmetry which is explicitly broken by the chiral anomaly. As such, the η' mass is not protected against quantum corrections and acquires a mass at the QCD scale. Conversely, the mesons of the octet are genuine pseudo-Goldstone bosons which would be exactly massless in the limit of vanishing quark masses. The properties of the η' will be further discussed in section B.4.

While the $U(1)_A$ symmetry is explicitly broken by the anomaly, the remaining chiral-flavour symmetry (associated with the meson octet) is broken spontaneously by the formation of chiral condensates $< \bar{q}_R q_L >$ in the QCD ground state. Because they couple quark fields of opposite chirality these vacuum states break the chiral symmetry of the Lagrangian B.1. The energy density scale for a quark condensate is approximately given by, $m_q < \bar{q}_R q_L > \sim m_q \Lambda^3_{QCD}$.

In the high temperature phase of QCD the condensates break down and chiral symmetry is restored. It is also believed that the $U(1)_A$ symmetry is at least partially restored in the high temperature phase as the instanton effects responsible for breaking it are screened at large temperatures [108].

B.3 The strong CP problem and axions

Combined charge conjugation and parity symmetry (CP) is known to be violated in many physical processes. For example CP violating phases appear in the CKM matrix [71] and PMNS matrix [88] describing the electroweak mixing of quarks and neutrinos, respectively. The resulting CP violation may then be observed in the decay rates of heavy mesons[40]. However, no such violation has been observed within the strong force interactions, where the gluons couple to vector currents rather than to chiral currents as do the gauge bosons of the weak interactions. The best constraints on the degree of allowed strong CP violation come from measurements of the electric dipole moment of the neutron, which will be exactly zero only if QCD respects CP symmetry. As CP symmetry is known to be broken in both the quark and neutrino sectors, we may well ask why it seems to be respected by QCD. That QCD apparently preserves CP symmetry is particularly interesting given that there exists a mechanism within QCD which would allow for CP violation. In addition to the standard terms in the QCD Lagrangian, given in equation B.1, we are free to introduce an additional term,

$$\Delta\mathcal{L} \sim i\theta G_{\mu\nu}\tilde{G}^{\mu\nu} \tag{B.2}$$

$$\tilde{G}_{\mu\nu} \equiv \epsilon_{\mu\nu\sigma\tau}G^{\sigma\tau}. \tag{B.3}$$

At this point θ may be thought of as a free parameter of the Standard Model whose value is to be determined experimentally, and which sets the degree of

[40]For example the kaons, mentioned in the previous section, have been observed to decay into pion states with opposite CP quantum numbers. This is possible as kaons, while strongly interacting, decay through the weak interactions where CP violation is known to occur.

CP violation present in the theory[41]. At present observational constraints demand $|\theta| < 10^{-10}$. As there is no explicit reason for this value to be small, this raises a possible fine-tuning problem. This problem is made even more important by the fact that, even if the value of θ were to be set to zero by hand, quantum fluctuations would generate non-zero corrections to this term, just as they do to the η' mass. The fact that QCD remains a CP preserving theory, despite this mechanism through which CP violation should be expected to occur, is known as the strong CP problem.

The strong CP problem has not yet been resolved, but one of the preferred solutions is that of the Peccei-Quinn mechanism [97]. In this model an additional symmetry is introduced which is then broken by the QCD vacuum. The pseudo-Goldstone boson resulting from this symmetry is known as the axion[42], and it enters the Lagrangian in the same way as the θ parameter. In this case θ may be absorbed by a redefinition of the axion field. The axion field then relaxes down to $\theta \to 0$, resulting in the CP preserving theory we observe today. The axion has not been observed, but there are several experiments currently searching for it [25, 116] and, more than three decades after it was first proposed, it remains the only viable proposed solution to the strong CP problem. The properties of the axion, as relevant to this work, are its mass, which is believed to fall in the 10^{-3}eV$> m_a > 10^{-6}$eV range, and the fact that it is a singlet of the colour gauge group. These properties become important in the mechanism for compressing quarks of the early universe plasma into the high density phase which forms the quark nuggets in the dark matter model presented here. This will be briefly outlined in the following section.

B.4 Domain walls in QCD

Finally, I will present a brief overview of the domain walls involved in the formation of the quark nuggets. Domain walls are topological defects, know to exist in a wide range of field theories. These objects are generally the classical solutions of a field theory, which extrapolate between distinct ground

[41] This term is, in fact, a total derivative term representing a choice of vacuum state. As such, θ is a periodic variable such that the values θ and $\theta + 2\pi n$ describe identical physics. Where n is any integer.

[42] The axion model originally formulated by Wilczek and Weinberg [120, 121] produced an axion that was relatively heavy and strongly coupled to the particles of the Standard Model and has been ruled out by experiment. However, two subsequent models, the KSVZ axion [69, 107] and the DFSZ axion [34, 129], remain possible solutions to the strong CP problem.

states of the theory. In each domain the light degrees of freedom are excitations around the particular ground state configuration of the fields. Domain walls are the two dimensional surfaces at which two such distinct domains meet, and have energies at the scale of the barrier separating the different vacuum states. Associated with these objects is a conserved topological charge which makes them classically stable.

The domain walls considered here are a slight variation on this basic idea. As the θ parameter is 2π periodic, the states with θ and $\theta + 2\pi$ represent exactly the same physical ground state. Across the domain walls of this model the axion field (which has absorbed the bare value of θ into a dynamical field variable) varies by 2π, arriving back at a physically identical vacuum on the other side of the wall. These objects, involving a single winding through 2π are known as $N = 1$ domain walls. The physical length scale over which this transition occurs is set by the Compton wavelength of the axion, $\lambda \sim m_a^{-1}$, and is much larger than the typical QCD scale. Despite extrapolating between identical vacua, these field configurations still carry an associated topological charge which protects them from decay at the classical level [41].

The distinct vacuum states of QCD may be parameterized in the phases of the various condensates which they form. One may also consider transitions in the phase of the chiral condensates of the QCD ground state. As with the axion wall these involve the transition between two identical vacua, and possess a distinct topological charge. The transitions in these phases may be classified as belonging to rotations of the singlet or triplet configurations of the chiral-flavour symmetry group. The triplet field will have a relatively large length scale (somewhat larger than m_π^{-1}.) However, the singlet field (associated with the η') receives a correction from the gluon condensate, so that it exists at the QCD scale and has a length $\sim \Lambda_{QCD}^{-1}$. This range in length scales, from a few Fermi up to the macroscopic, will prove important in the considerations that follow.

It is also found that these transitions in the axion and condensate fields may overlap with each other forming a "sandwich" structure [41, 47]. The η' wall carries an energy density similar to that of the axion wall, but its narrower width implies that it is extended over a much smaller space, and contributes relatively little to the total energy associated with the wall. Partial mixing of the axion field with the η', which carries the same quantum numbers, also implies that a transition in one field may be accompanied by a transition in the other and, as such, some fraction of any axion walls which form will contain a hard η' core. The relatively small energetic cost implies that this fraction could be quite large.

With these preliminaries it is possible to outline the basic picture of nugget formation. As the early universe cools from the initial quark-gluon plasma to the baryonic phase, the axion fields condense out, on scales of order m_a^{-1}, and relax the CP violating θ term down to zero. These field configurations will include domain walls of the type described above. If the axion wall does not include an η' core[43] it is essentially transparent to fermions and the wall collapses down to R=0. If, however, the wall is of the sandwich type, with both a large axion scale component and a QCD scale core, it will be capable of trapping fermions within the collapsing wall. As the reflection process occurs at the centre of the wall where $\theta \neq 0$ this process will be CP violating, and the wall will preferentially trap either baryons or antibaryons. This process will continue until the Fermi pressure exerted by the trapped matter becomes comparable to the surface tension of the domain wall. As the trapped matter subsequently cools, the quarks will settle into a high density, superconducting phase forming nuggets with the properties discussed in the main body of this work.

B.5 Stability and lifetimes

The purpose of this section is to offer some brief arguments about the lifetime and stability of the quark nuggets and the axion domain walls which form and stabilize them. This discussion will necessarily be qualitative in nature as many exact calculations in high density QCD at $\theta \neq 0$ are not presently tractable. An analysis of the stability of the nuggets over a range of physical parameters was originally performed in [126] and the basic arguments will be presented here. An analysis of the stability of axion domain walls similar to those considered here was presented in [41] and in a slightly different geometry in [32], some qualitative results of this analysis will be sketched below.

The primary mode for the nuggets to decay into normal baryonic matter is through the emission of a nucleon or light nuclei. This process will be energetically favorable so long as the mass of the emitted nucleon is less than the decrease in the mass of the nugget, $m_N < M_B - M_{B-1}$. The stability of quark matter at zero external pressure is found to be highly model dependent [35, 122]. If the form of quark matter realized in the nuggets is absolutely stable with respect to nuclear matter then no external

[43] We could also consider η' walls without a surrounding axion wall, however these structures will form only over typical QCD length scales and be too small to be relevant here.

pressure from the axion wall is required and the wall's lifetime need only be long enough to provide the initial compression necessary to form the nuggets. This requires that the walls survive from the time of the QCD phase transition until the nuggets settle into the stable high density phase. A wider range of high density phases may become either stable or metastable in the presence of a confining domain wall. If this is the case the nuggets will remain stable over the lifetime of the wall and then begin to decay into free nucleons. For quark nuggets to serve as the dark matter this scenario would require domain wall stability over cosmological timescales.

In general the energy associated with a nugget of radius R and total baryonic charge B may be approximated as,

$$E = 4\pi R^2\sigma + \frac{4}{3}\pi R^3 \left[\frac{g\mu^4}{8\pi^2} + \epsilon_B\right]. \tag{B.4}$$

Here σ is the surface tension of the axion domain wall, μ is the quark chemical potential in the bulk of the nugget and ϵ_B is the binding energy of the quarks. As the chemical potential fixes the baryon density it is not independent from the baryon number and radius:

$$B = \frac{4}{3}\pi R^3 n_B(\mu) = \int_0^\mu g\frac{d\vec{p}}{(2\pi)^3} = \frac{2g\mu^3}{9\pi}R^3 \tag{B.5}$$

where g is the number of particle types present in the Fermi gas so that $g \approx$ (2 spins)$\times$(3 light flavours)$\times$(3 colours) ≈ 18. The stability of these objects may then be determined by minimizing the energy per baryon, E/B for a given value of σ and ϵ_B. If the energy at the minimization point is below the proton binding energy then nuggets in such a configuration will be stable. It is not necessary here to explore the full range of nugget parameters, allowed by expression B.4, that will result in long term stability. I will simply note that, as stable quark matter solutions have been found in the absence of a domain wall, adding this new component, which further compresses the quark matter, will necessarily increase the range of allowed phases. It should also be noted that at large radial sizes the pressure of the domain wall per quark in the nugget decreases. Thus, in the large R limit, the first term in equation B.4 becomes negligible and the situation becomes identical to that of quark matter not supported by the external pressure of the domain wall.

The domain walls themselves are topological defects which represent a solution to the classical field equations. This class of topological configurations generally arises when the theory under consideration contains a topological charge (for example a winding number) for which a conserved current may be derived. The conservation of this topological charge prevents the decay of the defect even in the case where such a decay would lower the total energy of the system.

The situation is more complicated when the walls are treated quantum mechanically. In that case the walls may decay through tunneling events even at temperatures well below the wall energy. A domain wall containing no hadronic matter will collapse down to an arbitrarily small size, and can decay relatively easily. If, however, the wall is supported against collapse by the Fermi pressure of matter trapped within it, the decay must occur through the nucleation of a hole in the wall. Holes of a sufficient size will expand rapidly and the wall will decay. The exact dynamics of this process are more complicated than will be considered here, but some basic scale arguments may be made. As with any tunneling process the rate of hole formation will be suppressed by a factor $\sim e^{-S_c/\hbar}$, where S_c is the classical action for the formation of the hole. In order for the hole to begin expanding it should be large with respect to the thickness of the wall $t \sim m_a^{-1}$. As this represents a macroscopically large area (comparable to the size of the quark nuggets themselves) and the energy density across the wall is large, the action for the formation of a hole will be large $S_c >> \hbar$. This leads to a strong exponential suppression of the wall decays and may allow these objects to be stable over cosmological timescales.

Appendix C

Nugget Thermodynamics

It is the purpose of this appendix to establish some of the basic thermal properties of the nuggets as required to determine their observational properties. Within the quark matter itself, the photon is screened at the QCD scale, so low energy thermal photons within the quark matter have no chance of escaping. Screening is also very efficient deep in the electrosphere where the positrons are at high densities. The first layer of the electrosphere from which low energy photons are able to escape occurs when the mean kinetic energy of the positrons becomes comparable to the temperature. This is precisely the Boltzmann regime discussed in section 2.2, and it will be the properties of this region which determine the thermal emission spectrum of the nuggets. In [43] the power emitted per unit volume at frequency ω of a Boltzmann gas of positrons of mass m_e was estimated as,

$$\frac{dE}{dt\ d\omega\ dV} \approx \frac{8\alpha}{15}\left(\frac{\alpha}{m_e}\right)^2 n_e^2(z,T)\sqrt{\frac{2T}{m\pi}}\left(1+\frac{\omega}{T}\right)e^{-\omega/T}F\left(\frac{\omega}{T}\right) \tag{C.1}$$

where the function $F(x)$ is defined as

$$\begin{aligned} F(x) = 17 \quad &- \quad 12ln\left(\frac{x}{2}\right) \quad x<1 \\ 17 \quad &+ \quad 12ln(2) \quad x>1. \end{aligned} \tag{C.2}$$

Here we may take the number density n_e to be given by 2.6 for the Boltzmann regime of the electrosphere. Note that the function $F(\omega/T)$ diverges in the $\omega \to 0$ limit. This divergence is unphysical and is a result of not imposing a long wavelength cutoff on the resulting photons. This cutoff will be imposed by the limited size of the Boltzmann regime of the electrosphere from which this radiation is emitted. As argued in section 2.2, the Boltzmann regime will persist from very near the nugget surface out to scales at which the plane parallel approximation fails. As this occurs at heights in the electrosphere for which the nugget's spherical geometry becomes important we should expect the emitting region to have a length on the order of the nugget's radius. The arguments leading to expression C.1 assumed a set of plane wave positron states of arbitrary long wavelength. If, however, we limit the allowed positron states[44] to a region with a scale of the size of the nugget we would expect a low momentum cutoff near $p_{min} \sim R_N^{-1}$. For photons emitted through elastic positron scattering this corresponds to a low frequency cutoff on the order of,

$$\omega_{min} \approx \frac{p_{min}^2}{2m_e} \approx \frac{\hbar}{2R_N^2 m_e} \approx 6 \times 10^9 \mathrm{s}^{-1} \tag{C.3}$$

while lower frequency radiation will be strongly suppressed. Thus, the emissivity given in C.1 and the emission spectrum to be derived from it should be considered valid only for frequencies above this limit. The exact way in which the spectrum falls from the value determined in C.1 near the cutoff will depend on the microscopic details of the electrosphere. For present purposes it will be sufficient to impose a hard cutoff at $\sim$ 6GHz, as implied by expression C.3, and limit ourselves to details of the spectrum above this frequency.

The expression C.1 may be integrated over the height of the Boltzmann regime to obtain a total surface emissivity as a function of temperature for the nuggets. In the plane parallel approximation roughly half of the emitted photons move upward and escape, the other half move downward and are reabsorbed. On performing this integration, one arrives at a final expression for the surface emissivity of a quark nugget of a given temperature:

$$\frac{dE}{dt\ dA\ d\omega} = \frac{4}{45}\frac{T^3\alpha^{5/2}}{\pi}\sqrt[4]{\frac{T}{m_e}}\left(1+\frac{\omega}{T}\right)e^{-\omega/T}\ F\left(\frac{\omega}{T}\right). \tag{C.4}$$

This will be the primary mechanism by which thermal energy is released from the nugget and, in addition to determining the spectral properties of the thermal emission, it is important for estimating the temperature evolution of the nuggets. As a general rule, the nuggets will be heated by nuclear annihilations and then radiate off this energy through low energy thermal radiation. The nuggets' temperature may then be estimated as the temperature for which the total thermal emission balances the energy input. To make this comparison we must integrate the surface emissivity across all

[44] Such a constraint is not placed on the photon states as they do not have to remain bound to the system. As such, the long wavelength radiation is not in equilibrium with the electrosphere and emission at these energies may exceed that expected from a blackbody.

frequencies [45] to obtain the total emitted energy:

$$\frac{dE}{dt\ dA} = \int \frac{dE}{dt\ dA\ d\omega} d\omega \approx \frac{16}{3} \frac{T^4 \alpha^{5/2}}{\pi} \sqrt[4]{\frac{T}{m_e}}. \tag{C.5}$$

This expression gives the total power output per surface area so that, if we assume the nugget to have a uniform surface temperature, the total power emitted through thermal radiation is simply

$$P(T) = 4\pi R_N^2 \left(\frac{dE}{dt\ dA} \right) \tag{C.6}$$

where R_N is the radius of the emitting quark nugget. In cases where the nugget is heated by the annihilation of matter falling onto the antiquark surface this total emitted power will be balanced by the flux of matter onto the nugget. This balance implies a temperature relation,

$$\left(\frac{T}{1\text{eV}} \right)^{17/4} \approx 10^{-9} f_T \ \frac{\Phi_{vis}}{1\text{GeVcm}^{-2}\text{s}^{-1}} \approx 30 f_T \ \frac{\rho_{vis}\beta}{1\text{GeVcm}^{-3}} \tag{C.7}$$

where Φ_{vis} is the visible matter energy flux onto the nugget, f_T is the fraction of this energy which is thermalized, ρ_{vis} is the visible matter density and $\beta = v/c$ is the boost factor of the matter. Note that for typical galactic values $\rho_{vis} \sim 100$ GeV cm^{-3} and $\beta \sim 10^{-3}$ so that this expression is of order one.

[45] As only a small fraction of the total energy is radiated at low frequencies this integral is not highly sensitive to the value of the low frequency cutoff given in expression C.3

Appendix D

Muon Propagation

Many of the observable properties of the air shower associated with a quark nugget passing through the atmosphere are dependent on its charged particle content. As argued in section 6.2, the charged particle content of the shower will primarily consist of muons. This appendix will discuss the treatment of muon propagation through the atmosphere to be used in estimating the observable properties of a quark nugget induced air shower.

In the study of cosmic ray induced air showers, the development of the shower as the secondary particles are produced and lose energy to the surrounding atmosphere is generally handled with large scale Monte Carlo simulations [20]. This level of detail is necessary in order to accurately calibrate the energy and composition of the primary cosmic ray, but goes well beyond the level of sophistication required for the simplified analysis presented here. Instead, I will use a highly simplified model of muon propagation which will allow a rough estimate of such important shower properties as the fluorescence profile, the surface distribution and the production of radio band geosynchrotron emission.

Here I will focus on the importance of a number of basic scales involved in muon propagation through the atmosphere. The lifetime of a muon at rest is $\tau_\mu = 2.2 \times 10^{-6}$s. For a relativistic muon this timescale is made longer by time dilation. The distance a muon can travel before it decays will be given by,

$$l_d = \gamma v \tau_\mu = \frac{p}{m_\mu} c \tau_\mu \tag{D.1}$$

where v is the muon's velocity and p is its momentum. This is the largest possible scale involved in muon propagation, and neglects energy losses to the atmosphere. Muons at the highest energies have very small interaction cross-sections with the surrounding matter and will generally travel about this distance. Muons decay to an electron and a neutrino pair. The neutrinos disappear from the shower while the electron is stopped much more rapidly than a muon and quickly becomes non-relativistic.

Muons at lower energies will loose a significant fraction of their energy to the atmosphere and may be stopped before they decay. The rate of energy loss will be dependent on the density of the background through which muons propagate. As the atmospheric molecules are neutral on scales larger than a few Bohr radii, scattering is only possible through the exchange of a photon with an energy of at least $\Delta E \sim m_e \alpha$. The cross section for this type of low energy scattering is approximately given by,

$$\sigma_{\mu e} \approx \frac{2\pi\alpha}{m_e^2}\frac{1}{v^2} \approx 7 \times 10^{-23}\text{cm}^2 \left(\frac{\text{c}}{\text{v}}\right). \tag{D.2}$$

The scattering length for a given muon is then given by finding the path length over which it is likely to encounter a single atmospheric molecule. This may be found by solving the expression

$$\sigma_{\mu e} \int_0^l ds\ n_{at}(s) = 1 \tag{D.3}$$

where l is the scattering length, s parameterizes the path along which the muon travels and n_{at} is the density of particles off of which the muon may scatter. The atmospheric depth is defined as

$$X = \int ds\ \rho(s) \tag{D.4}$$

and gives a measure of the amount of atmospheric material through which a particle moves [46]. Using this definition it is easier to express the scattering length in terms of the depth interval through which a muon can move:

$$\Delta X_s = \frac{m_p}{\sigma_{\mu e}}. \tag{D.5}$$

Here m_p is the mass per scattering site which is taken to be the mass of one proton.

The scattering amplitude is strongly peaked at small momentum transfer so that most scattering events will involve the muon losing roughly $m_e\alpha$ in energy. In this case the total number of scatterings required to stop a muon with total energy E is $(E - m_\mu)/m_e\alpha$. Thus the total depth interval across which a muon can travel is,

$$\Delta X_{tot} = \frac{E - m_\mu}{m_e \alpha}\frac{m_p}{\sigma_{\mu e}} \approx 6\ \text{kg cm}^{-2} \left(\frac{\text{E}}{\text{1GeV}}\right) \tag{D.6}$$

[46] This is a useful measure in studying a cosmic ray shower because the shower develops with depth rather than with the surrounding density as in the case of an antiquark nugget. This means, for example, that steeply inclined showers will leave a much longer fluorescence track than vertical ones. The atmospheric depth at which fluorescence peaks is referred to as X_{max} and is strongly correlated with the total energy initially carried by the primary cosmic ray.

where the final expression, intended only to give the scale involved, assumes that the muon energy is much larger than its rest mass. Note that the total atmospheric depth is on the order of 1kg cm^{-2}. So high energy particles will have no problem reaching the surface from most relevant heights. It is only relatively low momentum muons for which this energy loss scale will be important.

The basic muon propagation model I will use is simply to have the muon path length determined by either its decay length in equation D.1 or the maximum depth interval it can cross as given by expression D.6, depending on which is shorter. Until it reaches this distance the muon will be assumed to remain relativistic so that its velocity may be taken to be roughly the speed of light.

The muons originate at the nugget's location and propagate outward at a speed much larger than that of the nugget. As muons must be produced near the surface it will be assumed that the rate of muon emission is directly proportional to the matter flux onto the surface at any given time. This leads to preferential emission from the side of the nugget facing along the direction of motion. It will also be assumed that muon emission happens essentially perpendicular to the nugget surface as this implies the smallest distance within the quark matter that the muon must cross. Under these conditions the muon emission geometry may be expressed as the rate at which muons are emitted into a given solid angle:

$$\frac{dN_\mu}{d\Omega\ dt} = \frac{\Gamma_\mu}{2\pi} \cos\phi. \tag{D.7}$$

Here Γ_μ is the total muon production rate as given in 6.7 and ϕ is the angle between the direction that the muon is emitted and the direction of the nugget's motion. All emission will be taken to originate from the forward directed surface of the nugget so that $-\pi/2 < \phi < \pi/2$. In this geometry the muons are directed into a cone along the forward direction of the nuggets' motion.